Ion Binding Landscapes and Molecular Dynamics of Phospholipid Membranes

Jing Yang

PhD Thesis Supervised by

Dr. Jordi Martí and Dr. Carles Calero

October 2015

UNIVERSITAT POLITÈCNICA
DE CATALUNYA
BARCELONATECH

UNIVERSITAT POLITÈCNICA DE CATALUNYA
BARCELONATECH
Escola de Doctorat

Acta de calificación de tesis doctoral

Curso académico:

Nombre y apellidos

Programa de doctorado

Unidad estructural responsable del programa

Resolución del Tribunal

Reunido el Tribunal designado a tal efecto, el doctorando / la doctoranda expone el tema de la su tesis doctoral titulada _____

_____.

Acabada la lectura y después de dar respuesta a las cuestiones formuladas por los miembros titulares del tribunal, éste otorga la calificación:

☐ NO APTO ☐ APROBADO ☐ NOTABLE ☐ SOBRESALIENTE

(Nombre, apellidos y firma) Presidente/a	(Nombre, apellidos y firma) Secretario/a

(Nombre, apellidos y firma) Vocal	(Nombre, apellidos y firma) Vocal	(Nombre, apellidos y firma) Vocal

_____, _____ de _____ de _____

El resultado del escrutinio de los votos emitidos por los miembros titulares del tribunal, efectuado por la Escuela de Doctorado, a instancia de la Comisión de Doctorado de la UPC, otorga la MENCIÓN CUM LAUDE:

☐ SÍ ☐ NO

(Nombre, apellidos y firma) Presidente de la Comisión Permanente de la Escuela de Doctorado	(Nombre, apellidos y firma) Secretario de la Comisión Permanente de la Escuela de Doctorado

Barcelona a _____ de _____ de _____

Acknowledgements

First I gratefully thank my advisor Dr. Jordi Martí for his wonderful guidance throughout this thesis and kind help during my stay in Barcelona. I gratefully thank my advisor Dr. Carles Calero for his fruitful discussions and effort in revising the papers. I gratefully thank Dr. Massimiliano Bonomi for his expert advice and effort in reviewing my work. I gratefully acknowledge the financial support provided by the FI-AGAUR fellowship of the Generalitat de Catalunya, the computer resources and assistance provided by the Barcelona Supercomputing Center and the Red Española de Supercomputación, and the support of Universitat Politècnica de Catalunya.

Abstract

This thesis aims at studying the physical-chemical properties of phospholipid membranes in physiological environments. Molecular dynamics simulations and metadynamics simulations have been applied to study the interactions among membrane components, surrounding ions, and interfacial water. By applying metadynamics simulations, we have performed systematic free energy calculations of Na^+, K^+, Ca^{2+}, and Mg^{2+} bound to DMPC phospholipid membrane surfaces for the first time. The free energy landscapes unveil specific binding behaviors of metal cations on phospholipid membranes. We further propose a general methodology to explore the free energy landscapes for ions at complex biological interfaces and apply this methodology to examine the binding of Na^+ at cholesterol-containing membranes. The resulting free energy landscapes further validate our methodology and unveil the cholesterol effects on Na^+ binding at phospholipid membranes. We also study the microscopic structure and dynamics of water and lipids in a DMPC membrane in the liquid-disordered phase by molecular dynamics simulations. The diffusive dynamics of the membrane lipids and of hydration water, their reorientational motions, and their corresponding spectral densities reveal a variety of time scales playing a role in membrane dynamics. We have performed microsecond molecular dynamics simulations on the ternary mixtures of DPPC/POPC/cholesterol in the liquid-ordered and the liquid-disordered phases. The results show that the interactions of lipid-lipid and lipid-cholesterol are nontrivial properties depending on the lipid saturation and also on the mixture phase, which are consistent with the push-pull forces derived from experiments and give general insights on the interactions among membrane components.

Contents

1 General Introduction and Aims of This Thesis

1.1 Biological membranes in physiological environments

Biological membranes are ubiquitous in nature as limiting structures of cells, separating cell contents from external environments but also allowing the passage of nutrients and wastes through them. Cell membranes are involved in various cellular processes and play a vital role in protecting the integrity of the cell and maintaining the shape of the cell. While mammalian cell membranes are highly complex systems in terms of heterogeneous components, the predominant components are phospholipids and cholesterol. Phospholipid membranes provide the framework to biological membranes, to which other molecules such as proteins or cholesterol attach. Phospholipids are amphipathic molecules composed of a hydrophilic head group (easily attracted to water) and two hydrophobic tails (not dissolving in water). When placed in water, phospholipids self-assemble into a lipid bilayer with the hydrophillic heads facing outward and tails facing inward because of the hydrophobic effects. Lipid bilayers are simplified but commonly applied physical models for studying biological membranes. Exploring the physical-chemical properties of model lipid bilayers is important for the understanding of membrane functioning and cellular processes [1, 2, 3].

The first phospholipid to be discovered was phosphatidylcholine (PC) in the egg yolk of chickens by Theodore Gobley in 1847 and was named lecithin [4]. PC lipids such as di-myristoyl-phosphatidyl-choline (DMPC), di-palmitoyl-phosphatidyl-choline (DPPC), and palmitoyl-oleoyl-phosphatidyl-choline (POPC) that incorporate a choline headgroup are a major component of biological membranes. For instance, DPPC contributes approximately 40% to the compositions of pulmonary surfactant of lungs [5].

Cholesterol is another crucial component in mammalian cell membranes, constituting up to 50% of their weight in some cases [6]. Cholesterol can modulate the structural and mechanical properties of membranes and can induce a phase transition from a liquid-disordered phase to a liquid-ordered phase. While phospholipids are both translationally and conformationally disordered in the liquid-disordered phase, they are translationally disordered and conformationally ordered in the liquid-ordered phase [7, 8].

Cholesterol is also a key component of membrane rafts, which are lipid-cholesterol-protein assemblies functioning in membrane trafficking and signalling [9]. Membrane rafts are enriched in cholesterol and probably exist in the liquid-ordered phase. A number of physiologically important proteins are targeted to rafts, which plays a role in signal transduction, sorting in intracellular membranes, and regulation of cell-surface proteolysis [10]. Therefore, the study on cholesterol-containing lipid bilayers is of interest to understand membrane properties more realistically.

Moreover, biological membranes are surrounded by electrolyte solutions in physiological environments. The interactions of membranes with water and with ions are essential for several cellular processes, and should be taken into account when studying membrane properties. A snapshot of a cholesterol-containing phospholipid bilayer immersed in a $CaCl_2$ aqueous solution is shown in Figure 1.1.

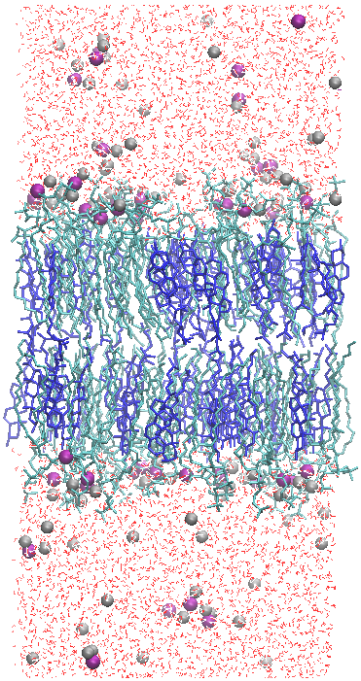

Figure 1.1: Snapshot of a cholesterol-containing phospholipid bilayer immersed in a $CaCl_2$ aqueous solution with phospholipids in cyan, cholesterol in blue, Ca^{2+} ions in purple, and Cl^- ions in silver.

1.2 Computational models

In general, there are two kinds of computational models widely used for biological membranes, i.e. the coarse-grained model and the all-atom model. In coarse-grained models, groups of atoms are treated as single particles, which can significantly increase system sizes and timescales of the simulations. Coarse-grained models have been applied to simulate large scale and long time processes such as membrane phase transitions, hydrophobic matching, and membrane-protein interactions[11]. However, coarse-grained models lack atomic resolutions and are therefore not appropriate

for studying phenomenons such as molecular vibration, ion binding, and hydration bonding. All-atom models, though more computationally expensive, can give physical insights on relevant dynamics at atomic levels. This thesis is based on all-atom models and includes analysis of microscopic processes such as ion binding to membranes and lipid vibrations.

1.3 CHARMM36 force field

The core of molecular modeling is the force field, which describes how the atoms interact. The interactions are classified into bonded and nonbonded ones. The bonded interactions include bond, angle, and dihedral terms. The nonbonded interactions include Lennard-Jones and electrostatic terms. The functional form for these interactions and parameter values used to calculate the potential energy of a system constitute the force field [1, 12]. MARTINI [13] force field is a coarse-grained force field for biomolecular systems. GROMOS [14], AMBER [15], and CHARMM [16] force fields are frequently used in atomic simulations of lipid bilayers. The potential energy in the CHARMM force field takes the form

$$\begin{aligned} U_{\text{total}} = & \sum_{\text{bonds}} K_b(b-b_0)^2 + \sum_{\text{angles}} K_\theta(\theta-\theta_0)^2 \\ & + \sum_{\text{dihedrals}} \sum_{j} K_{\varphi,j}[1+\cos(n_j\varphi-\delta_j)] \\ & + \sum_{\text{vdW}\ i,j} \varepsilon_{ij}\left[\left(\frac{R_{\min,ij}}{r_{ij}}\right)^{12} - \left(\frac{R_{\min,ij}}{r_{ij}}\right)^{6}\right] \\ & + \sum_{\text{Coulomb}\ i,j} \frac{q_i q_j}{\varepsilon_D r_{ij}}. \end{aligned} \tag{1.1}$$

The first three terms describe the stretching, bending, and torsional bonded interactions, and the final two terms describe nonbonded interactions. K_b, K_θ, and $K_{\varphi,j}$ are force constants for the bond, angle, and dihedral potential. b_0 and θ_0 are equilibrium values for bond lengths and angles.

n_j is multiplicity and δ_j is offset. The van der Waals interactions are modeled by Lennard-Jones potential, where ε_{ij} is the potential energy minimum between two particles separated by r_{ij}, and $R_{\min}$ is the position of this minimum. For the Columbic term, q_i and q_j are the partial atomic charges, and the dielectric constant ε_D equals 1 in explicit solvent simulations [16, 17].

The recently released CHARMM36 lipid force field [17] is one of the most used all-atom force fields for lipid membrane simulations. Motivated by the flaws of previous version CHARMM27 [18] and CHARMM27r [19] which yield large positive surface tension for fluid phase bilayers and gel-like structures of bilayers well above the gel transition temperature, selected parameters were modified. The resulting CHARMM36 lipid force field allows for molecular dynamics simulations to be run in the tensionless ensemble, and is desirable for simulations of pure lipid systems and heterogeneous lipid systems [17]. This thesis includes simulations of pure lipid bilayers and lipid mixtures, and uses the CHARMM36 lipid force field throughout the whole set of works.

1.4 Molecular dynamics simulations and enhanced sampling techniques

Molecular dynamics (MD) simulations [20, 21] have been widely employed to study lipid bilayer membranes. In MD simulations, the instant positions and velocities of atoms in the system are calculated by numerical integration of Newton's equations of motion as the simulation evolves. The potential energy $U(\boldsymbol{r}_1, ..., \boldsymbol{r}_n)$ of N interacting atoms depends on all atomic positions $\boldsymbol{r}_i = (x_i, y_i, z_i)$. The force acting on ith atom is determined by the gradient of the potential with respect to atomic displacements as [22]

$$\boldsymbol{F}_i = -\nabla_{\boldsymbol{r}_i} U(\boldsymbol{r}_1, ..., \boldsymbol{r}_n) = -\left(\frac{\partial U}{\partial x_i}, \frac{\partial U}{\partial y_i}, \frac{\partial U}{\partial z_i}\right). \tag{1.2}$$

The time evolution of a set of interacting atoms is obtained by the solution of Newton's equations of motion, i.e.,

$$\boldsymbol{F}_i = m_i \frac{\mathrm{d}^2 \boldsymbol{r}_i(t)}{\mathrm{d}t^2}, \tag{1.3}$$

where $\boldsymbol{r}_i(t) = (x_i(t), y_i(t), z_i(t))$ is the position of ith atom at time t, $\boldsymbol{F}_i$ is the force acting upon this atom at time t, and m_i is the mass of this atom.

The positions of atoms at time $(t+\triangle t)$ can be obtained by the numerical integration of Newton's equations of motion and expressed in terms of the previous positions [22]. The Verlet algorithm is commonly used in MD simulations. The basic idea for this algorithm is to express the atomic positions $\boldsymbol{r}$ at time $(t + \triangle t)$ and $(t - \triangle t)$ by Taylor expansions [20]

$$\boldsymbol{r}(t + \triangle t) = \boldsymbol{r}(t) + \frac{\mathrm{d}\boldsymbol{r}(t)}{\mathrm{d}t}\triangle t + \frac{1}{2!}\frac{\mathrm{d}^2\boldsymbol{r}(t)}{\mathrm{d}t^2}\triangle t^2 + \frac{1}{3!}\frac{\mathrm{d}^3\boldsymbol{r}(t)}{\mathrm{d}t^3}\triangle t^3 + O(\triangle t^4),$$

$$\boldsymbol{r}(t - \triangle t) = \boldsymbol{r}(t) - \frac{\mathrm{d}\boldsymbol{r}(t)}{\mathrm{d}t}\triangle t + \frac{1}{2!}\frac{\mathrm{d}^2\boldsymbol{r}(t)}{\mathrm{d}t^2}\triangle t^2 - \frac{1}{3!}\frac{\mathrm{d}^3\boldsymbol{r}(t)}{\mathrm{d}t^3}\triangle t^3 + O(\triangle t^4).$$

The atomic positions $\boldsymbol{r}(t + \triangle t)$ can be obtained by

$$\begin{aligned}\boldsymbol{r}(t + \triangle t) + \boldsymbol{r}(t - \triangle t) &= 2\boldsymbol{r}(t) + \frac{\mathrm{d}^2\boldsymbol{r}(t)}{\mathrm{d}t^2}\triangle t^2 + O(\triangle t^4) \\ &= 2\boldsymbol{r}(t) + \frac{\boldsymbol{F}(t)}{m}\triangle t^2 + O(\triangle t^4),\end{aligned}$$

$$\boldsymbol{r}(t + \triangle t) \simeq 2\boldsymbol{r}(t) - \boldsymbol{r}(t - \triangle t) + \frac{\boldsymbol{F}(t)}{m}\triangle t^2. \tag{1.4}$$

The atomic velocities $\boldsymbol{v}(t)$ can be obtained by

$$\begin{aligned}\boldsymbol{r}(t + \triangle t) - \boldsymbol{r}(t - \triangle t) &= 2\frac{\mathrm{d}\boldsymbol{r}(t)}{\mathrm{d}t}\triangle t + O(\triangle t^3) \\ &= 2\boldsymbol{v}(t)\triangle t + O(\triangle t^3),\end{aligned}$$

$$\boldsymbol{v}(t) \approx \frac{\boldsymbol{r}(t+\triangle t) - \boldsymbol{r}(t-\triangle t)}{2\triangle t}. \tag{1.5}$$

The equilibrium properties of the system can be obtained by time averaging the corresponding physical quantities if the MD trajectories are ergodic in the timescale of the simulation. However, in some systems, the relevant configurations are separated by high free energy barriers, making it a challenge to achieve ergodicity by standard MD simulations [23, 24, 25].

To enhance the sampling of relevant configurations, a number of methods have been proposed, such as umbrella sampling [26], adaptive biasing force algorithm [27], steered molecular dynamics[28], and metaynamics [29]. These methods are often referred to as enhanced sampling techniques or as free energy methods due to their close relations with free energy calculations [23, 24, 25, 30].

1.5 Metaynamics

In metadynamics, an external history-dependent bias potential is constructed in the space of one or a few predefined collective variables (CVs). This potential is built as a sum of Gaussians deposited along the system trajectory in the CVs space to discourage the system from revisiting configurations that have already been sampled [29, 25, 23].

Let $\boldsymbol{S}$ be a set of CVs described by the microscopic coordinates $\boldsymbol{R}$ of the system

$$\boldsymbol{S}(\boldsymbol{R}) = (S_1(\boldsymbol{R}), ..., S_d(\boldsymbol{R})). \tag{1.6}$$

At time t, the metadynamics bias potential is

$$V_{\mathrm{G}}(\boldsymbol{S}, t) = \int_0^t dt' \omega \exp\left(- \sum_{i=1}^{d} \frac{(S_i(\boldsymbol{R}) - S_i(\boldsymbol{R}(t')))^2}{2\sigma_i^2} \right), \tag{1.7}$$

where σ_i is the width of the Gaussian for the ith CV, and ω is a con-

stant energy rate depending on the Gaussian height W and the Gaussian deposition stride τ_G as

$$\omega = \frac{W}{\tau_G}. \tag{1.8}$$

The effect of the metadynamics bias potential is to push the system away from local free energy minima into visiting new regions of the CVs space. After the free energy minima are filled up by Gaussians, the bias potential V_{G} will approximately flatten the underlying free energy $F(\boldsymbol{S})$. In the long time limit, the bias potential V_{G} converges to

$$V_{\mathrm{G}}(\boldsymbol{S}, t \to \infty) = -F(\boldsymbol{S}) + C, \tag{1.9}$$

where C is an irrelevant constant.

Since Gaussians of constant height are added during a metadynamics simulation, the system is eventually pushed to explore high free energy regions and the estimate of the free energy calculated from the bias potential V_{G} oscillates around the real free energy $F(\boldsymbol{S})$.

1.6 Well-tempered metaynamics

Well-tempered metadynamics [31, 25, 23], a variant of metadynamics, has been proposed to decrease the error between the metadynamics estimate of the free energy and the real free energy. In well-tempered metadynamics, the height of the Gaussian is decreased with simulation time as

$$W = \omega \tau_G e^{-\frac{V_{\mathrm{G}}(\boldsymbol{S},t)}{k_{\mathrm{B}} \triangle T}}, \tag{1.10}$$

where $\triangle T$ is an input parameter with the dimension of a temperature, and k_{B} is the Boltzmann constant.

With this rescaling of the Gaussian height, the bias potential V_{G} does not fully compensate the underlying free energy $F(\boldsymbol{S})$, but it smoothly

converges to

$$V_{\mathrm{G}}(\boldsymbol{S}, t \to \infty) = -\frac{\triangle T}{T + \triangle T} F(\boldsymbol{S}) + C, \tag{1.11}$$

where T is the temperature of the system and C is an irrelevant constant. In the long time limit, the CVs thus sample an ensemble at a temperature $T + \triangle T$ which is higher than the system temperature T. While $\triangle T = 0$ corresponds to standard molecular dynamics, $\triangle T \to \infty$ corresponds to standard metadynamics. The ratio between the temperature of the CVs $(T + \triangle T)$ and the system temperature (T) is named as the bias factor γ in well-tempered metadynamics simulations, which is

$$\gamma = \frac{T + \triangle T}{T} \tag{1.12}$$

The bias factor γ should be carefully chosen in order for the relevant free energy barriers to be crossed efficiently in well-tempered metadynamics simulations.

1.7 Aims of this thesis

This thesis aims at studying the physical-chemical properties of model lipid bilayers in physiological environments. Since biological membranes composed of phospholipids and cholesterol are surrounded by electrolyte solutions in physiological environments, understanding the interactions of phospholipids with cholesterol, lipid bilayers with surrounding ions, and lipid bilayers with interfacial water are of great fundamental importance. Moreover, phospholipids are classified into saturated ones and unsaturated ones according to the tail saturation. Therefore, considering the tail saturation is another important issue when studying lipid bilayers.

The lipids involved in this thesis include the saturated phospholipids DMPC and DPPC, the unsaturated phospholipid POPC, and cholesterol. The chemical structures of these lipids are shown in Figure 1.2. While all

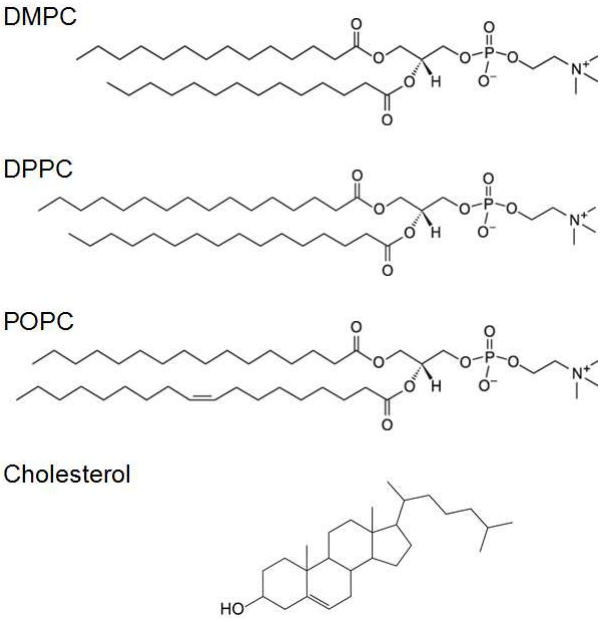

Figure 1.2: Chemical structures of phospholipids DMPC, DPPC, and POPC and cholesterol.

the phospholipids DMPC, DPPC, and POPC have the same phosphatidylcholine (PC) head group, DPPC has slightly longer tails than DMPC and POPC has an unsaturated double bond in the tails.

Classical molecular dynamics simulations and well-tempered metadynamics simulations have been applied in this thesis. The outline of the thesis is as follows.

In Chapter 2, we study the microscopic structure and dynamics of water and lipids in a DMPC phospholipid membrane in the liquid-disordered phase by classical molecular dynamics simulations. The diffusive dynamics of the membrane lipids and of its hydration water, their reorientational motions as well as their corresponding spectral densities, related to the absorption of radiation, have been considered for the first time using the

CHARMM36 force field. In addition, structural properties such as density and pressure profiles, a deuterium-order parameter, surface tension and the extent of water penetration in the membrane have been analyzed. Molecular self-diffusion, reorientational motions and spectral densities of atomic species reveal a variety of time scales playing a role in membrane dynamics. The mechanisms of lipid motion strongly depend on the time scale considered. Lipid reorientation along selected directions agree well with reported nuclear magnetic resonance data and indicate two different time scales. Calculated spectral densities corresponding to lipid and water reveal an overall good qualitative agreement with Fourier transform infrared spectroscopy experiments. The physical meaning of all spectral features from lipid atomic sites is analyzed and correlated with experimental data.

In Chapter 3, we study the ion binding landscapes of phospholipid membranes. By applying well-tempered metadynamics simulations, we have performed systematic free-energy calculations of Na^+, K^+, Ca^{2+}, and Mg^{2+} bound to DMPC phospholipid membrane surfaces for the first time. The free-energy landscapes unveil specific binding behaviors of metal cations on phospholipid membranes. This work provides a general methodology to explore the free-energy landscapes for ions at complex biological interfaces which can be extended to study other interactions of interest between ions and charged headgroups in colloidal chemistry and biology.

In Chapter 4, we further apply this methodology to cholesterol-containing membranes by means of systematic free energy calculations of Na^+ bound to DMPC phospholipid membranes of several cholesterol concentrations. The resulting free energy landscapes further validate our methodology at membrane interfaces with higher complexity and unveil the cholesterol effects on Na^+ binding at phospholipid membranes.

In Chapter 5, we have performed microsecond molecular dynamics simulations on the ternary mixtures of DPPC/POPC/cholesterol to systematically examined lipid-lipid and lipid-cholesterol interactions in the liquid-

ordered and the liquid-disordered phases. The results show that the interactions of lipid-lipid and lipid-cholesterol are nontrivial properties depending on the lipid saturation and also on the mixture phase. The results are consistent with experiments and give systematical descriptions of the mutual interactions between various like or unlike species in different phases.

The conclusions of each chapter are summarized in Chapter 6.

2 Diffusion and Spectroscopy of DMPC Phospholipid Membranes

Microscopic structure and dynamics of water and lipids in a fully hydrated DMPC phospholipid membrane in the liquid-disordered phase have been analyzed with all-atom molecular dynamics simulations based on the recently parameterized CHARMM36 force field. The diffusive dynamics of the membrane lipids and of its hydration water, their reorientational motions as well as their corresponding spectral densities, related to the absorption of radiation, have been considered for the first time using the present force field. In addition, structural properties such as density and pressure profiles, a deuterium-order parameter, surface tension and the extent of water penetration in the membrane have been analyzed. Molecular self-diffusion, reorientational motions and spectral densities of atomic species reveal a variety of time scales playing a role in membrane dynamics. Our findings include a "wagging of the tails" frequency around 30 cm^{-1}, which essentially corresponds to motions of the tail-group along the instantaneous plane formed by the two lipid tails, i.e., in-plane oscillations are clearly of bigger importance than those along the normal-to-the plane direction.

2.1 Introduction

Biological membranes are ubiquitous in nature as limiting structures of cells, separating cell contents from external environments, but allowing the passage of nutrients and wastes through them. Phospholipid membranes provide the framework to biological membranes, to which other molecules (such as proteins or cholesterol) attach. They consist of two leaflets of amphiphilic lipids which self-assemble due to the hydrophobic effect [3]. The study of pure component membranes can help understand basic biological membrane functions and its interaction with the environment. Among a wide variety of lipids, DMPC are phospholipids incorporating a choline as a headgroup and a tailgroup formed by two myristoyl chains. They are usually synthesized to be used for research purposes (studies of liposomes and bilayer membranes). Their properties are very similar to those of DPPC which has the same structure but slightly longer tails, being a major constituent of pulmonary surfactants of lungs[32] (about 40%).

Structure and dynamics of lipid bilayers in water environments have been thoroughly analyzed from long time ago from the experimental and theoretical points of view, including water permeation and lipid hydration [33, 34, 35]. Structure has been well characterized by Fourier transform infrared spectroscopy (FTIR) and from quasielastic neutron scattering (QENS), whereas hydration of lipid membranes can be probed by means of ultrafast polarization selective vibrational pump-robe spectroscopy[36], among a variety of techniques. Nevertheless, its microscopic dynamics remains controversial due to the multiple time scales involved (see for instance Ref.[37]). Indeed, while at short timescales the dynamics of lipids is dominated by fast translations restricted by their neighbors (*rattling in a cage* effect), at long timescales the motion of lipids exhibits a slower long-range diffusion. To reconcile both regimes, a mechanism based on the hopping of lipids to nearby spontaneously created voids was proposed. This paradigm offered an explanation to the apparent contradiction of

the lipid motion at different timescales and was instrumental to interpret QENS backscattering experiments [38]. However, this mechanism was recently challenged by different computational[39] and experimental studies [40, 41], in which it is found that the dynamics of lipids at long timescales is collective in nature, strongly correlated over tens of nanometers to the dynamics of the neighboring lipids. This concerted motion creates lipid flow patterns at the mesoscopic scale. In addition, lipid dynamics can be affected by rare event phenomena such as lipid flip-flops (translocations of a lipid chain between the two leaflets composing a membrane), occurring at a time scale of the order of hundreds of nanoseconds [42] and for that reason requiring specific computational tools to analyze them, such as transition path sampling[43].

Spectroscopic methods provide a valuable tool to help uncover the mechanisms of lipid dynamics. Together with FTIR and QENS mentioned above, other techniques such as small angle scattering of synchrotron radiation, dielectric spectroscopy and nuclear magnetic resonance have also provided valuable information on the properties of lipid bilayers[44, 45]. However, experimental data is often not conclusive and it requires theoretical interpretation. In that respect, molecular dynamics simulations of lipid bilayers can be used to ascertain the microscopic mechanisms responsible for experimental observations. In that spirit, we report in the present work a detailed study of the structure and dynamics of DMPC lipid bilayers. Similar works have been already published using other force fields[44, 46, 47] but, up to our knowledge, this is the first work where results of dynamical properties such as long time diffusion and spectroscopy have been obtained using CHARMM36 force field [17]. In particular, we focussed our view on three particular issues: (1) the characterization of the structure and dynamics of DMPC, (2) the analysis of the microscopic mechanisms of diffusion at different timescales, and (3) the characterization of the motion of atoms by calculating spectral densities, which can be related to a variety of spectroscopic experimental techniques.

2.2 Methods

Our system is a prototype model of an aqueous bilayer membrane composed by 128 lipids distributed in two leaflets of 64 flexible DMPC molecules surrounded by 4377 TIP3P[48] water molecules. In contrast to the original TIP3P force field, the water model employed in this work allows flexible internal motions (bending, stretching) of water molecules, in order to compute specific spectral densities (see section 2.3.5). With $\sim$ 34.2 water molecules per lipid, our simulated lipid bilayer can be considered fully hydrated [49]. A general view of the system is represented in Figure 2.1. Each DMPC molecule is described with atomic resolution (118 sites). Some of the most relevant sites considered in this work, which will be referred to in the analysis of the results, are highlighted in Figure 2.2.

Molecular dynamics simulations were performed by means of the NAMD2 molecular dynamics simulation package[50] at a temperature of 303 K and an average pressure of 1 atm. The simulation time step was set to 2 fs for a long 200 ns run and to 0.5 fs for additional short runs, used to analyze vibrations of hydrogens. The recently parameterized force field CHARMM36, which is able to reproduce the area per lipid in excellent agreement with experimental data, has been used. For the long 200 ns run, all molecular bonds have been left non rigid, except the bonds made with hydrogens. For the short runs, fluctuations of bond distances and angles associated to hydrogens have been allowed as well. Van der Waals interactions were cut off at 12 Åwith a smooth switching function starting at 10 Å. Long ranged electrostatic forces were computed with the help of the particle mesh Ewald method[51], with a grid space of about 1 Å. Electrostatic interactions were updated every 2 fs. Periodic boundary conditions were applied in all three dimensions. After energy minimization, the system was equilibrated in the NPT ensemble at 1 atm for 30 ns. During the NPT simulation run we monitored the surface area per lipid considering the total surface along the XY plane (plane parallel to the

bilayer surface) divided by the number of lipids in one lamellar layer[52]. The final area per lipid was 60.5 Å^2 (see top panel of Figure 2.3), which is consistent with the expected result of CHARMM36 force field (60.8 Å^2)[17] and also with the experimental value (60.6 Å^2)[53]. The reader should note that this value for the area per lipid arises naturally from the relaxation of the system at a given temperature, pressure and number of particles rather than being an imposition to fit the experimental value. Its agreement with the experimental value validates both the use of the CHARMM36 force field and the chosen equilibration procedure.

Next, a 200 ns production run was performed in the NVT ensemble, with XY plane fixed at 67.4 Å$\times$ 57.4 Å, which was the final size of the previous equilibrating NPT simulation, and Z direction (normal to the XY plane) fixed at 140 Å . The temperature was controlled by a Langevin thermostat[54] with a damping coefficient of 1 ps^{-1} for both NPT and NVT simulations, whereas the pressure was controlled by a Nosé-Hoover Langevin barostat[55] with a piston oscillation time of 200 fs and a damping time of 100 fs for the NPT simulation. Since one important goal of this work is to characterize the diffusion of water and lipids over several time scales, we conducted simulation runs of different lengths with appropriately chosen data recording frequencies (see Table 2.1). Finally, in order to eliminate any artificial drift of the center-of-mass of the system in the simulations, the coordinates of lipid atoms were corrected for the motion of the center-of-mass of the monolayer they belong to[56].

To ensure that we are simulating the liquid phase of the model system as well as to efficiently characterize the order of the aqueous lipid bilayer, we computed the deuterium order parameter S_{CD} which can be obtained from ^{2}H NMR experiments. This quantity was first reported by Stockton and Smith[57] and later on adapted by Hofsäss et al.[58], by means of an order parameter defined for each CH_2 group as follows:

$$S_{CD} = \frac{1}{2}(3 < \cos^2 \theta_{CD} > -1), \tag{2.1}$$

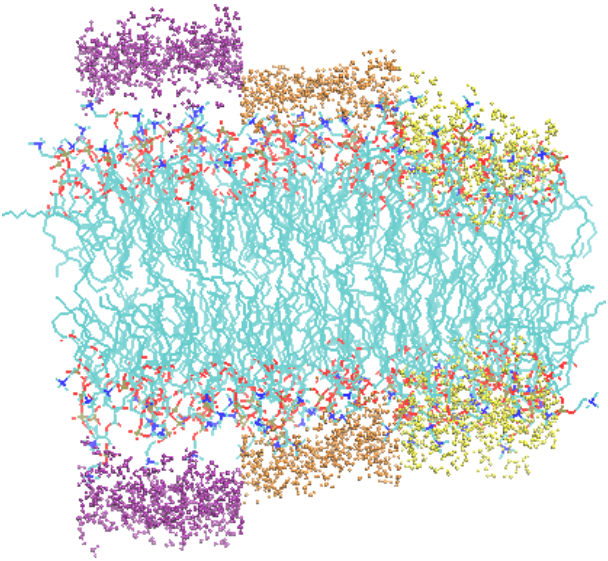

Figure 2.1: Snapshot of the DMPC bilayer membrane simulated in this work. The carbon chains of DMPC molecules are shown in cyan. Nitrogen atoms are depicted in blue, phosphorus in green and ester oxygens in red. Water molecules have been represented in different colors depending on their location: in purple those located at 6 Å or more from any site of a lipid chain ("bulk"); in orange those located between 6 and 3 Å from any lipid site ("intermediate") and in yellow those located closer than 3 Å of any lipid site ("contact").

where θ_{CD} is the angle between the membrane normal and a CH-bond (a CD-bond in the experiments). Brackets in Eq.2.1 indicate ensemble average for all lipids. The results are shown in the bottom panel of Fig.2.3 for the two chains (sn1, sn2) of a DMPC molecule. The results are in good agreement with both experimental [59, 60] and simulation works [58, 61, 62] and confirm that the system, in the simulation conditions assumed in the present work, pertains to the liquid phase.

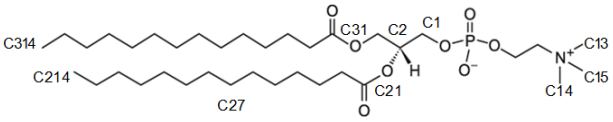

Figure 2.2: DMPC molecule with highlighted sites considered in this work. Hydrogen atoms not shown.

Table 2.1: Simulation lengths and frequency of recording data for the study of diffusion of water and dynamics of lipids at the *ballistic, sub-diffusive* and *diffusive* regimes.

Purpose	Length	Frequency
Ballistic	10 ps	1 fs
Sub-diffusive	1 ns	100 fs
Fickian (longtime)	200 ns	10 ps
Water diffusion	50 ps	5 fs

2.3 Results

2.3.1 Pressure profile and surface tension of the membrane

The pressure profile, i.e. lateral minus normal pressure as a function of the Z coordinate, has been obtained from a series of 10 additional simulations (total run length of 20 ns) in the NPT ensemble, in order to better control pressure fluctuations of the system, which strongly affect the pressure at the membrane. Along such short runs, the XY dimensions were fixed at 67.4 Å$\times$ 57.4 Å while the box Z coordinate (fluctuating around 70 Å) was allowed to adjust to the pressure of 1 atm. The remaining parameters were kept the same as those employed during the equilibration run.

The result is displayed in Figure 2.4. Our results agree qualitatively well with those reported in a previous work [63], with some differences observed at relevant regions of the membrane, i.e. the water-lipid interface and the center of the membrane where the two leaflets are in close contact through

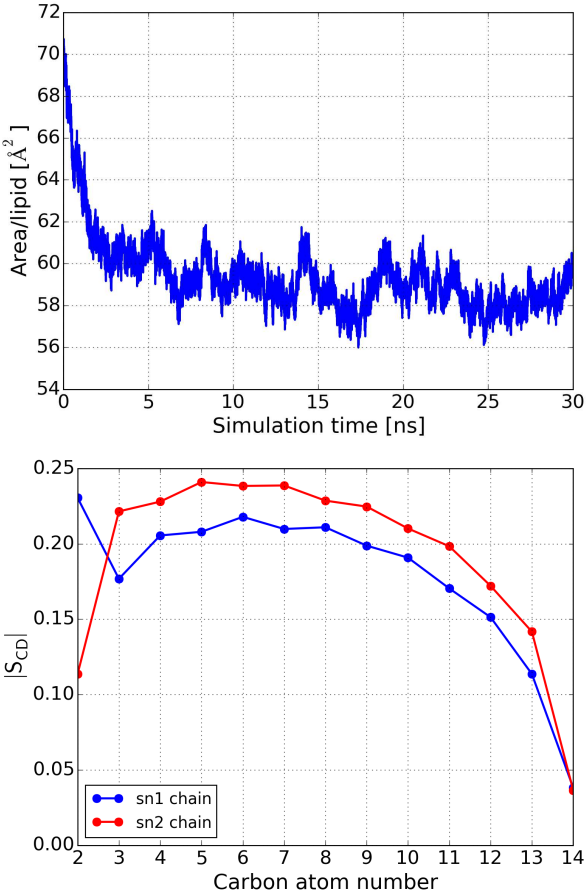

Figure 2.3: Area per lipid as a function of simulation time (top) and order parameter for selected carbon sites at the tailgroups (bottom).

tail-tail interactions. We observe significant fluctuations alongside the bilayer of the same order of magnitude already found in previous simulation works[63]. The uncertainty of the pressure profile, represented in the error bars of Figure 2.4, was estimated by calculating the absolute difference

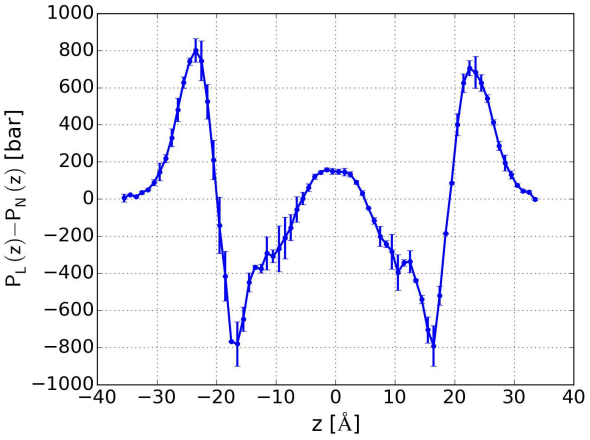

Figure 2.4: Pressure profile: $P_L(z) - P_N(z)$.

of the results obtained from each of the ten independent simulations and their average. From the pressure profile we calculated the surface tension γ using[64], i.e.,

$$\gamma = \int_{-\frac{h}{2}}^{\frac{h}{2}} \mathrm{d}z \, [P_N - P_L] \,, \tag{2.2}$$

where h is the height of the simulated system's volume, with the normal and lateral pressures given by $P_N = P_{zz}$ and $P_L = \frac{1}{2}(P_{xx} + P_{yy})$, respectively. Here, P_{ii} with $i = x, y, z$ are components of the stress tensor for a bilayer whose normal is parallel to the Z-axis. From Eq.2.2, we obtain for the surface tension $\gamma = -0.1 \pm 1.2$ mN/m, again in good agreement with previous works[65] (gel phase, low hydration), [63] (liquid phase). From experimental and theoretical previous works, the expected surface tension of a lipid bilayer membrane should be zero [65, 66, 67, 68, 69].

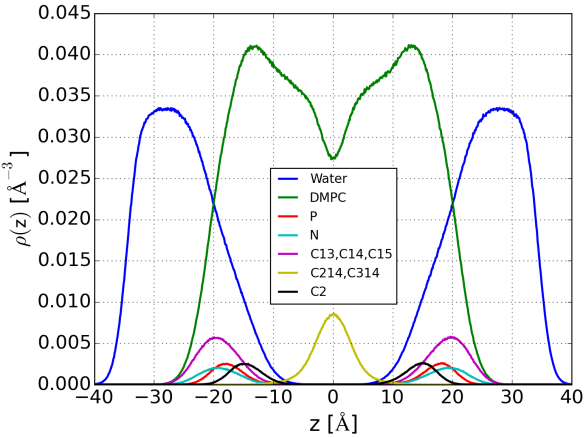

Figure 2.5: Density profiles of water, lipid chains and lipid atoms. Nitrogen (N), phosphorus (P), carbons: C2 (close to center of mass of the lipid), C13, C14 and C15 (headgroup) and C214 and C314 (tailgroup).

2.3.2 Structure

The local structure of the system can be resolved by means of atomic density profiles, shown in Figure 2.5. We sliced the system into 0.1 Å- width layers perpendicular to the Z-axis. The overall results are in accordance with those of Griepernau and Böckmann [62], who employed a different force field in the description of the lipids.

We have considered the densities of nitrogen, phosphorus, and carbon atoms close to the center of mass of the lipids, carbons at the head and tails of lipids, water, and the lipid backbone (excluding hydrogens). A closer look into water densities allows us to distinguish the three regions sketched in the snapshot of Figure 2.1: Region (a) "bulk" water (more than 6 Å away from the position of any lipid site); (b) "intermediate" water (between 3 and 6 Å of any lipid site) and (c) "contact" (interfacial)

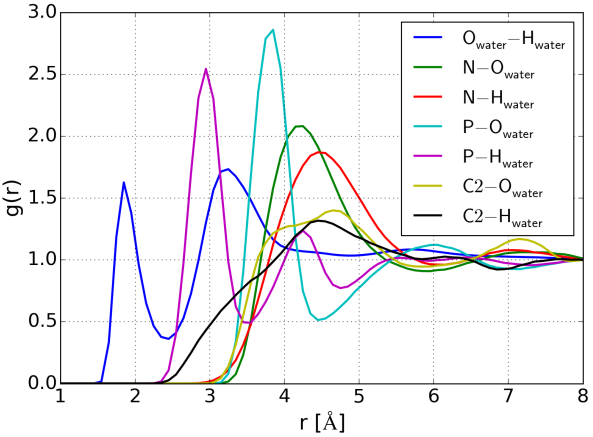

Figure 2.6: Radial distribution functions of water (Oxygens, Ow and Hydrogens, Hw) related to several species: nitrogen (N), phosphorus (P), carbon (C2).

water (within 3 Å of any lipid site). From a general perspective, the structure of the lipid bilayer shows few differences compared to the one obtained by means of the previous CHARMM27 force field [47].

To investigate the distribution of water molecules around lipid species, we also report selected water-lipid radial distribution functions in Figure 2.6. Our results are in good agreement with those recently reported by Hansen et al. [47] and indicate a selective binding of water around atoms such as nitrogen and phosphorus and a weak affinity for intermediate carbons as C2, located very close to the center of mass of a lipid chain. As a general fact, water shows a tendency to place around phosphorus at shorter distances (3.8 Å) than around nitrogen (4.3 Å). Further, a second water layer around P can be observed at $\sim$ 6 Å, whereas no second layer around N has been detected.

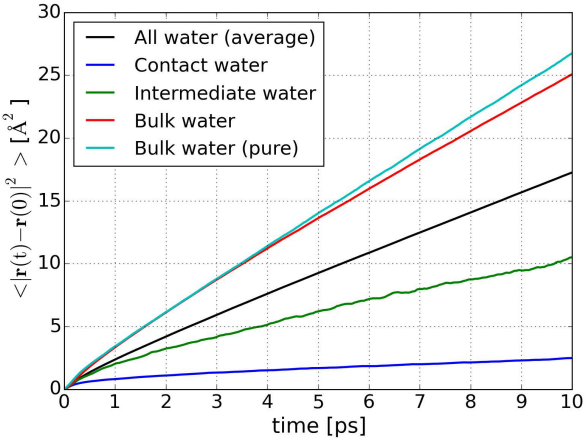

Figure 2.7: Mean square displacement of water oxygens. The result from the bulk of pure TIP3P water employed in the present work has been included for the sake of comparion with our system's bulk.

2.3.3 Water diffusion

Water dynamics in phospholipid membranes has been from long time a controversial issue, with different approaches referring water hydration and its behavior in the vicinity and inside the membrane [70, 71, 72]. Water self-diffusion coefficients D_w have been obtained from the analysis of the time-dependence of the mean square displacement (MSD) of oxygen atoms, displayed in Figure 2.7. The calculation of D_w renders an overall value of 2.66×10^{-5} cm^2/s, obtained from all water molecules independently of their positions in the system. This can be compared with the self-diffusion of water in a pure system, simulated with the same force field employed in the present work. To do so, we conducted a 50 ps simulation run (after equilibration) in the NVT ensemble. The value of D_w^{pure} has been of 4.0×10^{-5} cm^2/s, indicating that the TIP3P model employed in this work tends to overemphasize water's diffusion. Similar results were

obtained by Rosso and Gould [35].

We have also considered the diffusion of water located in the three different regions defined above: bulk, intermediate, and contact regions. The diffusion coefficient obtained for water in the "contact" region is 0.26×10^{-5} cm^2/s, much smaller than the values obtained for the "intermediate" (1.29×10^{-5} cm^2/s) and "bulk" (3.77×10^{-5} cm^2/s) regions. The latter value is in excellent agreement with the value reported above for pure water, which validates the choice of the "bulk" like region considered in the present work. So, although the water model employed in this work considerably overestimates water diffusion in bulk (the experimental value for the water diffusion coefficient is 2.3×10^{-5} cm^2/s [73]), the drastic drop in water diffusion at the interface should be model independent and related to the interaction of water molecules with the hydrophilic lipid heads.

During the calculation time-window of 10 ps, about $\sim$24% of water molecules remained in the "bulk" group, $\sim$6% water molecules stayed in the "contact" zone, while only $\sim$0.5% of them were accounted as "intermediate" water molecules, with the remaining water molecules fluctuating between different zones. For this reason, statistics at the intermediate zone are much worse than those from the other two regions, which is reflected in the noise observed in the MSD of "intermediate water" reported in Figure 2.7.

2.3.4 Mechanisms of lipid diffusion

One of most relevant issues in the study of phospholipid membranes concerns the lateral diffusion of lipid chains. Different factors such as temperature, pressure, amount of cholesterol and proteins, hydration, concentration of salts, etc. may have strong influence on lipid dynamics. Further, a variety of experimental methods report significantly different values for the diffusion coefficient. Experimental studies using pulsed gradient nuclear magnetic resonance [74], single particle tracking [75], fluorescence recovery after photobleaching [38], or from fluorescence correlation spec-

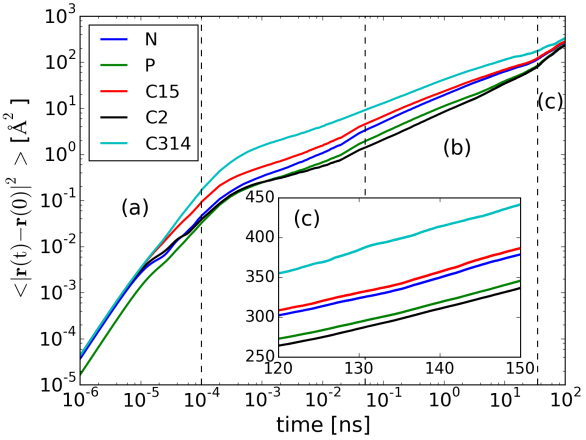

Figure 2.8: Mean square displacement of lipid atoms. (a) Sub-picosecond time scale; (b) nanosecond time scale; (c) hundred nanoseconds time scale. The inset shows the range of longest time, between 120 and 150 ns.

troscopy [76] report values within 0.5×10^{-7} cm^2/s and 1×10^{-7} cm^2/s. Neutron scattering experiments, operating in the picosecond range, produce diffusion coefficients significantly higher [37, 38, 77], in the range of 1 to 10×10^{-7} cm^2/s.

Furthermore, there exists a controversy concerning the existence of two regimes working on the dynamics of lipids, namely (1) the fast confined motion limited by the neighboring lipids, i.e. *rattling in a cage* effect[44], probably due to the wagging of lipid tails, as it has been observed for some fatty acids[78] at short timescales and (2) the slower long-range diffusion exhibited at longer timescales. The accepted paradigm is based on a mechanism of lipid hopping out of the neighbor cage to nearby spontaneously created voids, which successfully accounts for QENS backscattering experiments[38]. Such a mechanism was put in question by Falck et al.[39], who studied the lateral diffusion of lipid membranes with MD

Table 2.2: Exponent β of lipid atoms corresponds to *ballistic motion*, *sub-diffusion*, and *long time (Fickian) diffusion*.

Atom	$\beta_{ballistic}$	$\beta_{sub-diffusive}$	$\beta_{Fickian}$
N	1.94	0.57	1.04
P	1.96	0.62	1.08
C15	1.94	0.54	1.04
C2	1.92	0.62	1.11
C (at tail's end)	1.94	0.49	0.90

simulations. They concluded that the dynamics of lipids at long timescales is collective in nature, strongly correlated over tens of nanometers to the dynamics of their neighbors. Later on it was shown that such mechanism was consistent with experiments [40, 41].

Generally, the time-dependence of the lateral MSD of membrane lipids can be described by a power law as follows:

$$< \vec{r}^2(t) > \sim A \cdot t^{\beta}, \tag{2.3}$$

where the exponent β changes for different time scales. At the shortest time scale, lipids undergo ballistic motion (with $\beta \sim 2$), followed by sub-diffusion (with $0 < \beta < 1$) at some intermediate scale, and ending with continuous Brownian motion with $\beta \sim 1$ at the longest time scale available in our computer simulations. We have separated these three time regimes from different parts of the MSD, as illustrated in Figure 2.8. The results of β computed for selected lipid atoms (N, P, C15, C2, C at tail's ends) at different time scales are reported in Table 2.2. The results corroborate the choice and denomination of the three relevant time scales.

To characterize the dynamics of lipids at the different time-scales we have computed lateral diffusion coefficients D_L of selected lipid atoms (N,

Table 2.3: Effective and real diffusion coefficients of atomic species in lipids (in 10^{-7} cm^2/s) obtained at different time scales. *Ballistic* corresponds to the 0.1 ps time scale, *sub-diffusive* corresponds to the 0.3 ns time scale and *Fickian* has been obtained at the 150 ns time scale.

Atom	$D_{ballistic}$	$D_{sub-diffusive}$	$D_{Fickian}$
N	92	4.30	0.65
P	48	2.84	0.61
C15	120	5.05	0.66
C2	105	2.18	0.61
C (at tail's end)	121	8.8	0.65

P, C15, C2 and C at tail's ends), given by

$$D_L = \lim_{t\to\infty} \frac{< |\vec{r}_i(t) - \vec{r}_i(0)|^2 >}{4t}. \tag{2.4}$$

Full results of diffusion coefficients of lipids are reported in Table 2.3, where we have separated results corresponding to the three time scales indicated above, obtained from different parts of the time-dependence of the MSD of selected lipid sites. We refer to them as *diffusion* coefficients, although real diffusion is only achieved at the longest time scale and in the two shorter time scales we can only compute *effective* diffusion coefficients, which will provide valuable information on the rapidity of atomic motions.

In the sub-picosecond time scale (between 1 fs and 0.1 ps, part (a) of Figure 2.8) β ranges between 1.92 and 1.96, indicative of ballistic motion (see Table 2.2). In that regime we observe fast motion of all atoms in the lipids, with effective diffusion coefficients of the order of 10^{-5} cm^2/s (see Table 2.3). This is an indication of flow-like ballistic diffusion, with all atoms acting as free inertial particles. We note that atoms belonging to the same lipid can move up to 2.5 times faster than others, e.g. tail carbons (C214 and C314) compared to phosphorus. In between, carbons at lipid heads (C15) tend to move at rates of $\sim 120\times10^{-7}$ cm^2/s.

At a longer time scale (range between 0.01 and 10 ns, part (b) of Figure 2.8), the so-called *sub-diffusive* regime[46], we obtain different values for the effective diffusion coefficient, of the order of $\times 10^{-7}$ cm^2/s. In this regime the MSD scales with $0 < \beta < 1$, see Eq.2.3. We obtained values for β between 0.49 for carbons at the final sites of tailgroups and 0.62 for phosphorus or C2. These values are in good agreement with those recently reported by Jeon et al.[79] for several different membranes. In this time scale the dynamics is slower due to interactions of the lipid chains with neighboring ones, although they have not reached a pure diffusive regime yet. Our results for the effective diffusion coefficients range between ~ 2 and 9×10^{-7} cm^2/s. Now the fastest motions are due to carbons located at the lipid tail whereas C2 carbons, close to the center-of-mass of the lipid chain, are the slowest.

Lipid sub-diffusion has been observed in several experiments [80]. The main observation is that MSD can be described by a power law $< \vec{r}^2(t) > \sim A \cdot t^\beta$, with a time dependence of MSD in sub-diffusive time scale ($0 < \beta < 1$) weaker than that in Fickian diffusion, where $\beta \sim 1$. However, the physical mechanisms behind sub-diffusion could be diverse according to specific environments. Models such as continuous time random walk, fractional Brownian motion and the fractional Langevin equation (FLE) have been proposed [81]. Based on extensive molecular dynamics simulations, Jeon et al. [79] showed that sub-diffusion in lipid bilayers can be described by a FLE-type stochastic motion. We see in our simulations that the length scale explored by lipids in the sub-diffusive regime is comparable and slightly over the typical lipid-lipid distance (see Figure 2.8). This suggests that the sub-diffusive regime is reached when a lipid chain crosses a given energy barrier created by the interaction with its nearest neighbors. Lipid bilayer membrane is a crowded environment, where a mobile lipid molecule will be constrained continually by rattling in a cage motion due to its local environment. As a result its effective motion is offset, corresponding to a slower MSD increment, i.e., weaker time depen-

dence. After colliding with environments during a given transient time, a lipid chain will move towards a direction where it will have a chance to surmount the energy barrier and escape from its neighbors' cage. The typical time needed for a lipid to find such a comfortable direction, i.e., a place with lower energy barrier is the intermediate time scale with β observed before the linear MSD is achieved. This interpretation is in overall agreement with previous ones [44].

Finally, full diffusion is practically achieved at the time scale of hundreds of nanoseconds (part (c) of Figure 2.8, where $\beta \sim 1$). In that regime the dynamics of lipids is governed by *Fickian* diffusion, i.e. due to gradients of concentration and not mediated by local, short ranged effects as in the case of the previous regimes. Interestingly, at this time scale, all (selected) atoms in the lipid diffuse at approximately the same rate, with diffusion coefficients between 0.61 and 0.66×10^{-7} cm^2/s. This suggests that lateral diffusion of a lipid chain is the result of its global motion. The diffusion coefficient of atom C2, located next to the center-of-mass of the lipid, $D_L = 0.61\times10^{-7}$ cm^2/s, is in close agreement with the experimental result obtained from FRAP experiments (at 30°C) of 0.59×10^{-7} cm^2/s [82]. In contrast, the diffusion coefficient reported from simulations based on the CHARMM27[18] force field by Flenner et al. [46], 1.46×10^{-7} cm^2/s, is in clear discrepancy with the experimental value. Thus, it seems clear that the CHARMM36 force field accounts better than CHARMM27 for the diffusion of DMPC lipids in bilayer membranes.

To further investigate the diffusive dynamics of lipids at long timescales, we have depicted in Figure 2.9 the time evolution of the displacements of lipid chains pertaining to one single monolayer. The physical features reported here were observed independently for the two lipid monolayers. We tracked three atoms of each lipid chain (C15, C2, C314, located at the lipid head, center and tail, respectively) during different instants of the simulated trajectory (50, 100, 150 and 200 ns). As shown in Figure 2.9, after 50 ns the displacements of all lipid sites considered are already evident.

After 100 ns, longer displacements are seen in all cases, with some indication of the appearance of *nanodomains* or collective local motions, for all classes of particles considered, identified in Figure 2.9 with red ellipses. For longer times, the regions where lipid species move in a concerted way are evident for all sites. At times up to 200 ns, the particles keep moving same way. Within the timescales explored, the direction of the motion of the identified nanodomains seem to be conserved in time, with all three sites (C15, C2 and C314) moving roughly towards the same direction. This is in agreement with the fact that diffusion coefficients are fully equivalent at the Fickian regime (variations smaller than 10%, see Table 2.3).

In summary, we observed that neighboring lipids forming nanodomains move concertedly in a particular direction within the plane of the membrane. This reveals a mechanism of diffusion based on collective flows of a limited number of lipid chains, which results in diffusion coefficients of the order of 0.6×10^{-7} cm^2/s. This conclusion is in overall agreement with the computer simulation's findings of Falck et al. [39] and the QENS data of Busch et al.[40], although in our case the size of the lipid clusters formed is smaller, in the order of 10 lipid chains.

2.3.5 Spectral densities of water and lipid species

In this section we analyze the spectral densities of water oxygens, water hydrogens, as well as of selected atomic sites at the DMPC molecules. Experimental infrared spectra are usually obtained through the absorption coefficient $\alpha(\omega)$ or the imaginary part of the frequency-dependent dielectric constant. These properties are directly related to the absorption lineshape $I(\omega)$, which can be obtained from molecular dynamics simulations[83, 84] in certain cases, as it will be highlighted below.

The spectral density $S(\omega)$ is defined as

$$S_i(\omega) = \int_0^\infty \mathrm{d}t\; C_i(t)\cos(\omega t) \tag{2.5}$$

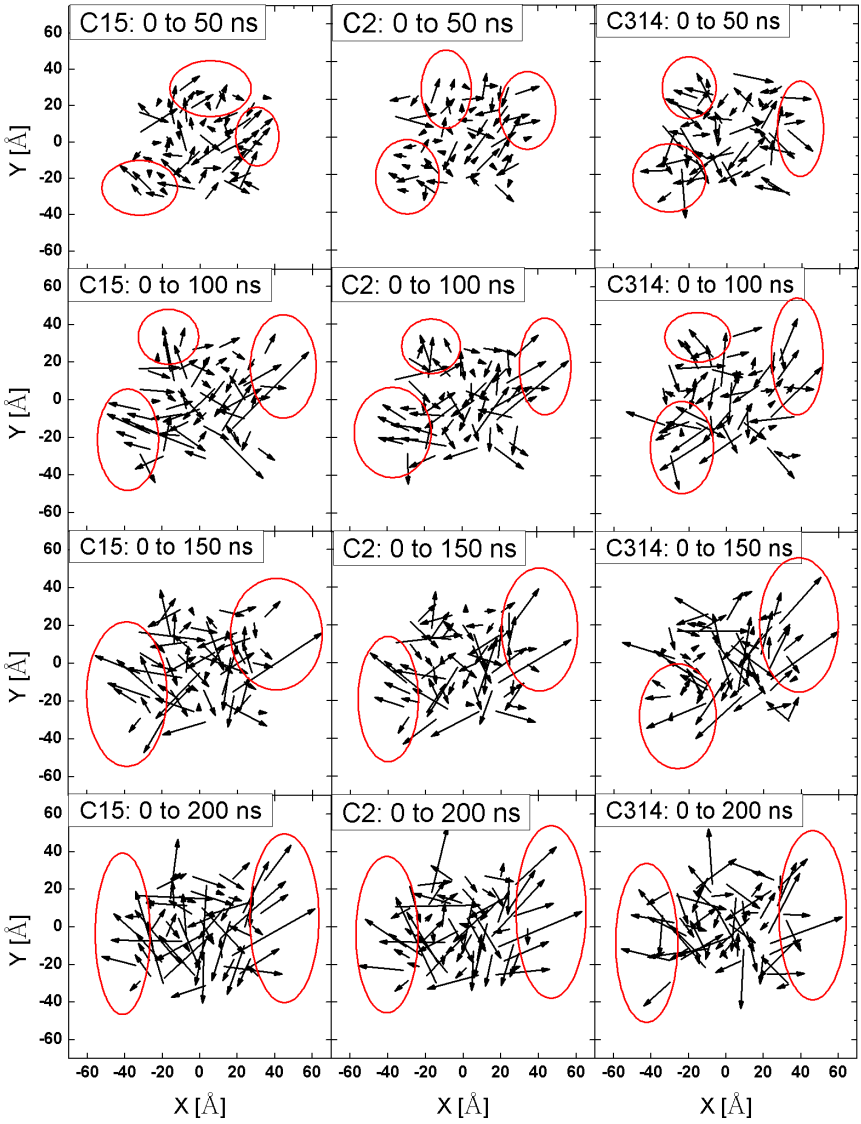

Figure 2.9: Contour plots of lipid displacements as a function of time. The displacements are real, i.e. no periodic boundary conditions have been considered. Some nanodomains have been highlighted with red lines.

where $C_i(t) =< \vec{v}_i(t)\vec{v}_i(0) >$ is the velocity autocorrelation function for atom i. In our case $i = \mathrm{O}_{water}, \mathrm{H}_{water}, \mathrm{H}_{lipid}$, N, P, C2, C15, C27, C214 and C314 (average of the latter two), with the brackets $\langle \cdots \rangle$ denoting equilibrium ensemble average.

In the case of water, it has been shown that $S(\omega)$ is directly related to $I(\omega)$, giving

$$\begin{aligned} I(\omega) =& \frac{1}{2\pi} \int_{-\infty}^{\infty} \mathrm{d}t \ < \vec{M}(t)\vec{M}(0) > \cos(\omega t) \\ =& \frac{1}{\pi\omega^2} \int_{0}^{\infty} \mathrm{d}t \ < \dot{\vec{M}}(t)\dot{\vec{M}}(0) > \cos(\omega t), \end{aligned} \tag{2.6}$$

where $\vec{M}(t)$ is the total dipole moment of water [84]. The final expression has been obtained by repeated integration by parts and using time symmetry. For three-site water models with partial charges (such as the TIP3P model), we can write

$$\dot{\vec{M}}(t) = q \sum_{i=1}^{2N} \vec{v}_{H_i}(t) - 2q \sum_{i=1}^{N} \vec{v}_{O_i}(t) \tag{2.7}$$

where q stands for the effective hydrogen charge, N the total number of water molecules in the system and $\vec{v}_{O_i(H_i)}$ is the velocity of the oxygen (hydrogen) of atom i at time t. Using this expression in Eq.2.6 we obtain terms with self and cross velocity correlation functions. It has been proven[84] that the terms including oxygen velocities have minor influence in the final result of the absorption lineshape and can be neglected, and Eq.2.6 becomes

$$I(\omega) \approx \frac{2Nq^2}{\pi\omega^2} S_{H_{water}}(\omega). \tag{2.8}$$

From Eq.2.8 we see that knowledge of the lineshape $I(\omega)$ can be used to study the motion of water hydrogens. Hence, although classical molecular dynamics simulations are not able to fully reproduce experimental absorption coefficients, these being quantum properties, they can be used

to locate the position of the spectral bands since in the harmonic (oscillator) approximation classical and quantum fundamental frequencies are the same.

We characterize the vibration of the center of mass of water by computing its corresponding spectral density $S_{water}(\omega)$, which is displayed in Figure 2.10. Such spectral densities are directly related with low frequency bands observed at far infrared and Raman spectroscopy measurements of liquid water[85, 86]. The three groups of water molecules defined in section 2.3.2 have been considered. We observe spectral shifts in good qualitative agreement with results obtained for a DPPC membrane[87]. For bulk water, the two main bands in the range of mid-infrared vibrations (experimentally located at 60 and 170 cm^{-1}[88]) are present, the lowest frequency centered at about 35 cm^{-1} and the highest one at around 225 cm^{-1}. For water molecules located next to lipid atoms (intermediate and contact regions) the first low frequency peak blueshifts, whereas the highest frequency band remains unchanged. In addition, for water in close contact with lipid sites, the signature of hydrogen-bonding shows a marked tendency to disappear. The first peak is usually related to hindered vibrations of a water molecule in the cage of its nearest neighbors (*rattling* in a cage), whereas the band centered around 200 cm^{-1} is associated to stretching vibrations of hydrogen-bonds [89]. The disappearance of this second peak seems to suggest that water molecules in contact with lipid sites tend to form a lower number of hydrogen-bonds.

The spectral density corresponding to the water's hydrogens, directly related to the absorption linewidth of radiation (see Eq.2.8), is shown in Figure 2.11. In the spectra, three regions need to be distinguished: one for frequencies up to 1000 cm^{-1} (librational motions), a second one for frequencies between 1000 and 2000 cm^{-1} (bending motions), and a third spectral band between 2000 and 4000 cm^{-1} (stretching motions). We observe in Figure 2.11 that stretching vibrations of water reveal a broad band centered at $\approx$3360 cm^{-1}, formed by two maxima at 3320 and 3375 cm^{-1}.

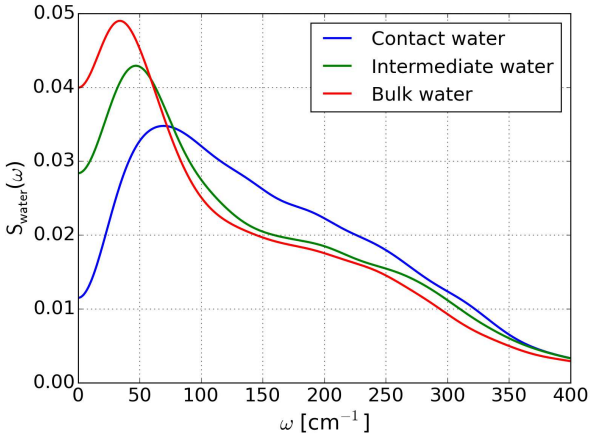

Figure 2.10: Spectral densities $S_w(\omega)$ of water's center-of-mass.

These results are in good overall agreement with very recent FTIR findings by Disalvo and Frias[90], who observed maxima at 3300 and 3550 cm^{-1} for water in DMPC at 25 °C, what indicates that our second maximum is underestimated by about 175 cm^{-1}. The location of the bending mode is also overestimated, centered around 1795 cm^{-1} in the present work, being the experimental value[90] of 1700 cm^{-1}. Finally, librations are fairly well reproduced, with maxima around 455 cm^{-1}. This agrees well with experimental information available for pure water[91], which indicates the existence of a broad band associated to librations between 300 and 900 cm^{-1}. From the results shown in Fig.2.11, we see that hydrogens pertaining to water molecules close to lipid chains (contact water) show the same bending and stretching vibrations as bulk water, but at the librational region, associated to molecular rotations, a neat blue shift of $\sim$ 90 cm^{-1} is observed. In contrast, water located between 3 and 6 Å of lipid sites (intermediate) shows the same frequency vibrations as bulk water for all three bands.

Vibrations of hydrogens pertaining to lipid chains exhibit significant

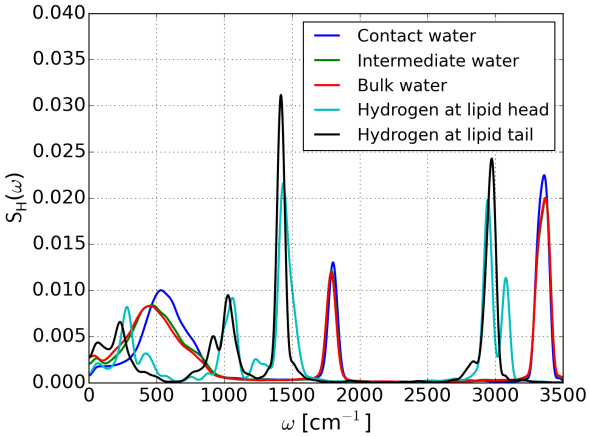

Figure 2.11: Hydrogen spectral densities $S_H(\omega)$ for lipid and water species.

changes when compared with those of water hydrogens, revealing that molecular motions of hydrogens in lipid chains are significantly slower than those in water: firstly, the high-frequency stretching band is centered around 3000 cm^{-1} and split into two contributions for hydrogens pertaining to lipid heads (2945, 3080 cm^{-1}). This vibration should correspond to CH_3 choline (C-H) stretch vibrations, as we will explain below. This is excellent agreement with findings of Pohle et al. [92] and Binder [93]. Secondly, a very intense band around 1430 cm^{-1} is observed and it should be attributed to the bend of internal CH angles[93]. Further, a band of smaller intensity around 1000 cm^{-1} is also observed and, as we will discuss below, it can be directly attributed to vibrations of carbon units. From the experimental side, Hübner and Mantsch[94] who analyzed phosphatidylcholine multilayers by means of FTIR spectroscopy, attributed this band to vibrations of N-$(CH_3)_3$ units, reported around 970 cm^{-1}. In other experiments, Binder et al.[93, 95] employed infrared linear dihcroism spectroscopy to assign a band around 970 cm^{-1} again to the asymmetrical stretch of CN-$(CH_3)_3$ units. Finally, a libration band is now located

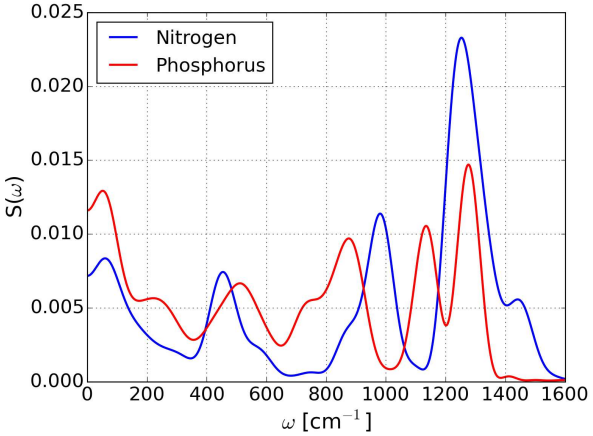

Figure 2.12: Spectral densities of nitrogen and phosphorus atoms.

around 230-280 cm^{-1}. Remarkably, the values obtained in the present work for lipid hydrogen vibrations are in very good agreement with theoretical data [96] obtained by means of density functional conformational analysis of DMPC membranes.

We have also considered vibrations of other particles pertaining to lipid chains, such as nitrogen, phosphorus and a variety of carbons. The results are reported in Figure 2.12 and 2.13. As expected, the frequency range for N and P is shorter than that of hydrogens, now ranging from 0 to 1600 cm^{-1}. Three different frequency domains may be defined: (1) at low frequencies, $\omega < 300$ cm^{-1}, restricted translational motions are described; (2) in the range of $400 < \omega < 800$ cm^{-1}, librational motions, including those around dihedral angles as well as slow vibrational modes are involved; (3) for $800 < \omega < 1600$ cm^{-1}, faster vibrational modes, related to bending and stretching along molecular bonds.

The spectral densities of nitrogen and phosphorus reported in Figure 2.12 reveal restricted *rattling-in-a-cage* vibrations for both particles (around 50-60 cm^{-1}) and librational peaks around 460 and 520 cm^{-1}, respectively.

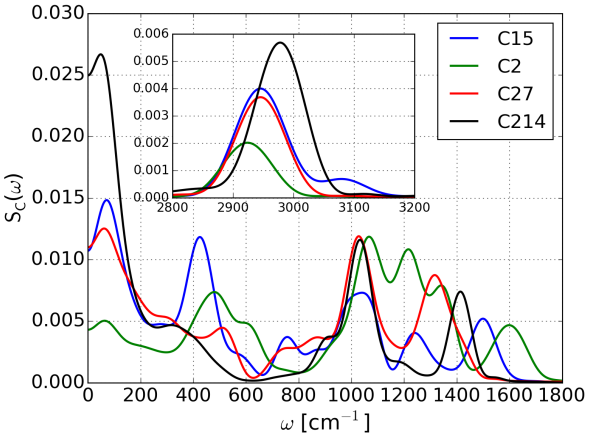

Figure 2.13: Carbon spectral densities $S_C(\omega)$. The inset shows the range of highest frequencies, around 3000 cm^{-1}, of small relative intensity.

This suggests a N-P collective vibrational motion of the full headgroup. At higher frequencies, some significant differences arise, indicating that atomic motions of N and P are not directly related. Nitrogen shows a vibration at 980 cm^{-1} that can be associated with the mode obtained around 1000 cm^{-1} for hydrogens (see Figure 2.11) and attributed to vibrations of N-(CH_3)$_3$ units (see above). Two additional maxima for N are observed around 1250 and 1450 cm^{-1}. Both should obviously be related to CH_3-N-CH_2 vibrations, since we found evidence of those bands in the C15 spectrum (Figure 2.13), but located at 1240 and 1490 cm^{-1}. In the same frequency range, we found a $\sim$ 875 cm^{-1} frequency peak for P that might be associated to the asymmetric $P-(OC)_2$ stretching motions observed by Binder around 800-830 cm^{-1} [93, 95]. At even higher frequencies other two vibrational motions of $O-PO_2-O$ units are seen: one at 1135 cm^{-1} and another one around 1280 cm^{-1}, assigned to the symmetric and asymmetric stretch of $O-PO_2-O$ units[94, 95], respectively. Other authors

(Kozak et al.[45]) found a single maximum around 1209 cm^{-1}, associated to a PO_2^- stretching mode. The numerical agreement of our data with experimental data of Hübner and Mantsch[94] and with Binder et al. [93, 95] is quite remarkable.

Finally, spectral densities of carbons are reported in Figure 2.13. Four carbon sites at the lipid chains have been selected: C15, C2, C27 and C214 at the head, body center, central part of tails and tail's end of DMPC, respectively. In this case, four frequency domains can be distinguished: (1) $\omega < 300$ cm^{-1} (restricted translations) all of them in the range of 45-75 cm^{-1}, i.e. slightly higher than those reported for N and P; (2) $300 < \omega < 900$ cm^{-1} (molecular librations), (3) $900 < \omega < 1800$ cm^{-1} (low frequency vibrations of molecular groups) and (4) $2800 < \omega < 3100$ cm^{-1} (high frequency vibrations of molecular groups). In domain (1) the usual hindered translations are seen in all cases; in domain (2) we can observe two prominent peaks around 425 and 490 cm^{-1} for C15 and C2 but no clear vibrations of tailgroup carbons are seen. Following this, rotation of lipids may be attributed to librational motions of the headgroups (including C2) in motions which are essentially independent of those performed by tailgroups. Density functional calculations by Krishnamurty et al.[96] showed the existence of frequencies in this domain, which were assigned to symmetric deformation modes involving oxygen and carbon units.

In contrast, vibrations in domains (3) and (4) can be related to experimental findings. In the main Figure 2.13 we can distinguish two groups of vibrations: one at frequencies around 1000-1200 cm^{-1} and another one for values in between 1315 and 1600 cm^{-1}. For the two cases, all classes of carbons are involved. Vibrations at the lowest frequencies have been related to the motion of phosphorus as well as to the so-called *wagging* motions of CH_2 and CH_3 chains[92, 96, 97], whereas at the highest frequencies the bands have been attributed to bending motions of CH_2 groups (located around 1450 cm^{-1}) and to C=O stretching vibrations[96, 97]. From our

findings, we observe that all spectra considered (including carbon sites not shown, such as C22, C24, C26, C28, C210 and C212) show the two vibrational features, indicating that they can be related to stretch modes along C-C directions (range of highest frequencies) and also bend of C-C-C and C-N-C units. Finally, vibrations around 2950 cm^{-1} assigned to CH_3 choline (C-H) stretch are also observed for carbons and presented in the inset of Figure 2.13. There we can observe that carbons at the end of tailgroups show stretching frequencies around 2975 cm^{-1}, i.e. slightly blue-shifted from those of the rest of carbon units. Interestingly, these frequencies have been assigned to vibrations of "head" (CH_3) and "neck" (CH_2) groups [92, 93], assignments which are in excellent qualitative agreement with our present interpretation.

2.3.6 Low frequency vibrations of lipid tails and reorientational motions

Among the frequency ranges explored in the present work, perhaps the less known is the one related to low frequency vibrations, up to 100 cm^{-1}, which corresponds to slow motions of parts of the lipid chains. In such range we expect to observe restricted translational motions of few atomic units and also signatures of collective displacements of a group of particles. To further explore the lowest frequency range, we have analyzed the slow motions of lipid tails, and computed reorientational correlation functions and their corresponding characteristic decay times.

A detailed analysis of lipid tailgroup motions has been performed through the calculation of velocity autocorrelation functions (VACF) of the center-of-mass (CoM) of each tail $\vec{v}_{\mathrm{CoM}}$ (labeled "total" in Figure 2.14). To provide further insight into the librational motion of the lipid tails, we decomposed $\vec{v}_{\mathrm{CoM}}$ into its parallel (called "in-plane") and perpendicular (called "normal") components to the instantaneous plane of the lipid. This

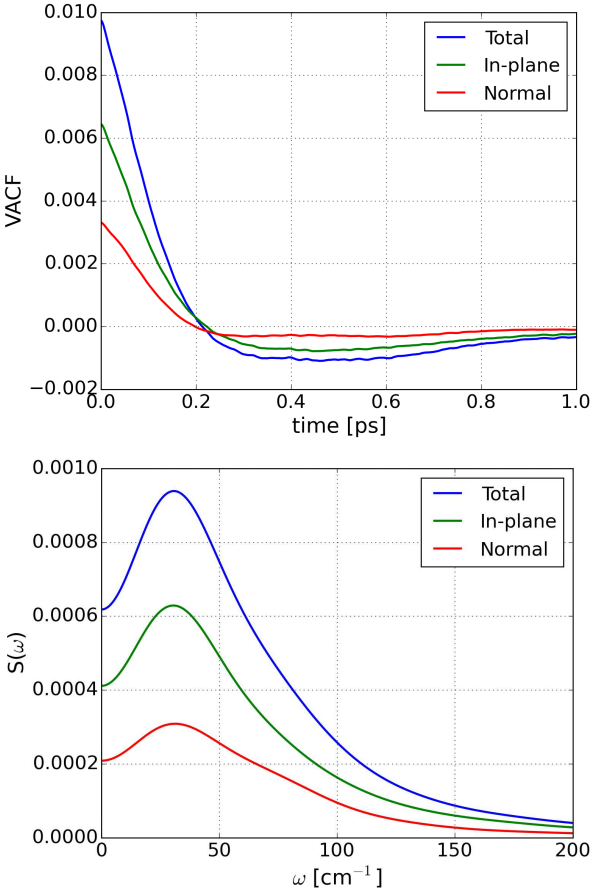

Figure 2.14: Velocity autocorrelation functions of single tail's center-of-mass (CoM) and their spectral densities. The velocities of the CoM of lipid tails (black lines) have been projected on: (1) the instantaneous plane formed by the two lipid tails (red line); (2) the direction normal to the instantaneous plane indicated above (green line).

plane is defined by the vectors

$$\begin{aligned}\vec{T_1}(t) &\equiv \vec{r}_{tail1\ CoM}(t) - \vec{r}_{C2}(t),\\ \vec{T_2}(t) &\equiv \vec{r}_{tail2\ CoM}(t) - \vec{r}_{C2}(t),\end{aligned} \tag{2.9}$$

where $\vec{r}_{tail1(2)\ CoM}(t)$ is the instantaneous position of the center of mass of tail 1 (2) of a lipid and $\vec{r}_{C2}(t)$ is the position of carbon C2. The perpendicular direction is defined by $\vec{N} \equiv \vec{T_1} \times \vec{T_2}$. The results for the VACF of the velocity of the center of mass of lipid tails, as well as of its in-plane and normal components are shown at the top plot of Figure **??**. As it can be directly observed from the non-normalized VACF, the largest contribution is that of the in-plane component. The spectral densities of formed VACF are reported at the bottom of Figure 2.14. We note that a 30 cm^{-1} peak appears in all three spectra, being a new feature not observed in the previous spectral densities of Figure 2.12, 2.13. Directly from our analysis, we believe that this is a clear indication that tailgroups perform "wagging" motions of low frequency, composed by motions along the in-plane direction, with some smaller component along the normal direction.

We have also analyzed the orientation and reorientation dynamics of some relevant directions of the lipid, namely (a) P-N, (b) C21-C31, (c) C2-CoM of lipid tails and (d) the normal direction to the instantaneous plane formed by lipid tails. In Figure 2.15 we show the angular distribution for each direction with the bilayer normal direction (Z). Additionally, following previous works[44, 98, 99, 100, 101, 102], we computed the reorientational correlation functions

$$C_2(t) =< P_2[\hat{u}(0) \cdot \hat{u}(t)] >, \tag{2.10}$$

where $P_2(x)$ is the second Legendre polynomial and $\hat{u}(t)$ is the unit vector along the selected directions. We considered a double exponential to fit the decay of $C_2(t)$, with characteristic times τ_1 and τ_2. The results for the reorientational times are summarized in Table 2.4. We observe that the

Table 2.4: Reorientational times of selected vectors in lipids (in ns).

Vector	τ_1	τ_2
P-N	0.3	2.4
$C2 - CoM_{tails}$	1.5	8.3
C21-C31	0.8	6.4
Normal to tails' instantaneous plane	1.1	6.0

decay of the P-N vector is the fastest. The direction C21-C31 (roughly normal to the C2-tails' CoM) is the second fastest, whereas the two remaining vectors show the slowest decay times. These results are in good agreement with those obtained by Patra et al.[100].

A detailed inspection of such angular distributions can be performed considering angular variations of each selected direction with respect to its initial orientation at a given time (regardless of its orientation from the bilayer normal), considering time intervals of lengths τ_1 and τ_2. We obtained that at the scale of τ_1 (short reorientational times), the angle formed by each vector fluctuates around low values (around 15-20° related to its initial orientation), whereas at the τ_2 time scale (long reorientational times), the distribution of angular variations spreads out significantly, with maxima up to 40° for the P-N direction, covering almost the full angular range. In summary, at the scale τ_1 unit vectors fluctuate narrowly and when they reach the τ_2 time scale, their orientations fluctuate to a wide range of values.

2.4 Conclusions

A series of molecular dynamics simulations of a fully hydrated DMPC lipid bilayer membrane in its liquid-disordered phase has been performed using the recently parameterized CHARMM36 force field. The system is described in atomic detail and molecules are held together with flexible

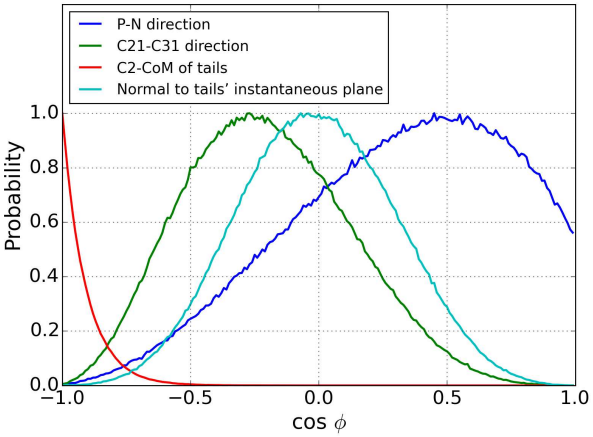

Figure 2.15: Angular distributions of unit vectors **u** along selected directions. ϕ are the angles formed by **u** and the Z-axis. P-N direction (black line), C21-C31 direction (red line), C2-CoM of lipid tails (green line), direction normal to the instantaneous plane of the lipid tails (blue line).

bonds.

Using this description, a surface area per lipid of 60.5 $Å^2$ is obtained after a 30ns equilibration in the NPT ensemble, in good agreement with the experimental value of 60.6 $Å^2$. From the pressure profile along the lipid bilayer we obtain the surface tension of the membrane to be of -0.1±1.2mN/m, close to the expected value of zero. Other structural properties obtained from our description, such as the density profiles or the deuterium order parameter, are in good agreement with experimental and simulation works.

Diffusion of lipids in the membrane and of its hydration water has also been considered. Three regions were defined for water: "bulk" water (more than 6 Å away from the position of any lipid site), "intermediate" water (between 3 and 6 Å of any lipid sites), and "contact" water (within 3 Å of any lipid sites). We found that water molecules located close to lipid

sites diffuse about one order of magnitude slower than those at intermediate and bulk-like regions. Lipid lateral diffusion is one of most challenging properties to obtain, since it requires long simulation runs, of the order of hundreds of nanoseconds. In the present work, we studied diffusion at different time scales, from the sub-picosecond time scale (ballistic motions) to the scale of hundred nanoseconds (Fickian diffusion). In between, we found a sub-diffusive regime (range between 0.01 and 10 ns), where lipid diffusion is about 2-9$\times 10^{-7}$ cm^2/s. In this regime, particles at the lipid headgroup move significantly faster than those located at the body center and slower than those at tailgroups. In the longest time scale analyzed in the present work, lateral diffusion of lipid chains is essentially Fickian, as the result of a global motion of each lipid chain. In this regime we obtained a diffusion coefficient of 0.61×10^{-7} cm^2/s, very close to the experimental result obtained from FRAP experiments of 0.59×10^{-7} cm^2/s[82]. Regarding the mechanism of lipid diffusion at long timescales, we have identified the existence of nanodomains in which the dynamics of lipids is strongly correlated, creating concerted local lipid flow in particular directions, in overall agreement with previous works[39, 40]. The typical length of displacement of a nanodomain can be of 2 nm after 100 ns; they are formed by less than 10 lipid units.

We have also performed a thorough analysis of the spectroscopic properties of the lipid membrane and its hydration water by calculating the spectral densities of the corresponding atomic velocity autocorrelation functions. Our analysis gives some clues to interpret the location of frequency maxima experimentally observed in these systems using different spectroscopic techniques. Overall, our results for lipid atoms are in good agreement with available experimental data [92, 93, 95, 94, 97] measured by means of FTIR spectroscopy, mostly concerning vibrational modes of CH_2 and CH_3 units, as well as a variety of motions mediated by oxygen, phosphorus and nitrogen. From our analysis we also obtain vibrational modes related to $N-P$ vibrations and located around 500 cm^{-1}. The

spectroscopic properties of hydration water are also well accounted for by our simulations, reproducing the three vibrational bands observed in experiment[90, 91]. We also obtain the spectral band related to the motion of the center of mass of water at low frequencies, in agreement with far infrared and Raman spectroscopy measurements [85, 86]. The effect of the interaction with the lipids on the spectroscopic properties of hydration water is also studied, resulting in the blueshift of certain bands for water molecules in contact with the lipid membrane.

A detailed analysis of lipid reorientations and slow motions has revealed the existence of a low frequency band around 30 cm^{-1} that can be assigned to wagging of the tail vibrations which are motions of the tailgroups along the instantaneous plane formed by the two tails of each lipid. In addition, we have analyzed the reorientation dynamics of lipid tails, which can be characterized by two time-scales.

3 Specific Ion Binding at Phospholipid Membrane Surfaces

Metal cations are ubiquitous components in biological environments and play an important role in regulating cellular functioning and membrane properties. By applying metadynamics simulations, we have performed systematic free-energy calculations of Na^+, K^+, Ca^{2+}, and Mg^{2+} bound to phospholipid membrane surfaces for the first time. The free-energy landscapes unveil specific binding behaviors of metal cations on phospholipid membranes. Na^+ and K^+ are more likely to stay in the aqueous solution, and can easily bind to a few lipid oxygens by overcoming low free-energy barriers. Ca^{2+} is most stable when bound to four lipid oxygens of the membranes, rather than being hydrated in the aqueous solution. Mg^{2+} is tightly hydrated, and can hardly lose a hydration water and bind directly to the membranes. When bound to the membranes, the cations' most favorable total coordination numbers with water and lipid oxygens are the same as their corresponding hydration numbers in aqueous solution, indicating a competition between ion binding to water and lipids. The binding specificity of metal cations on membranes is then highly correlated with the hydration free-energy and the size of the hydration shell.

3.1 Introduction

Specific ion effects on biological systems have drawn great attention during last decades [103]. In general, specific effects for cations are less pronounced than those for anions when ion-water interactions are dominant[104]. However, for biological membranes in physiological environments, the interactions between metal cations and charged lipid headgroups are also essential and significant. Metal cations bound to membranes have been found to regulate membrane properties and membrane functioning, and such regulations deeply depend on the ion specificity [105, 106]. Therefore, the understanding of specific interactions of metal cations with membranes is of great fundamental importance.

Several experiments suggest that metal cations are bound to the phosphate and carbonyl regions of phospholipid membranes [107, 108, 109, 110]. While bound to membranes in aqueous solution, a hydrated metal cation will lose one or more water molecules from its first hydration shell, resulting in several possible bound configurations [111, 112]. Although the binding constant and Gibbs free-energy of metal cation can be estimated from experiments [111], detailed studies of the relative stabilities of different bound states are difficult. Molecular dynamics (MD) simulations have been widely employed to investigate the role of metal cations in solvated phospholipid membranes from an atomic point of view [112, 113, 114, 115, 116, 117, 118, 110]. Nevertheless, the theoretical study of ionic binding to membranes is a computationally demanding task due to the long simulation times required to probe ion-membrane association and dissociation events. In addition, various bound configurations are separated by high free-energy barriers, making it difficult for MD simulations to sample them adequately [25]. Free-energy calculations using enhanced sampling techniques provide a method to address the problem. However, despite the significant progress of free-energy calculations achieved in recent years [119], to the best of our knowledge, the binding free-energy landscape of

metal cations on membrane surfaces is still missing. This is partially due to the difficulty of applying appropriate sampling techniques to address the problem, and also because of the complexity of the membrane environments, making the determination of the proper collective variables a difficult challenge [120].

In this work, we have performed a systematic free-energy calculation of the binding states of metal cations at phospholipid membrane surfaces. The specific interactions of biologically relevant cations Na^+, K^+, Ca^{2+}, and Mg^{2+} with membranes are revealed and interpreted from a free-energy perspective. The competition between ion-water and ion-membrane binding is also studied. Although such competition has been discussed before [114, 116], here we provide for the first time a quantitative free energy characterization of the relevant ion binding states to water and lipids. Our work provides a general methodology to explore the free-energy landscapes for ions at complex biological interfaces which can be extended to study other interactions of interest between ions and charged headgroups in colloidal chemistry and biology [121].

3.2 Methods

3.2.1 System setup and equilibration

Four sets of lipid bilayer systems were generated by CHARMM-GUI [122, 123] to study the binding of biologically relevant cations Na^+, K^+, Ca^{2+}, and Mg^{2+} at neutral zwitterionic phospholipid membranes. Each system consisted of 50 DMPC lipid molecules [124, 125], 2500 TIP3P water molecules [48], a metal cation, and one or two Cl^- anions to neutralize the system.

Each membrane system was equilibrated for 100 ns in the NPT ensemble at 1 atm and 303 K. MD simulations for equilibration were performed using NAMD 2.9 [50] and the CHARMM36 force field [17]. A time step of 2 fs was

used. Covalent bonds with hydrogen atoms of lipids were kept rigid using SHAKE [126], and water molecules were kept rigid using SETTLE [127]. The particle mesh Ewald method was employed to compute long-range electrostatic interactions [51]. The cutoff for Lennard-Jones interactions was set to 12 Å, with a switching distance of 10 Å. Pressure was controlled by the Langevin piston Nosé-Hoover method and the ratio of the unit cell in the x-y plane was kept constant [128]. Temperature was controlled by the Langevin dynamics with a damping coefficient of 1 ps^{-1} [55].

3.2.2 Collective variables

Applying proper enhanced sampling methods and defining proper collective variables (CVs) are essential for the success of free-energy calculations. Recently, Jämbeck et al. showed that missing an essential CV in the construction of free energy profiles for membrane partitioning of solute can lead to divergences on the permeability of solute.[129] While the normal direction to the plane of the membrane, Z, has been typically adopted as the reaction coordinate for the calculation of solute partitioning [129, 130] and ionic permeation [131, 132], the problem of ion binding to membranes is more complex. Membranes are composed of a large number of lipid molecules with numerous conformations, and each lipid molecule has several binding sites at its headgroup, making it a challenge to define proper CVs to describe the interaction between ions and membranes. Moreover, ions are hydrated by water molecules, and the hydration level depends on the locations of ions at the membrane surfaces. Therefore, considering the interactions between ions and both lipid and water molecules could be a rational way for CV definition. A number of experiments [107, 108, 109, 110] and simulation works [112, 113, 114, 115, 116, 117, 118, 110] have shown that metal cations directly coordinate with the oxygen atoms of phosphate (PO_4^-) and carbonyl (C=O) groups of lipid molecules, indicating that the oxygens in the lipid headgroup are the binding sites for metal cations. Accordingly, in this work we defined two CVs to describe the ion-membrane

binding: the coordination number between a metal ion and lipid oxygens (CLP), and the coordination number between a metal ion and water oxygens (CWT).

The coordination number [133] is defined by

$$s = \sum_{i \in G_1} \sum_{j \in G_2} s_{ij}, \tag{3.1}$$

where s_{ij} is a differentiable switching function defined as

$$s_{ij} = \frac{1 - (\frac{|\mathbf{r}_i - \mathbf{r}_j| - d_0}{r_0})^6}{1 - (\frac{|\mathbf{r}_i - \mathbf{r}_j| - d_0}{r_0})^{12}}. \tag{3.2}$$

For CLP, G_1 is the metal ion, G_2 is all the lipid oxygens. For CWT, G_1 is the metal ion, G_2 is all the water oxygens. The values of d_0 and r_0 were determined from the radial distribution function g(r), which was calculated from unbiased simulations on membrane systems containing 128 DMPC lipids, 6400 water molecules, 46 metal ions, and 46 or 92 Cl^- ions (corresponding to the ionic concentration of 0.4 M). d_0 is the position of the first peak of g(r), and r_0 is the width at half maximum of the peak. The determination of the parameters for coordination number, i.e. d_0 and r_0, is essential for the accuracy of the resulting free-energy surfaces. An example on choosing d_0 and r_0 for CLP of Na^+ is given in Figure 3.1. The values for d_0, r_0, and other parameters are listed in Table 3.1.

The determination of d_0 and r_0 for CLP of Na^+ is described in Figure 3.1. The radial distribution function g(r) of lipid oxygens with respect to Na^+ is normalized and shown as the blue lines in all the subplots. The switching function s_{ij} (Eq. 3.2) with $d_0 = 2.3$, $r_0 = 0.25$ is shown as the red line in Figure 3.1a. Figure 3.1b is a close look on the first coordination shell of Figure 3.1a. The peak of g(r) is located at $d_0 = 2.3$, and the width at half maximum of the peak is $r_0 = 0.25$. The first minimum of g(r) is at $r = 2.9$. If we only set $r_0 = 2.9$ and don't consider d_0 (keep $d_0 = 0$ as default), then s_{ij} (green line in Figure 3.1c) will cover g(r) outside the first

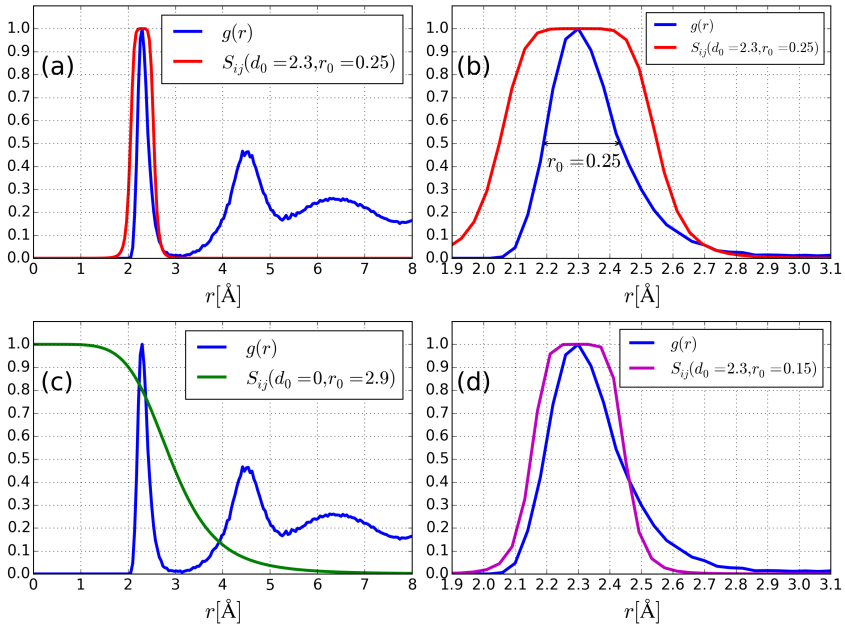

Figure 3.1: The determination of d_0 and r_0 for CLP of Na^+.

minimum from $r = 2.9$ to $r = 6.0$. In this case, the lipid oxygens outside the first coordination shell of Na^+ ($2.9 < r < 6.0$) still contribute to s_{ij} and are counted into CLP, which can overestimate CLP. If we set $d_0 = 2.3$, but $r_0 = 0.15$, then s_{ij} (purple line in Figure 3.1d) can't completely cover g(r) within $2.6 < r < 2.9$. In this case, some of the lipid oxygens inside the first coordination shell of Na^+ ($2.6 < r < 2.9$) are not counted into CLP, which can underestimate CLP. Overall, by setting $d_0 = 2.3$ and $r_0 = 0.25$ (red line in Figure 3.1b), the lipid oxygens inside the first coordination shell of Na^+ are accurately counted into CLP, which determines the accuracy of the resulting free-energy surfaces.

Table 3.1: Simulation parameters

Parameter	Na^+	K^+	Ca^{2+}	Mg^{2+}
d_0 of CLP[Å]	2.3	2.64	2.12	1.85
r_0 of CLP[Å]	0.25	0.32	0.12	0.13
d_0 of CWT[Å]	2.35	2.7	2.24	1.95
r_0 of CWT[Å]	0.25	0.36	0.22	0.18
Gaussian width of CLP	0.2	0.2	0.2	0.2
Gaussian width of CWT	0.2	0.2	0.2	0.2
Starting hill [kcal/mol]	0.3	0.3	0.5	0.5
Deposition stride [ps]	1	1	1	1
Bias factor	5	3	20	15
Simulation time [ns]	800	800	800	100

3.2.3 Well-tempered metadynamics simulations

Well-tempered metadynamics [31], a variant of metadynamics [29, 25] capable of enhancing the sampling of coordination numbers in multiple CV dimensions, was employed to calculate the free-energy landscape of ion binding to the membrane. Four sets of two-dimensional (2D) well-tempered metadynamics simulations based on the above CVs were performed to calculate the free-energy surfaces of Na^+, K^+, Ca^{2+}, and Mg^{2+} ions at neutral zwitterionic phospholipid membranes. After equilibration for 100 ns in the NPT ensemble as described above, 1000 ns well-tempered metadynamics simulations were performed on each system in the NVT ensemble. All the simulations were performed using NAMD 2.9 [50] together with PLUMED2 plugin [134] and the CHARMM36 force field [17]. The simulation parameters are described in Table 3.1.

Metadynamics [29, 25] is a powerful enhanced sampling method. In metadynamics simulations, an external history-dependent bias potential is constructed in the space of a few selected CVs. This potential is built as a sum of Gaussians deposited along the system trajectory in the CV space to push the system away from local free-energy minima that have already been sampled. In standard metadynamics simulations, the height

of Gaussian is kept constant along the simulations, and the resulting free-energy calculated from the bias potential oscillates around the underlying free-energy landscape. In well-tempered metadynamics [31, 25], the height of Gaussian is decreased along the simulations, and the bias potential converges more smoothly to the underlying free-energy landscape, provided that the bias factor is sufficiently high for the relevant free-energy barriers to be crossed. Therefore, bias factor should be carefully chosen in well-tempered metadynamics.

In general, for a barrier of the order of $\triangle G$, a feasible choice for the bias factor is $\gamma \approx \frac{\triangle G}{2k_{\mathrm{B}}T}$. As shown in Table 3.1, we choose different bias factors for different ions. Indeed, for each ion, we have tried several bias factors in short runs and checked if they are sufficiently high for the relevant free-energy barriers to be crossed. The bias factors listed in Table 3.1 are those sufficiently high for the ions (except Mg^{2+}) to cross the free-energy barriers between bound and unbound states, and at the same time not too high in order to avoid visiting very high free-energy CV space. Using a too high bias factor very high free-energy CV space are visited, which slows down the free-energy convergence. Take K^+ as an example, when setting the bias factor $\gamma = 5$, we observe the visit to the high free-energy states with CLP=9 or CWT=11, and the convergence is slower than setting $\gamma = 3$.

3.3 Results

The resulting 2D free-energy surface (FES) of Na^+ bound to DMPC membranes is shown in Figure 3.2. A staircase pattern is present in the FES. The Na^+ ion is considered to be in the aqueous solution at CLP = 0, where it can be hydrated by at most 8 water molecules. When it is fully dehydrated (CWT = 0), Na^+ can be bound to at most 7 lipid oxygens. Between these two extreme cases, Na^+ is bound to oxygens of both water and lipids. The fact that the states at local free energy minima are those with integer numbers of CLP and CWT validates our choice of CVs

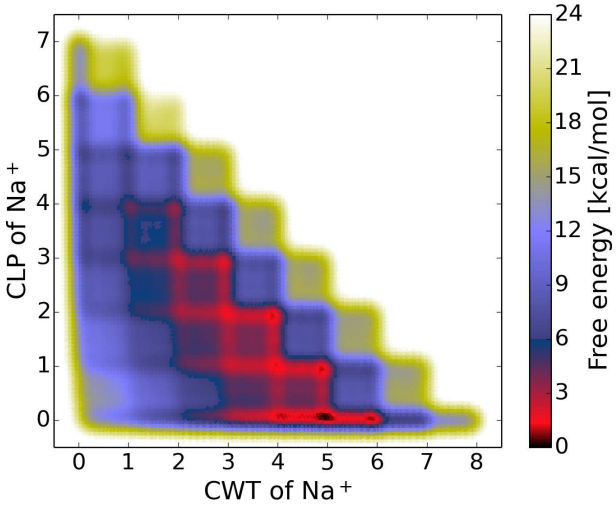

Figure 3.2: Free-energy surface as a function of the coordination number of water oxygens (CWT) and the coordination number of lipid oxygens (CLP) for Na^+.

to explore the binding processes. The pattern shown in Figure 3.2 is a consequence of the competition between the binding of the ion to lipids and to water. Indeed, paths of approximately the same binding free energy are found for integer values of CLP and CWT with the same total coordination number (CLP+CWT). The global minimum of the FES is at the (CWT=5, CLP=0) state, revealing that being hydrated by 5 water molecules in the aqueous solution is the most favorable state for Na^+. When Na^+ is bound to the membranes, the stable bound states are located in the region with CLP$\in [1, 4]$ and CWT$\in [1, 5]$ with the total coordination number (CLP+CWT)$\in [4, 6]$. A representative snapshot of a bound state of Na^+ coordinated with 6 oxygens is shown in Figure 3.5a.

Similar patterns are also present in the 2D FES of K^+ in Figure 3.3, revealing similar binding behaviors of K^+ and Na^+ at aqueous membrane interfaces. Because of a larger atomic size, K^+ has a larger first coordina-

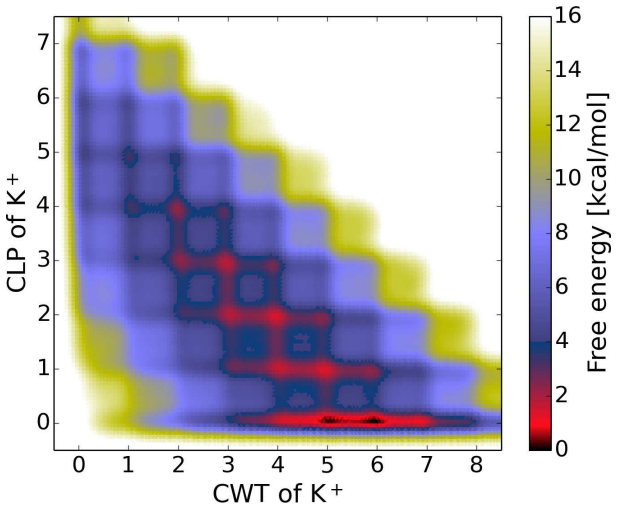

Figure 3.3: Free-energy surface as a function of CWT and CLP for K^+.

tion shell but a relatively lower surface charge density. The global minima states are at (5, 0) and (6, 0). Therefore, being hydrated by $5 \sim 6$ water molecules in the aqueous solution is most favorable for K^+. When bound to membrane surfaces, K^+ can be coordinated to more water oxygens and lipid oxygens than Na^+. The stable bound states for K^+ are in the region with CLP$\in [1, 4]$ and CWT$\in [2, 6]$ with the total coordination number (CLP+CWT)$\in [5, 7]$.

While staying in the aqueous solution is most favorable for the monovalent metal cations, i.e. Na^+ and K^+, being bound to the membrane surfaces is most stable for Ca^{2+}. The global free-energy minimum at (2, 4) in Figure 3.4 indicates that Ca^{2+} is preferably bound to 4 lipid oxygens (see Figure 3.5b), rather than being hydrated in the aqueous solution. In contrast to the stable bound states of Na^+ and K^+ with CLP$\in [1, 4]$, those for Ca^{2+} are located in the region with CLP$\in [2, 6]$, which suggests a significantly greater affinity of Ca^{2+} to lipid oxygens than that of monovalent metal cations.

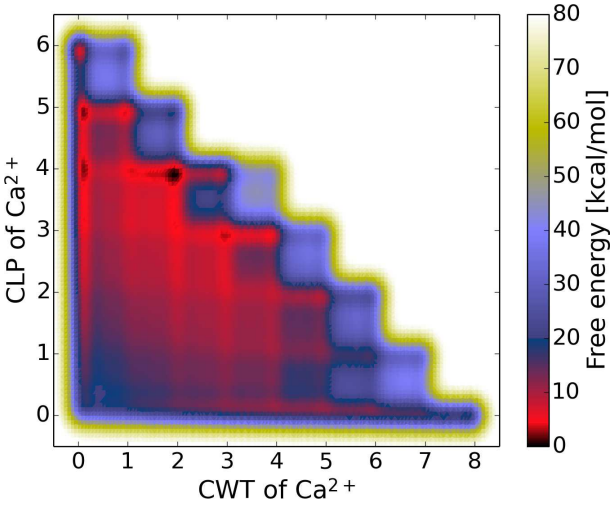

Figure 3.4: Free-energy surface as a function of CWT and CLP for Ca^{2+}.

The case of Mg^{2+} is different from the other ions considered. The bound states of Mg^{2+} to lipid oxygens (CLP≥1) are separated from the unbound states in the aqueous solution (CLP = 0) by high free-energy barriers, and could not be appropriately sampled by our calculations. This is attributed to the high energy required for partial dehydration of the first hydration shell of Mg^{2+}, which is shown in Figure 3.9, where only the case with CLP = 0 is considered. The strong binding of Mg^{2+} to its hydration layer has been also reported recently by Allnér et al. They calculated the potential of mean force between Mg^{2+} and water oxygens and that between Mg^{2+} and phosphate oxygens, and showed extremely high free-energy barriers for water dehydration and direct phosphate binding [135].

The quantitative representations of the above FES are given in Figure 3.6, 3.7, and 3.8, where the free-energies are plotted as a function of CWT at various CLP, and in Table 3.2, where the most relevant binding states are selected. As shown in Figure 3.6, several hydration free-energy basins have been found for CLP = 0, where Na^{+} is unbound to mem-

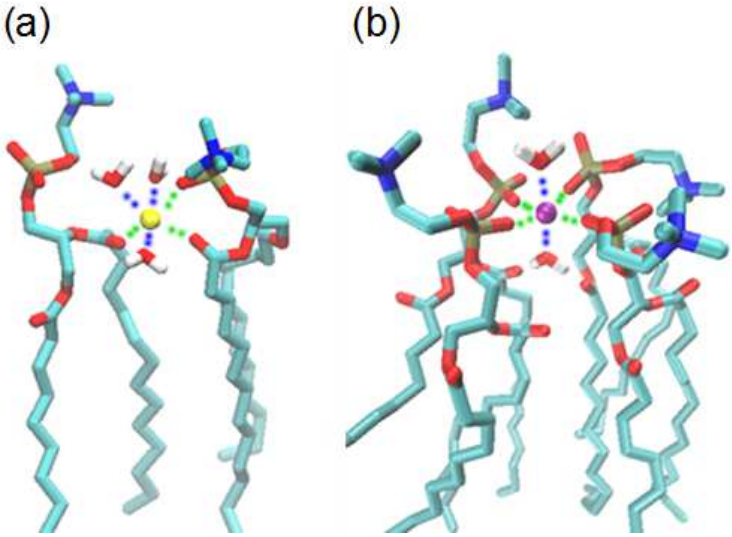

Figure 3.5: (a) A representative bound state for Na^+ coordinated to 3 lipid oxygens and 3 water molecules. (b) The most stable bound state for Ca^{2+} coordinated to 4 lipid oxygens and 2 water molecules. Na^+ is in yellow and Ca^{2+} is in purple. The binding to lipid oxygens and to water oxygens are shown in green and blue respectively.

branes. The most stable hydration state for Na^+ is the hydration with 5 water molecules, in agreement with the hydration number measured by experiments [136, 137]. The ion is considered bound to the membrane when CLP > 0. For Na^+ at low binding, i.e. for CLP = 1, 2, 3, the corresponding minimum free-energies are located at hydration levels CWT = 4, 3, 2, respectively, being 5 the total coordination number, which is the same as experimental hydration number [136, 137]. At high binding, i.e. for CLP = 4, 5, 6, the most stable hydration levels are CWT = 2, 1, 0, respectively, being 6 the total coordination number. The states with CLP = 1, 2, 3 and total coordination number of $5 \sim 6$ are the lowest free-energy

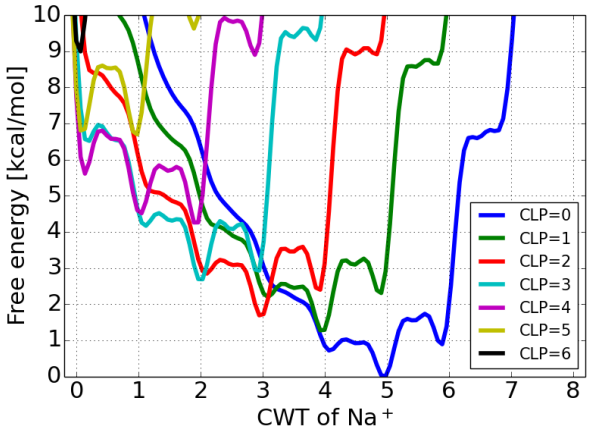

Figure 3.6: Free-energy as a function of CWT at various CLP for Na^+. The data are extracted from Figure 3.2.

bound states, which are $1 \sim 2$ kcal/mol higher than the global minimum at CLP = 0. A quantitative characterization of the free-energies of those states is given in Table 3.2. Consequently, those are the most likely bound states of Na^+ that one is expected to find in a DMPC membrane immersed in a NaCl aqueous solution.

As shown in Figure 3.7, the profiles for K^+ are similar to those for Na^+. The hydration with 5 or 6 water molecules is most stable for K^+ at CLP = 0, in agreement with the experimental hydration number [136, 137]. Free-energy barriers constraining K^+ at the stable hydration states (CWT = 5, 6) are smaller than those for Na^+ (CWT = 5), indicating a weaker affinity for water molecules of K^+. At low binding, i.e. for CLP = 1, 2, 3, the corresponding minimum free-energies are located at hydration levels CWT = 5, 4, 3, respectively, resulting in a total coordination number of 6, which is the same as the experimental hydration number of K^+ [136, 137]. Note that the free-energy barriers for the lowest energy bound states of K^+ are also smaller than those for Na^+, indicating an easier release from

Table 3.2: Free-energies for the lowest states of Na^+, K^+, and Ca^{2+} with respect to the global minimum.

ion	binding state			F[kcal/mol]
	CLP	CWT	CLP+CWT	
Na^+	0	5	5	0.0
	1	4	5	1.28
	2	3	5	1.69
	3	2	5	2.69
K^+	0	6	6	0.0
	0	5	5	0.11
	1	5	6	1.23
	2	4	6	1.46
	3	3	6	1.78
	4	2	6	2.26
Ca^{2+}	4	2	6	0.0
	4	0	4	2.07
	5	0	5	2.74
	3	3	6	3.13

lipid binding sites.

Although being hydrated in aqueous solution (CLP=0) is the most favorable state for Na^+ and K^+, for Ca^{2+} that state is ~ 16 kcal/mol higher than the global minimum, as shown in Figure 3.8. This shows that staying in the aqueous solution is greatly unfavorable for Ca^{2+} compared to being bound to the membranes. In aqueous solution, the most stable hydration states for Ca^{2+} are CWT = 6, 7, consistent with experimental hydration number [138, 139]. The most stable bound state for Ca^{2+} is at (CWT = 2, CLP = 4), where the total coordination number is 6. Other stable bound states are at CLP = 3, 4, 5 with total coordination number of $4 \sim 6$, which are $2 \sim 4$ kcal/mol higher than the global minimum (see Table 3.2). These bound states are also the global minima of the FES, which are $12 \sim 16$ kcal/mol lower than the lowest energy unbound states at CLP = 0. For Ca^{2+}, we obtain a significantly stronger binding to phospholipid membranes over aqueous solution than for Na^+ and K^+ where the binding is

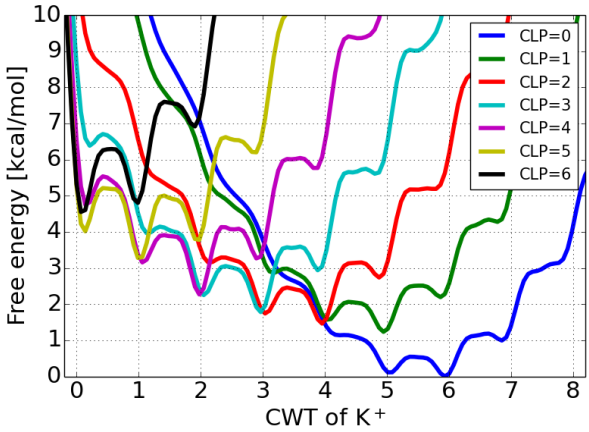

Figure 3.7: Free-energy as a function of CWT at various CLP for K^+. The data are extracted from Figure 3.3.

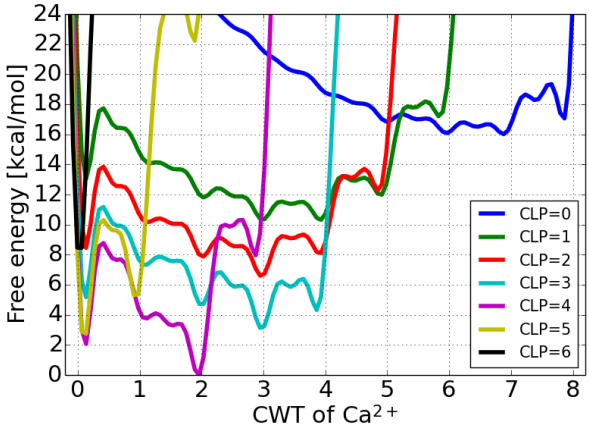

Figure 3.8: Free-energy as a function of CWT at various CLP for Ca^{2+}. The data are extracted from Figure 3.4.

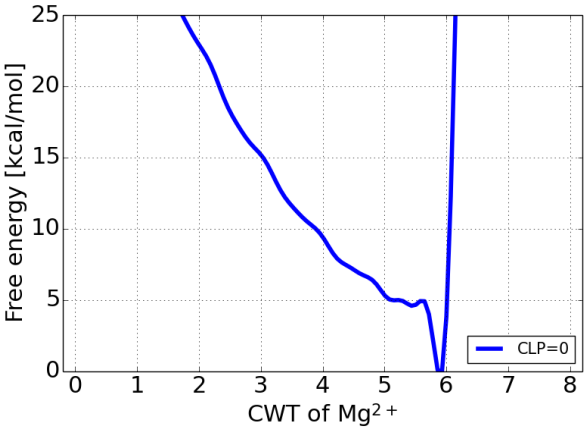

Figure 3.9: Free-energy as a function of CWT for Mg^{2+}. Only the case with CLP = 0 is considered.

weak, in agreement with experiment [109]. For the ions considered, the ion binding free-energy has its minimum at the same total coordination number (CLP+CWT), irrespective of CLP or CWT, as shown in Table 3.2 and Figure 3.10, and coincides with the hydration number in solution. This is a clear indication of the competition between ion binding to water and lipids, and is responsible for the correlation between ion hydration and ion binding specificity at the membranes.

Figure 3.9 shows that in aqueous solution the hydration with 6 water molecules is the most stable state for Mg^{2+}, in accordance with experiments [138, 139]. However, in contrast to the other cations which in solution have several hydration free-energy basins, Mg^{2+} has only one basin at CWT=6, and the corresponding hydration free-energy barrier is very high ($\sim$ 5 kcal/mol) compared with Na^{+}, K^{+}, and Ca^{2+}. This is due to the strong binding of water molecules to Mg^{2+}, which makes the change of its hydration state to other hydration states (CWT < 6) and bound states (CLP > 0) a rare event phenomenon.

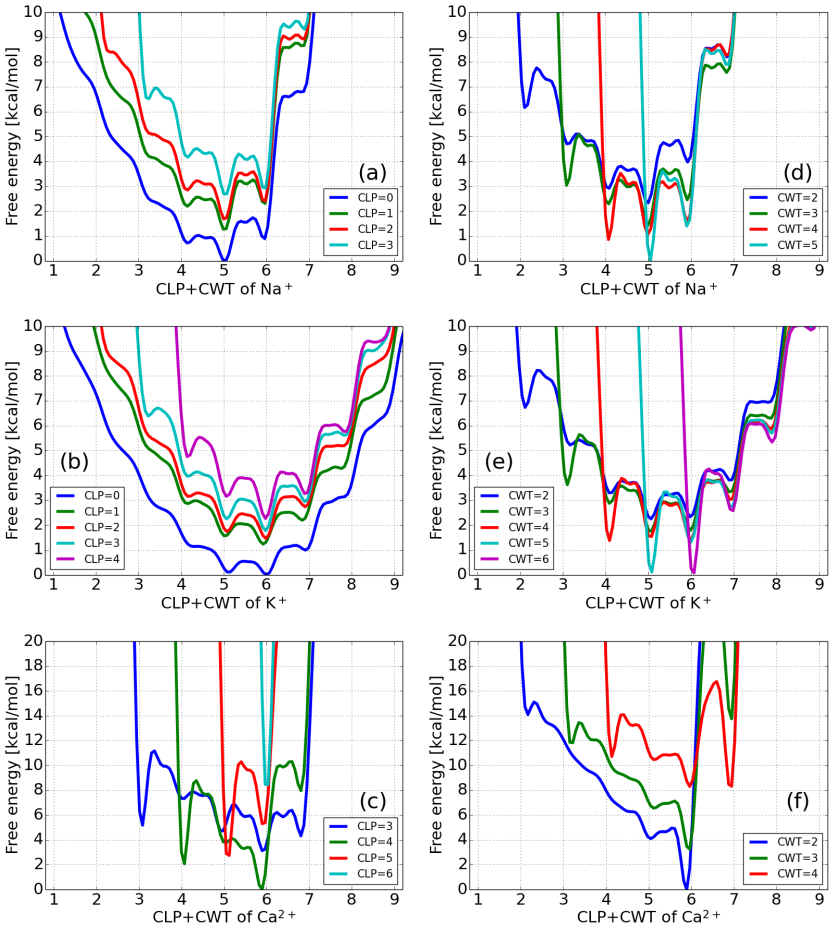

Figure 3.10: Free-energy as a function of total coordination number (CLP+CWT) for Na^+, K^+, and Ca^{2+} at various CLP ((a),(b),(c)) and at various CWT ((d),(e),(f)). The metal ions' most favorable total coordination numbers are 5, 6, and 6 for Na^+, K^+, and Ca^{2+}, respectively. For a given ion, the binding free-energy has its minimum at the same total coordination number, irrespective of CLP or CWT.

3.4 Conclusions

In summary, we have provided a quantitative characterization of the binding states of biologically relevant metal cations (Na^+, K^+, Ca^{2+}, and Mg^{2+}) at DMPC phospholipid membranes. With the help of well-tempered metadynamics simulations we have calculated the free-energies of the binding states, defined by the ion coordination to lipid (CLP) and water (CWT) oxygen atoms. Our results indicate that Na^+ and K^+ are more likely to stay in the aqueous solution, and can easily bind to $1 \sim 3$ lipid oxygens by overcoming free-energy barriers of $1 \sim 2$ kcal/mol. Ca^{2+} is most stable when bound to 4 lipid oxygens of the membranes, and the corresponding bound basin is ~ 16 kcal/mol lower than the unbound states in the aqueous solution. Mg^{2+} has a strong affinity to hydration water, which makes the direct binding to the membranes difficult. When bound to the membranes, the cations' most favorable total coordination numbers with water and lipid oxygens are 5, 6, and 6 for Na^+, K^+, and Ca^{2+}, respectively. Such coordination numbers coincide with their corresponding hydration numbers in bulk, suggesting a competition between ion binding to water and lipids.

3.5 Estimation of free-energy convergence

Figure 3.11 reports the well-tempered metadynamics trajectories of the collective variables. The free-energy convergence is estimated in Figure 3.12 and Figure 3.13.

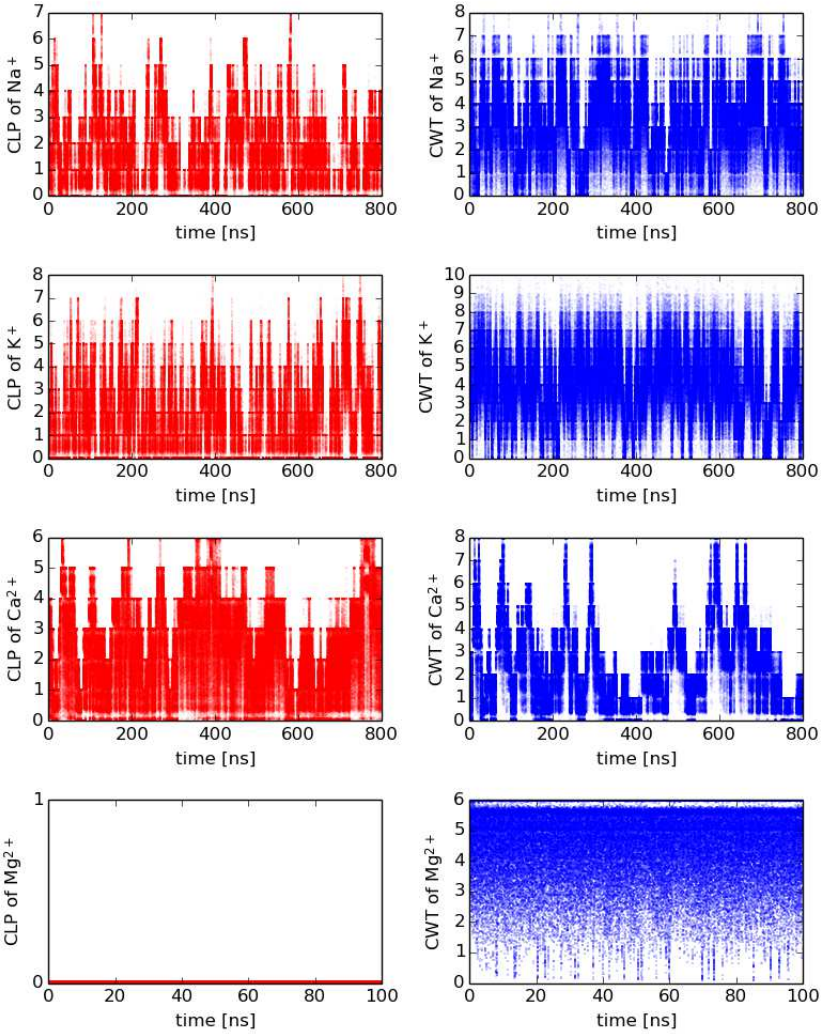

Figure 3.11: Well-tempered metadynamics trajectories of Na^+, K^+, Ca^{2+}, and Mg^{2+}. Left panels, red traces: CLP as a function of time. Right panels, blue traces: CWT as a function of time. The traces of Mg^{2+} show that CLP = 0 during 100 ns, indicating that the bound states of Mg^{2+} to lipid oxygens (CLP$\geq$1) are separated from the unbound states in the aqueous solution (CLP = 0) by high free-energy barriers, and could not be appropriately sampled by our calculations.

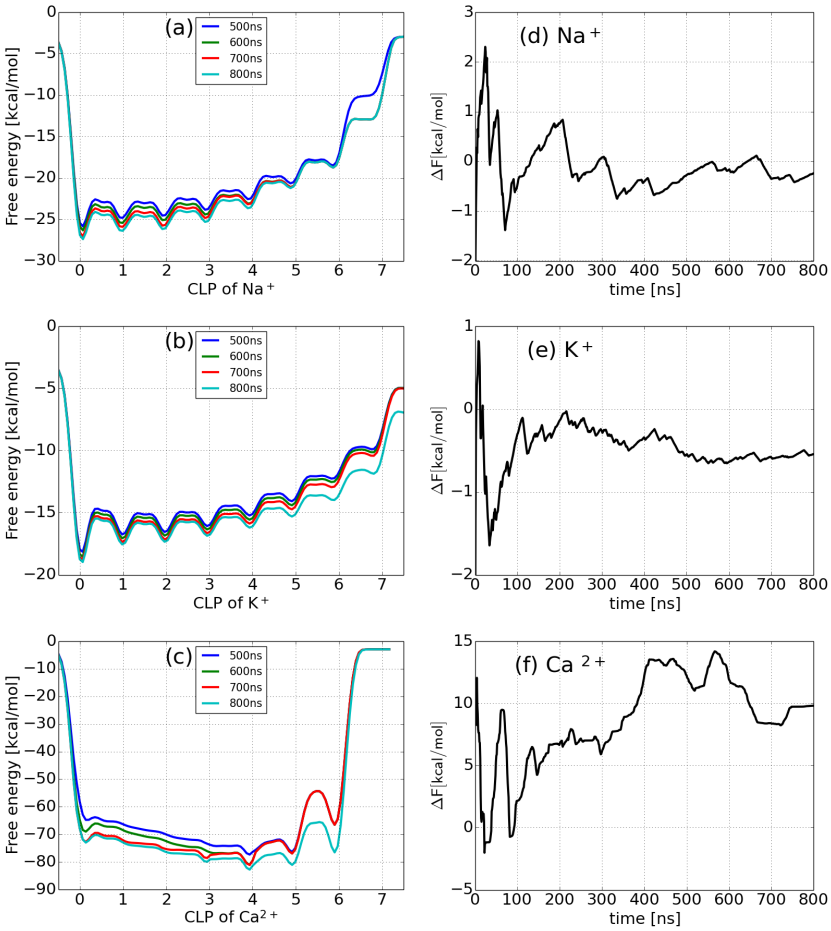

Figure 3.12: We monitor the convergence of the free-energy by projecting the free-energy surfaces on CLP (left panels) and calculating $\triangle$F, the free-energy difference between unbound states (CLP < 0.5) and bound state (CLP > 0.5) as a function of time (right panels). Figure S3(a), (b), and (c) show the projected free-energy as a function of CLP from 500 ns to 800 ns for Na^+, K^+, and Ca^{2+}.

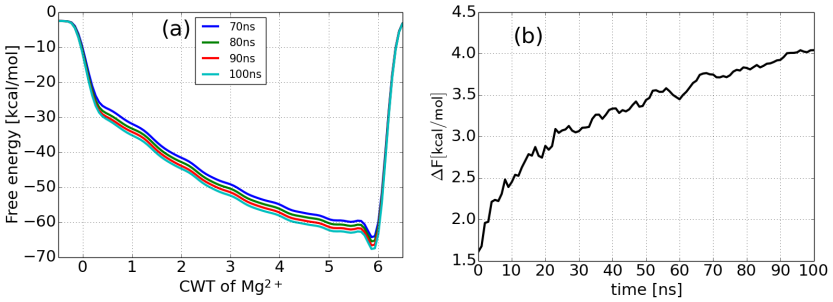

Figure 3.13: For Mg^{2+}, we monitor the convergence of the free-energy by projecting the free-energy surfaces on CWT (a) and calculating $\triangle$F, the free-energy difference between the basin of CWT < 5.5 and the basin of CWT > 5.5 as a function of time (b). Figure S4(a) shows the projected free-energy as a function of CWT from 70 ns to 100 ns.

4 Cholesterol Effects on Na^+ Binding at Phospholipid Membrane Surfaces

Exploring the free-energy landscapes of metal cations on phospholipid membrane surfaces is important for the understanding of chemical and biological processes in cellular environments. Using metadynamics simulations we have performed systematic free-energy calculations of sodium cations bound to DMPC phospholipid membranes with cholesterol concentration varying between 0% (cholesterol-free) and 50% (cholesterol-rich). The resulting free-energy landscapes reveal the competition between binding of sodium to water and to lipid head groups. Moreover, the binding competitiveness of lipid head groups is diminished by cholesterol contents. As cholesterol concentration increases, the ionic affinity to membranes decreases. When cholesterol concentration is greater than 30%, the ionic binding is significantly reduced, which coincides with the phase transition point of DMPC-cholesterol membranes from a liquid-disordered phase to a liquid-ordered phase. We have also evaluated the contributions of different lipid head groups to the binding free-energy separately. The DMPC's carbonyl group is the most favorable binding site for sodium, followed by DMPC's phosphate group and then the hydroxyl group of cholesterol.

4.1 Introduction

The interactions between metal cations and phospholipid membranes have drawn great attention during last decades [105, 106, 140]. Several experiments revealed that metal cations are bound to the negative charged head groups of phospholipid membranes [107, 108, 109, 110]. Meanwhile, numerous molecular dynamics (MD) simulations have been performed to study the binding of metal cations at phospholipid membranes from an atomic point of view [112, 113, 114, 115, 116, 117, 118, 110]. However, most of the experiments and simulation works on ionic binding to phospholipid membranes have been devoted to cholesterol-free environments. Cholesterol is a crucial component in mammalian cell membranes, constituting up to 50% of their weight [6]. Cholesterol can modulate the structural and mechanical properties of membranes and can induce a phase transition from a liquid disordered phase to a liquid ordered phase [7, 141, 8]. Therefore, the study of the binding of metal cations to cholesterol-containing membranes is of interest to understand ionic binding in realistic cellular environments. Only recently, experiments by Iraolagoitia et al. showed that cholesterol significantly reduced the Ca^{2+} binding to membranes [142]. More recently, Magarkar et al. performed both experiments and simulations, revealing that increasing cholesterol concentration decreased Na^{+} binding [143].

The binding of metal cations at membranes in aqueous solution can result in several possible bound configurations, as a consequence of the loss of water molecules and the gain of lipid atoms in the ion's first hydration shell. Exploring the binding processes and bound states of metal cations at phospholipid membrane surfaces is important for the understanding of chemical and biological processes such as binding, hydration, leakage, and dissociation in cellular environments. Nevertheless, a comprehensive study of the relative stabilities of different bound states is a difficult experimental task, and also difficult for classical MD simulations because of the high free-energy barriers among various bound states. To circumvent such difficulty,

free-energy calculations applying enhanced sampling techniques can be applied.

In this work, we have performed a systematic free-energy calculation of Na^+ bound to cholesterol-containing phospholipid membranes of various cholesterol concentrations by applying metadynamics simulations with appropriate collective variables. The resulting free-energy landscapes quantitatively reveal the relative stabilities of different bound states and unveil the cholesterol effects on Na^+ binding to phospholipid membranes.

4.2 Methods

4.2.1 System setup and equilibration

CHARMM-GUI [122, 123] was employed to generate six sets of lipid bilayers with cholesterol concentrations [CHOL] varying between 0 and 50% to study the cholesterol effects on Na^+ binding at phospholipid membrane surfaces. Each system consisted of 72 DMPC / cholesterol molecules, 3600 TIP3P water molecules [48] and a pair of Na^+ and Cl^- described by the CHARMM36 force field [17, 144]. The molar ratios of cholesterol/lipid were set to 0/72 (0%), 8/64 (10%), 14/58 (20%), 22/50 (30%), 30/42 (40%), and 36/36 (50%). Each membrane system was equilibrated for 100 ns in the NPT ensemble at 1 atm and 303 K. MD simulations for equilibration were performed using NAMD 2.9 [50]. A time step of 2 fs was used. Covalent bonds with hydrogen atoms of lipids were kept rigid using SHAKE [126], and water molecules were kept rigid using SETTLE [127]. The particle mesh Ewald method was employed to compute long-range electrostatic interactions [51]. The cutoff for Lennard-Jones interactions was set to 12 Å, with a switching distance of 10 Å. Pressure was controlled by the Langevin piston Nosé-Hoover method and the ratio of the unit cell in the x-y plane was kept constant [128]. Temperature was controlled by the Langevin dynamics with a damping coefficient of 1 ps^{-1} [55].

4.2.2 Collective variables

For membranes in ionic solutions, there exists a competition between ion binding to water molecules and to certain binding sites of phospholipids [114]. Therefore, a bound state can be characterized by the ion's coordination number with lipid binding sites and its simultaneous coordination number with water molecules. A number of experiments [107, 108, 109, 110] and simulation works [112, 113, 114, 115, 116, 117, 118, 110] have indicated that metal cations bind directly to the oxygen atoms of the negative charged phosphate (PO_4) and carbonyl (C=O) groups of lipid molecules. Accordingly, we defined two collective variables (CVs) to describe the ion's bound states: the coordination number between a Na^+ ion and lipid (including cholesterol) oxygens (CLP), and the coordination number between a Na^+ ion and water oxygens (CWT).

The coordination number [133] is defined by

$$s = \sum_{i \in G_1} \sum_{j \in G_2} s_{ij}, \tag{4.1}$$

where

$$s_{ij} = \frac{1 - (\frac{|\mathbf{r}_i - \mathbf{r}_j| - d_0}{r_0})^6}{1 - (\frac{|\mathbf{r}_i - \mathbf{r}_j| - d_0}{r_0})^{12}}. \tag{4.2}$$

The parameters for coordination numbers are taken from the previous work (Table 3.1). For CLP, G_1 is the Na^+ ion, G_2 is all the lipid oxygens (including oxygen atom in cholesterol for cholesterol-containing membranes), $d_0 = 2.3$ Å, and $r_0 = 0.25$ Å. For CWT, G_1 is the Na^+ ion, G_2 is all the water oxygens, $d_0 = 2.35$ Å, and $r_0 = 0.25$ Å.

4.2.3 Well-tempered metadynamics simulations

Six sets of two-dimensional (2D) well-tempered metadynamics [31] based on the above CVs were performed using NAMD 2.9 [50] together with

PLUMED2 plugin [134] and the CHARMM36 force field [17, 144]. After equilibration for 100 ns in the NPT ensemble as described above, 1000 ns well-tempered metadynamics simulations were performed on each system in the NVT ensemble. The Gaussian widths for both CLP and CWT were set to 0.2. The initial Gaussian deposition rate was 0.3 kcal/mol per ps, with a bias factor of 5.

4.3 Results

The resulting 2D free-energy surfaces (FES) of Na^+ bound to DMPC-cholesterol membranes with cholesterol concentrations [CHOL] = 0-50% are shown in Figure 4.1. Na^+ is considered bound to the membranes for CLP > 0 and unbound for CLP $= 0$. There are a number of bound states (CLP > 0) and several unbound states (CLP $= 0$) in each FES, and each state can be indexed by (CWT, CLP). A common feature for all the [CHOL] cases is the global minimum of the FES located at the (CWT=5, CLP=0) state, revealing that the hydration with 5 water molecules in the aqueous solution is most favorable for Na^+. In addition, we observe a staircase pattern in all of the FES, which is the consequence of the ionic binding competition between water and lipids. As [CHOL] increases, the stable bound states (represented by red color in the FES), which are $1 \sim 4$ kcal/mol higher than the global minimum, shift from the region with CLP$\in [1, 5]$ and CWT$\in [0, 5]$ for [CHOL]=0-10% to the region with CLP$\in [1, 4]$ and CWT$\in [1, 5]$ for [CHOL]=20-30%, and further to the region with CLP$\in [1, 3]$ and CWT$\in [2, 5]$ for [CHOL]=40-50%. This visible shifts of stable bound states clearly reveal that the binding competitiveness of lipid head groups has been diminished by cholesterol contents, and that the affinity of Na^+ to DMPC membranes becomes less favorable as cholesterol concentration increases, which is in agreement with experiments [143].

A more quantitative representation of the above results is given in Figure 4.2, where the free-energy as a function of CWT for several integer lipid

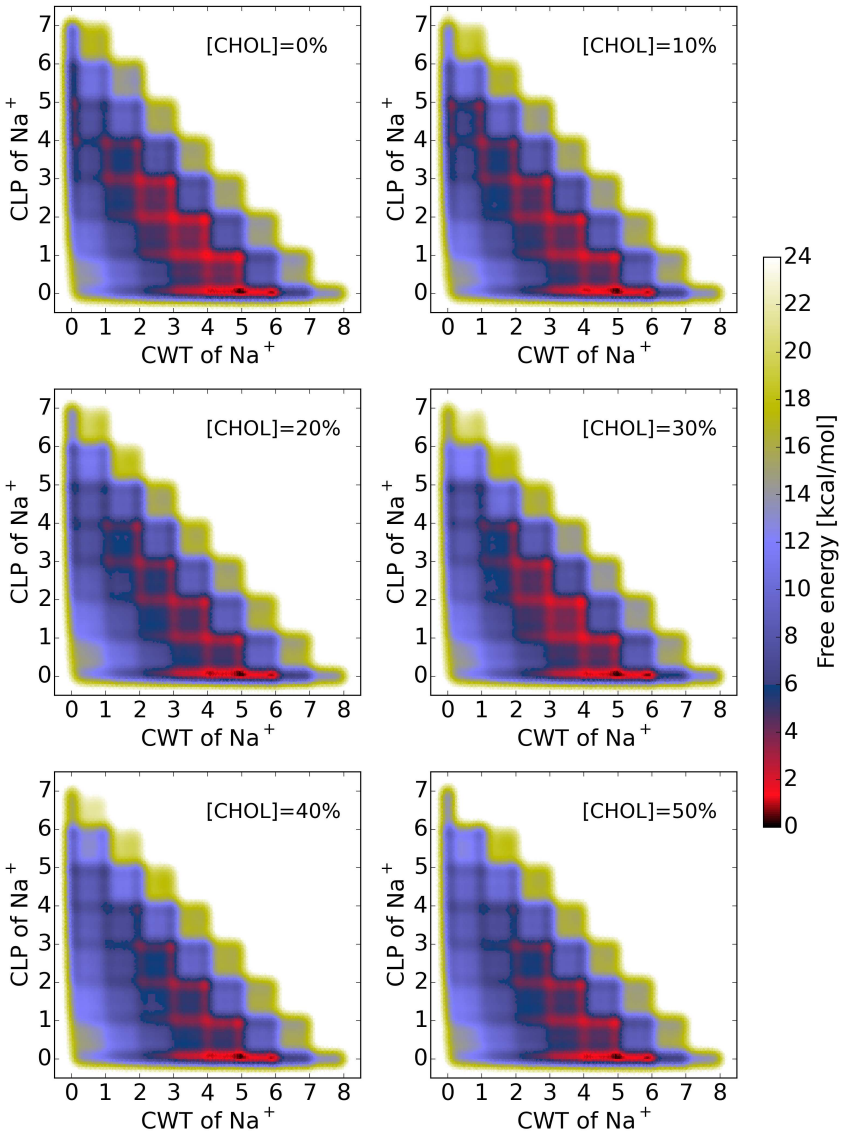

Figure 4.1: Free-energy surface (FES) as a function of the coordination number of lipid oxygens (CLP) and the coordination number of water oxygens (CWT) for Na^+ bound to DMPC membranes with cholesterol concentrations [CHOL] varying between 0 and 50%.

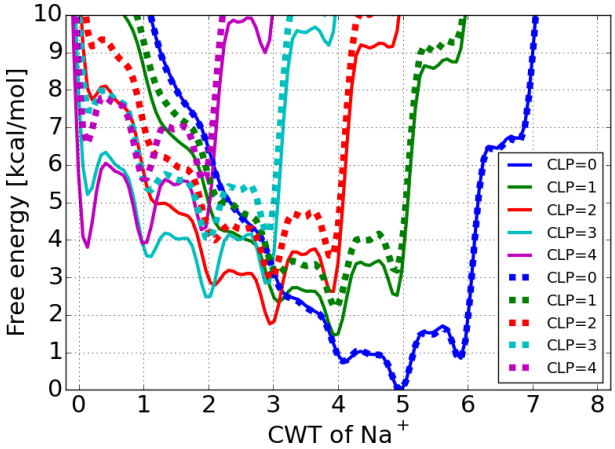

Figure 4.2: Free-energy as a function of CWT at CLP $= 0 - 4$ for Na^+ bound to DMPC membranes with cholesterol concentration [CHOL] of 0% (continuous lines) and 50% (dashed lines). The data are extracted from Figure 1.

binding levels (CLP) is extracted from the FES of Figure 4.1. Here we only represent the two extreme cases of [CHOL] = 0% (continuous lines) and [CHOL] = 50% (dashed lines). For CLP=0, the hydration free-energies of Na^+ unbound to membranes are exactly the same for both [CHOL] cases, indicating that, as expected, the hydration of Na^+ in the aqueous solution is not affected by the content of the membranes. There are several hydration free-energy basins, and the most stable one is coordinated with 5 water molecules, in agreement with the Na^+ hydration number measured by experiments [136, 137]. When bound to the membranes (CLP>0), the curves for the two cases become diverse. For each given CLP, the free-energy profiles for [CHOL] = 50% case increase $1 \sim 2$ kcal/mol compared to the cholesterol-free case ([CHOL] = 0%). Such increase evidences the decrease of Na^+ affinity to a membrane with high cholesterol contents. However, for both [CHOL] cases, the corresponding free-energy minimum for CLP = 1, 2, 3, 4, is located at CWT = 4, 3, 2, 1, respectively, keep-

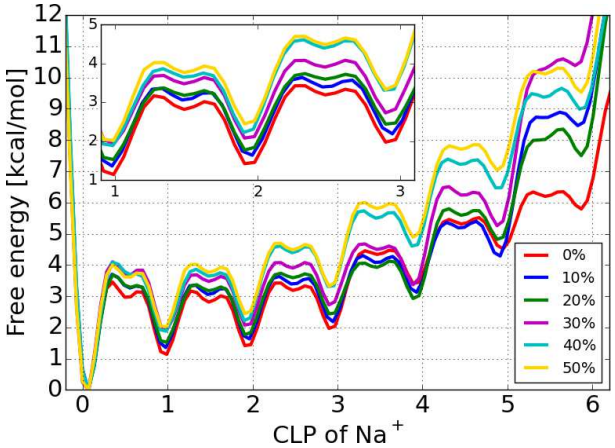

Figure 4.3: Free-energy as a function of the coordination number of lipid oxygens (CLP) for Na^+ bound to membranes with cholesterol concentration [CHOL] varying between 0 and 50%. (Inset) Zoom in the low CLP region.

ing 5 the total coordination number, which is the same as experimental hydration number of Na^+ in aqueous solution [136, 137].

In Figure 4.3, we represent the dependence of the binding free-energy on CLP for membranes with various cholesterol concentrations after integrating out CWT according to

$$F(s_1) = -k_{\mathrm{B}}T \log \int \exp^{-\frac{F(s_1,s_2)}{k_{\mathrm{B}}T}} ds_2, \tag{4.3}$$

where s_1 and s_2 are CVs, k_{B} is the Boltzmann constant, and T is the absolute temperature. As cholesterol concentration increases, the free-energy profiles corresponding to bound states (CLP>0) raise monotonically. To understand these changes, we should remember the well-known condensing effect of cholesterol in lipid bilayers, which produces higher membrane rigidity and ordering [145, 146]. For [CHOL] $\leq$ 20%, there are overlaps of the free-energy profiles at low bound states (CLP ≤ 3), indicating that

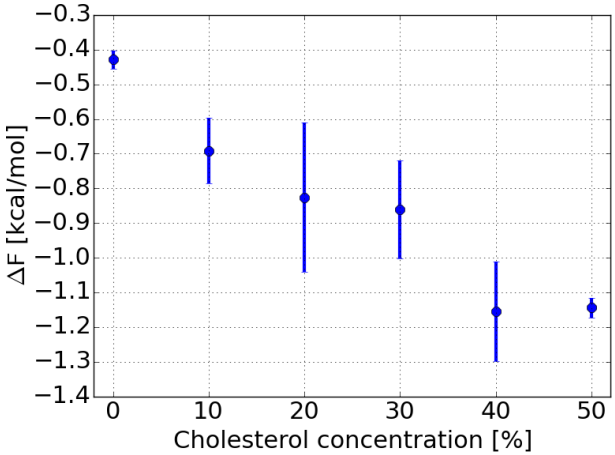

Figure 4.4: Average values and standard deviations of $\triangle$F, the free-energy difference between unbound states (CLP $<$ 0.5) and bound states (CLP $>$ 0.5) for different cholesterol concentrations.

Na^+ is easily bound to the membranes with low cholesterol concentration. When [CHOL] $\geq$ 30%, the ionic binding is significantly reduced (free-energy increases). Such transition in the ionic binding behavior at [CHOL] $\approx$ 30% coincides with the phase transition point of DMPC-cholesterol membranes, in which membranes change from a liquid-disordered phase to a liquid-ordered phase [8].

We monitor the convergence of the FES by calculating $\triangle$F, the free-energy difference between unbound states (CLP $<$ 0.5) and bound states (CLP $>$ 0.5) from the free-energy profiles of CLP as the simulations proceed (see Figure 4.9). The average values and standard deviations of $\triangle$F calculated from the last 100 ns of well-tempered metadynamics simulations are shown in Figure 4.4. The monotonic trend indicates that the energy gap between unbound and bound states increases with the increasing cholesterol concentration, which reduces the affinity of Na^+ to cholesterol-containing membranes. This is in good agreement with the results obtained

from the previous Figures 4.1, 4.2, and 4.3.

The above 2D FES (Figure 4.1) and 1D free-energy as a function of CLP (Figure 4.3) are based on the consideration that all the oxygen atoms from DMPC lipids (i.e. phosphate and carbonyl groups) and cholesterol (hydroxyl group in the polar head) are equivalent binding sites for Na^+. In order to understand the contributions of different head groups separately, we calculate the free-energy as a function of CLP between Na^+ and oxygen atoms from different head groups by applying a reweighting technique [147]. As shown in Figure 4.5, for a given CLP, the binding free-energy follows the order of C=O < PO_4 < -OH. Therefore, C=O is the most favorable binding site for Na^+, followed by PO_4 and then the -OH group of cholesterol. For DMPC binding sites (C=O and PO_4), we observe higher binding free-energy basins and higher binding free-energy barriers for higher [CHOL], which is in accordance with above results obtained when different CLP are considered equivalent. The situation for the CLP between Na^+ and cholesterol is radically different. At low [CHOL] (10%), only 1 cholesterol oxygen can be attached to Na^+. For [CHOL] $\geq$ 20%, it would be possible for Na^+ to bind up to 2 cholesterol oxygens. However, the free-energy barriers for high [CHOL] ($40-50\%$) are lower than those for the medium [CHOL] ($20-30\%$), which is in contrast to the trend observed for DMPC binding sites where higher free-energy barrier corresponds to higher [CHOL].

4.4 Conclusions

We have performed systematic free-energy calculations of Na^+ bound to DMPC-cholesterol membranes by means of well-tempered metadynamics simulations with two collective variables being the ion's coordination number to lipids (CLP) and to water (CWT). The free-energy surfaces reveal the competition between binding of ion to water and to lipids. However, the binding competitiveness of lipid head groups is diminished by

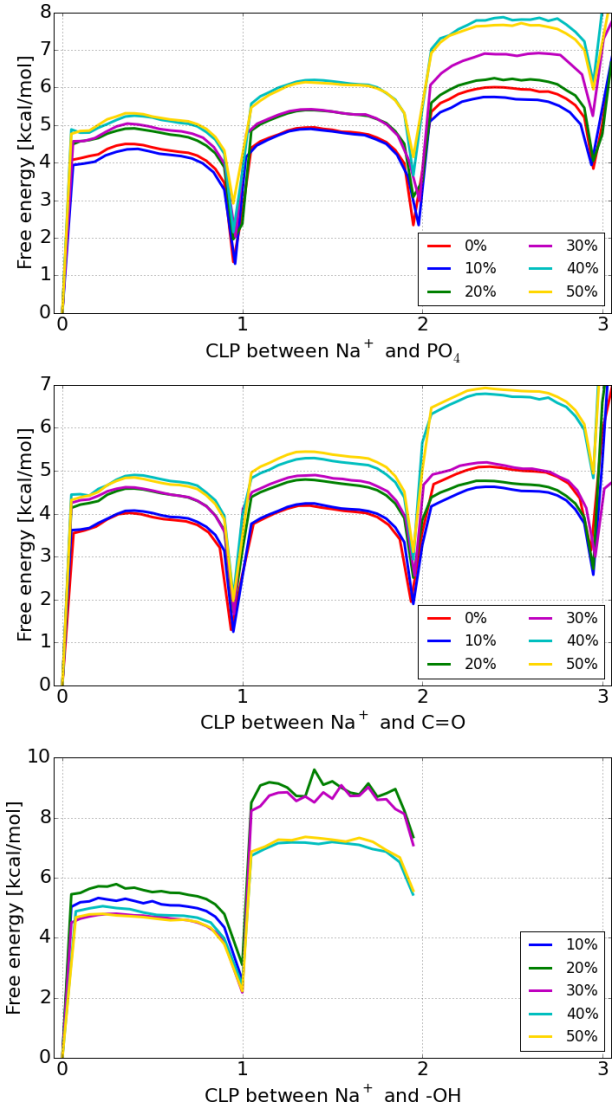

Figure 4.5: Free-energy as a function of CLP between Na^+ and oxygen atoms from different lipid head groups with cholesterol concentration [CHOL] varying between 0 and 50%. The three different lipid head groups are: DMPC's phosphate group PO_4 (top figure); DMPC's carbonyl group C=O (middle figure); and cholesterol's hydroxyl group -OH (bottom figure).

cholesterol contents. As cholesterol concentration increases, the ionic affinity to the membranes decreases, which is in agreement with experiments [142, 143]. When [CHOL] $\geq$ 30%, the ionic binding is significantly reduced. Such transition in the ionic binding behavior at [CHOL] $\approx$ 30% coincides with the phase transition point of DMPC-cholesterol membranes, in which membranes change from a liquid-disordered phase to a liquid-ordered phase. In contrast, the hydration free-energies of Na^+ in aqueous solution are not affected by the cholesterol content of membranes. The most stable hydration for Na^+ with 5 water molecules is in good agreement with experiments. We have also evaluated the contributions of different lipid head groups to the binding free-energy separately. The DMPC's carbonyl group (C=O) is the most favorable binding site for Na^+, followed by DMPC's phosphate group (PO_4) and then the hydroxyl group (-OH) of cholesterol.

The method employed can be widely applied to explore the free-energy landscapes of ions at complex biological interfaces. Furthermore, provided the importance in a variety of biological processes of the interaction of ions and charged interfaces in aqueous solution, our approach could be extended to explore other problems in colloidal chemistry and biology, and could be helpful to deepen our understanding of specific ion effects on soft matter and biological systems.

4.5 Estimation of free-energy convergence

Free-energy convergence is estimated by the diffusion behaviors of CVs (Figure 4.6 and 4.7), decay of HILLS Height (Figure 4.8), and free-energy difference between unbound states (CLP $<$ 0.5) and bound states (CLP $>$ 0.5)(Figure 4.9).

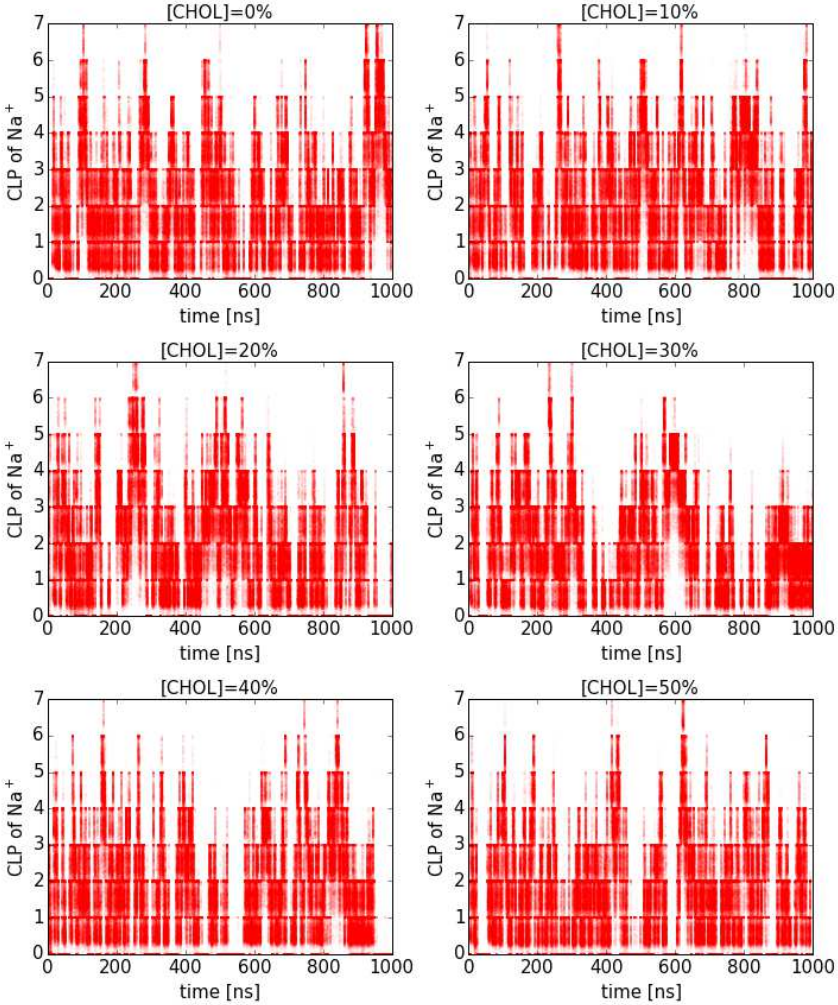

Figure 4.6: Coordination number between a Na^+ ion and lipid (including cholesterol) oxygens (CLP) as a function of time.

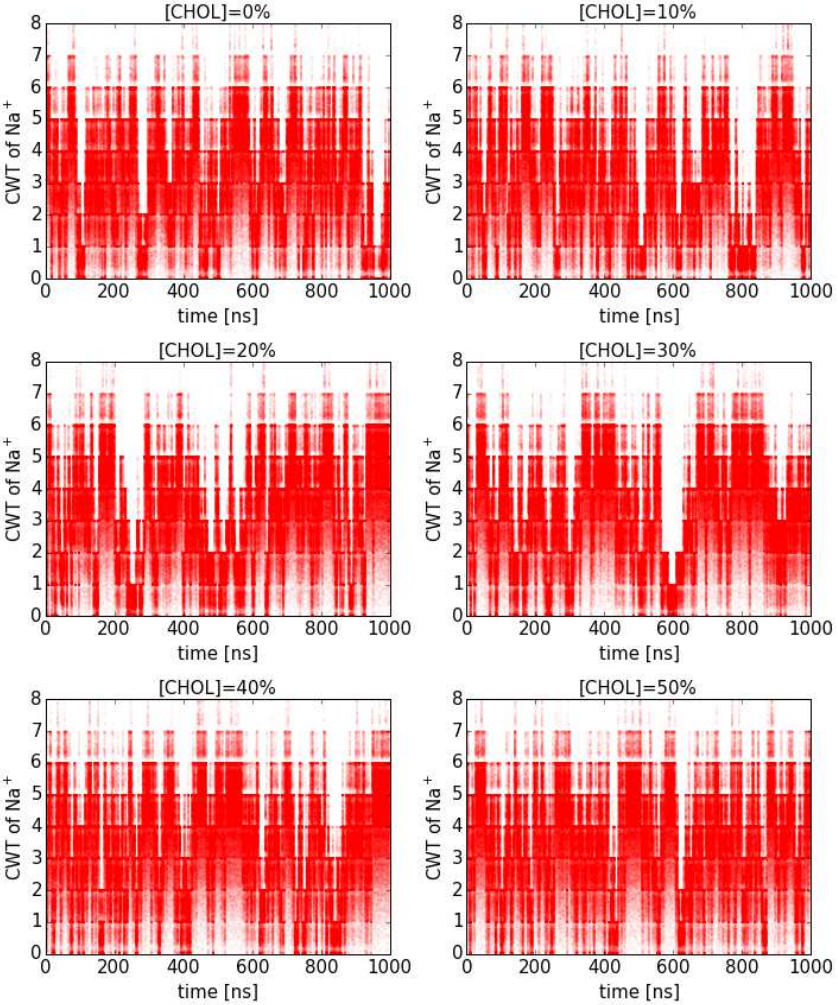

Figure 4.7: Coordination number between a Na^+ ion and water oxygens (CWT) as a function of time.

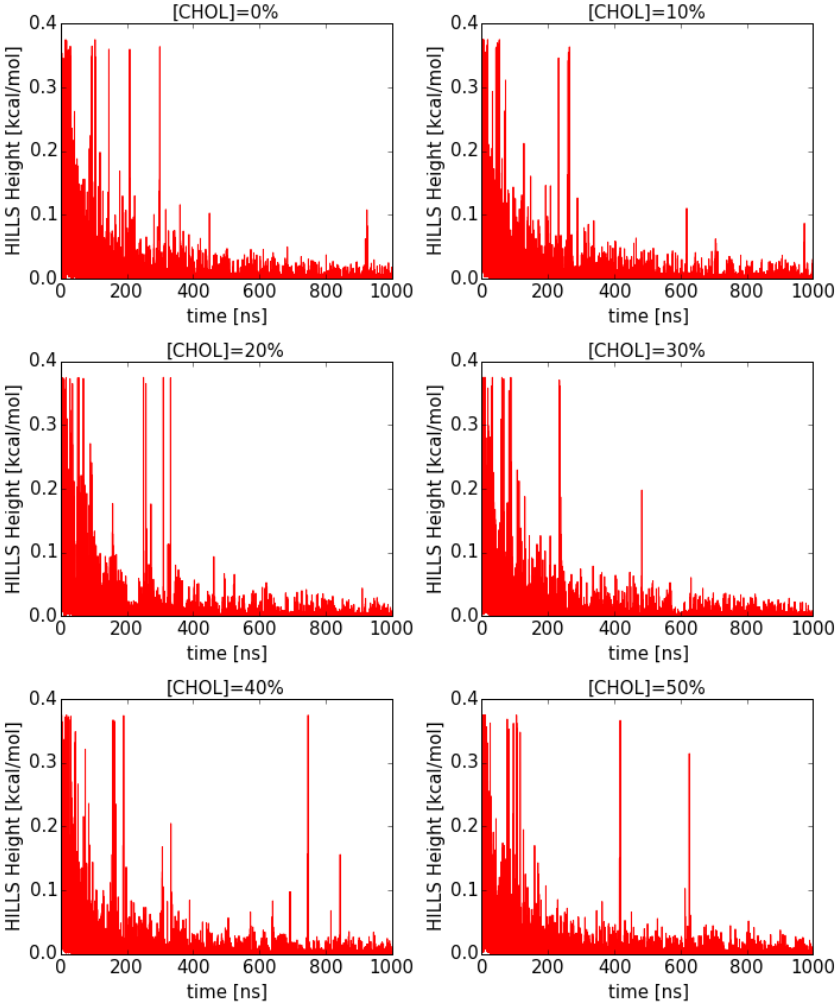

Figure 4.8: Well-tempered metadynamics HILLS Height as a function of time.

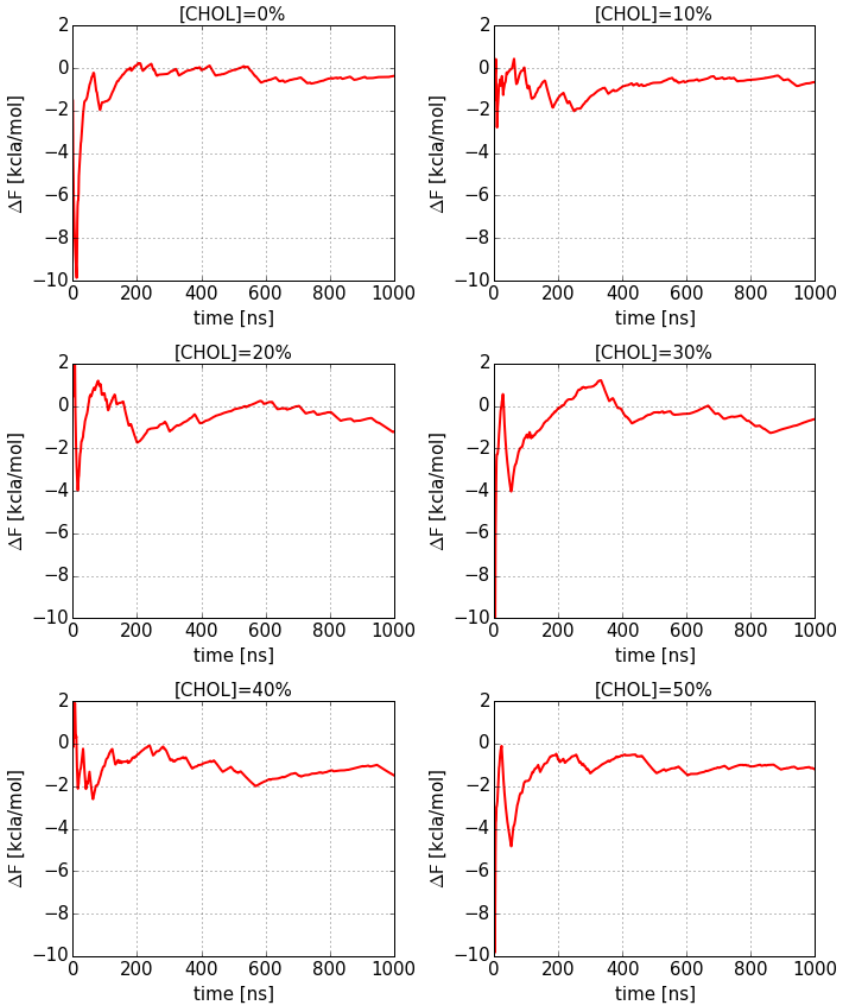

Figure 4.9: We monitor the convergence of the free-energy as a function of CLP (Figure 4.3) by calculating $\triangle$F, the free-energy difference between unbound states (CLP < 0.5) and bound states (CLP > 0.5) as a function of time. The average values and standard deviations of $\triangle$F calculated from the last 100 ns are shown in Figure 4 in the paper.

5 Pair Interactions among DPPC/POPC/Cholesterol Mixtures in Liquid-Ordered and Liquid-Disordered Phases

Saturated phospholipids, unsaturated phospholipids, and cholesterol are essential components of cell membranes, making the understanding of their mutual interactions of great significance. We have performed microsecond molecular dynamics simulations on the ternary mixtures of DPPC/ POPC/ cholesterol to systematically examined lipid-lipid and cholesterol-lipid interactions in the liquid-ordered and the liquid-disordered phases. The results show that there exits a competition between tighter packing of cholesterol-lipid and looser packing of lipid-lipid as the membrane changes from the liquid-disordered phase to liquid-ordered phase. Depending on the lipid saturation, the favor of lipid-lipid interactions is in the order of saturated-saturated > unsaturated-unsaturated > saturated-unsaturated. Cholesterol-saturated lipid interactions are more favorable than cholesterol-unsaturated lipid ones. The results are consistent with the push-pull forces derived from experiments and give general insights on the interactions among membrane components.

5.1 Introduction

Cholesterol is an essential component of cell membranes and plays important roles in maintaining membrane structures and regulating membrane functions [148, 149]. Mixtures of phospholipids and cholesterol form liquid-disordered (l_d) and liquid-ordered (l_o) phases at different cholesterol concentrations. While the l_o state has been considered as a good working model for lipid rafts, the l_d state well mimics the fluid lipids [150, 151]. Study of the interactions of lipid-lipid and cholesterol-lipid in both l_d and l_o phases is important for further understanding of cell membranes [152, 7].

Saturated and unsaturated phospholipids interact differently with each other and with cholesterol in different phases. The diversity of their mutual interactions determines their spatial distribution in the membrane [152]. Regen et al. provided the first direct experimental measurements of the interactions between unsaturated lipid POPC and cholesterol and that between saturated lipid DPPC and cholesterol in the l_d and l_o phases. They showed that DPPC and cholesterol exhibit strong attraction in the l_o phase but mix ideally in the l_d phase, and that POPC and cholesterol exhibit significant repulsion in the l_d phase but mix ideally in the l_o phase [150, 153]. More recently, they measured the interactions between DPPC and POPC and found that such interactions are significantly repulsive in the l_d phase but are neither attractive nor repulsive in the l_o phase [154].

The interactions of lipid-lipid and lipid-cholesterol are nontrivial properties depending on the lipid saturation and also on the mixture phase. Most of the simulations studying such interactions are based on binary mixtures, due to the difficulties of equilibrium issue in ternary mixtures [7]. However, since cell membranes are composed of saturated lipids, unsaturated lipids, and cholesterol, study on ternary mixtures can give more ideal descriptions of such mutual interactions. In this work, we perform microsecond all-atom molecular dynamics (MD) simulations on the ternary mixtures of DPPC/POPC/cholesterol in l_d and l_o phases. The results are

consistent with available experiments and give systematical descriptions of the mutual interactions between various like or unlike species in different phases, which could be helpful to deepen our understanding of lipid rafts [155].

5.2 Methods

Two lipid bilayer systems were generated by CHARMM-GUI [156, 157] to simulate membranes in the l_d and l_o phases. Each system has 128 lipid/cholesterol molecules and 5120 TIP3P water molecules [158], corresponding to a hydration of 40 water per lipid. For the l_d phase, the bilayer consisted of 52 DPPC, 52 POPC, and 24 cholesterol (CHOL), corresponding to a cholesterol concentration of 19%. For the l_o phase, the bilayer consisted of 36 DPPC, 36 POPC, and 56 CHOL, corresponding to a cholesterol concentration of 44%. MD simulations were performed using NAMD 2.9 [50] and the CHARMM36 force field [159, 160]. Each bilayer system was equilibrated for 100 ns in the NPT ensemble at 1 atm and 303 K. A time step of 2 fs was used. Covalent bonds with hydrogen atoms of lipids were kept rigid using SHAKE [126], and water molecules were kept rigid using SETTLE [127]. The particle mesh Ewald method was employed to compute long-range electrostatic interactions [51]. The cutoff for Lennard-Jones interactions was set to 12 Å and smoothly switched from 10 Å. Pressure was controlled by the Langevin piston Nosé-Hoover method [128]. Temperature was controlled by the Langevin dynamics with a damping coefficient of 1 ps^{-1} [55]. After equilibration, a 900 ns production run was performed in the NVT ensemble for each bilayer system.

5.3 Results

The deuterium order parameter S_{CD} of the lipid acyl tails is an important property to characterize the order of the lipid bilayer [161]. The order

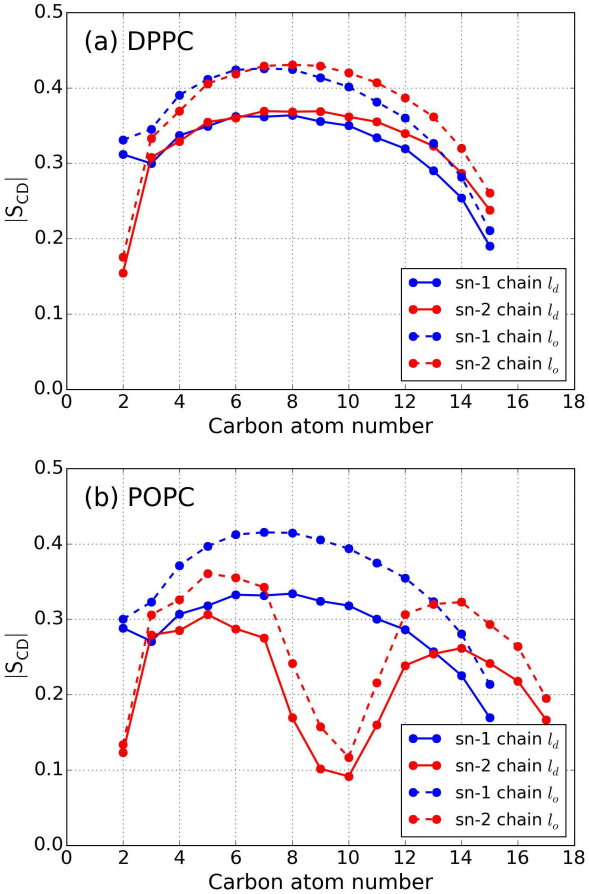

Figure 5.1: Order parameter $|S_{CD}|$ for the acyl tails of DPPC (a) and POPC (b) in the liquid-disordered phase (l_d) and the liquid-ordered phase (l_o).

parameter for each CH_2 group in the lipid tails is defined as

$$S_{CD} = \frac{1}{2}(3 < \cos^2\theta > -1), \tag{5.1}$$

where θ is the angle between a C-H vector and the bilayer normal, and the angular brackets denote both ensemble and time average. The resulting $|S_{CD}|$ obtained from the bilayer systems in the l_d and the l_o phases are shown in Figure 5.1. For both sn-1 and sn-2 chains of DPPC, the order parameters increase evidently from the l_d phase to the l_o phase (Figure 5.1a). The same trends are also observed for both chains of POPC with relatively small order parameters in the middle of the sn-2 unsaturated chain due to the double bond (Figure 5.1b). The results are in good agreement with other works [58, 162, 163, 164] and confirm that the bilayer systems containing 19% and 44% cholesterol make significant difference in modeling l_d and l_o phases in terms of the order parameter.

The packing of lipid-lipid and cholesterol-lipid pairs in the l_d and the l_o phases are characterized by the lateral radial pair distribution function $g(r)$, where r is the projected distance in the lateral plane between centers of mass (COM) of two molecules [165, 166]. As indicated by the decrease in the first peak of $g(r)$ in Figure 5.2a, the packing of DPPC-DPPC becomes looser when the bilayer changes from the l_d phase to the l_o phase. In contrast, the packing of POPC-POPC is almost not affected by the phases (Figure 5.2b). For DPPC-POPC, the packing also becomes looser in the l_o phase since the position of the first peak of $g(r)$ has been shifted far away (Figure 5.2c). The looser packing for DPPC-DPPC and DPPC-POPC and the unaffected packing for POPC-POPC in the l_o phase seems in contradiction with most of the experimental and computational results that lipid bilayers become more condensed and more tightly packed at higher cholesterol concentration [149, 7]. However, we should remember that there are also pairs involving cholesterol in the ternary bilayer systems. For CHOL-DPPC, the first peak of $g(r)$ becomes more apparent and increase significantly in the l_o phase, indicating a more condensed packing (Figure 5.2d). For CHOL-POPC, the packing is slightly tighter in the l_o phase as the first peak of $g(r)$ becomes more evident (Figure 5.2e). For CHOL-CHOL, the packing is tighter as the first, second, and third

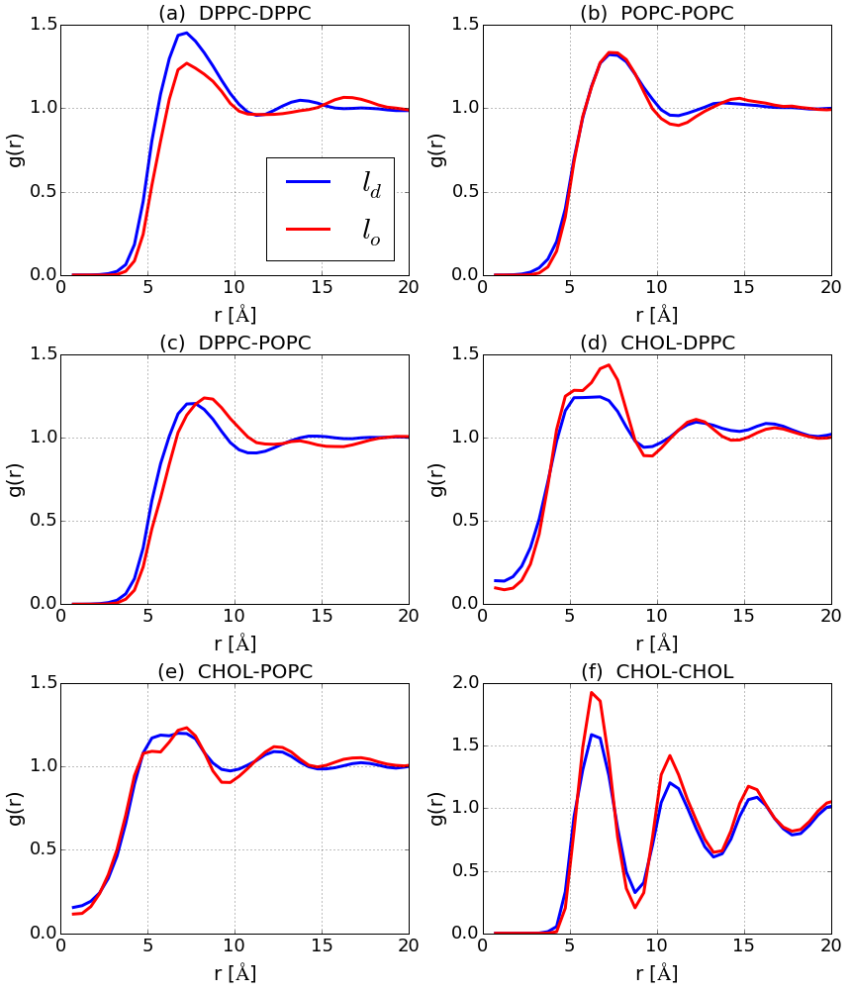

Figure 5.2: Lateral radial pair distribution function $g(r)$ for DPPC/POPC/CHOL mixtures in the l_d and l_o phases.

peak of $g(r)$ increase in the l_o phase (Figure 5.2f). Therefore, all the pairs involving CHOL become more tightly packed at higher cholesterol con-

centration, which compensates the looser packing effects of DPPC-DPPC and DPPC-POPC in the l_o phase and indicates a competition between tighter packing of cholesterol-lipid and looser packing of lipid-lipid as the mixtures condense.

In order to compare different kinds of interactions systematically, we calculate the potential of mean force (PMF) for lipid-lipid and cholesterol-lipid pairs by

$$\mathrm{PMF}(r) = -k_B T \ln g(r), \tag{5.2}$$

where $g(r)$ is the lateral radial pair distribution function [167]. The resulting PMF for lipid-lipid pairs in the l_d phase and the l_o phase are shown in Figure 5.3a. In the pair distance of 6Å $<$ r $<$ 10Å, the lowest profile is DPPC-DPPC in the l_d phase, indicating that interactions among saturated phospholipids in the l_d phase are most favorable. The highest profile is DPPC-POPC in the l_d phase, suggesting that interactions between saturated phospholipids and unsaturated phospholipids in the l_d phase are most unfavorable, which is consistent with the push force measured by Regen et al. [154] The resulting PMF for the pairs involving cholesterol are shown in Figure 5.3b. In 6Å $<$ r $<$ 10Å, there is a clear minimum for CHOL-DPPC in the l_o phase compared to the other cholesterol-lipid interactions, which corresponds to the strong pull proposed by Regen et al.[154] The interactions for CHOL-POPC in either the l_d phase or the l_o phase are clearly unfavorable with respect to the strong pull of CHOL-DPPC in the l_o phase, which can be attributed to the significant push between cholesterol and unsaturated phospholipids [154, 150]. In contract to the other interactions, the PMF for CHOL-CHOL has several local minima keeping the same positions in the l_d phase and the l_o phase, which indicates that the favorable packing distances among cholesterol are not affected by the phases.

The pull for CHOL-DPPC in the l_o phase and the push for CHOL-POPC shown in Figure 5.3b agree well with the experiments by Regen et

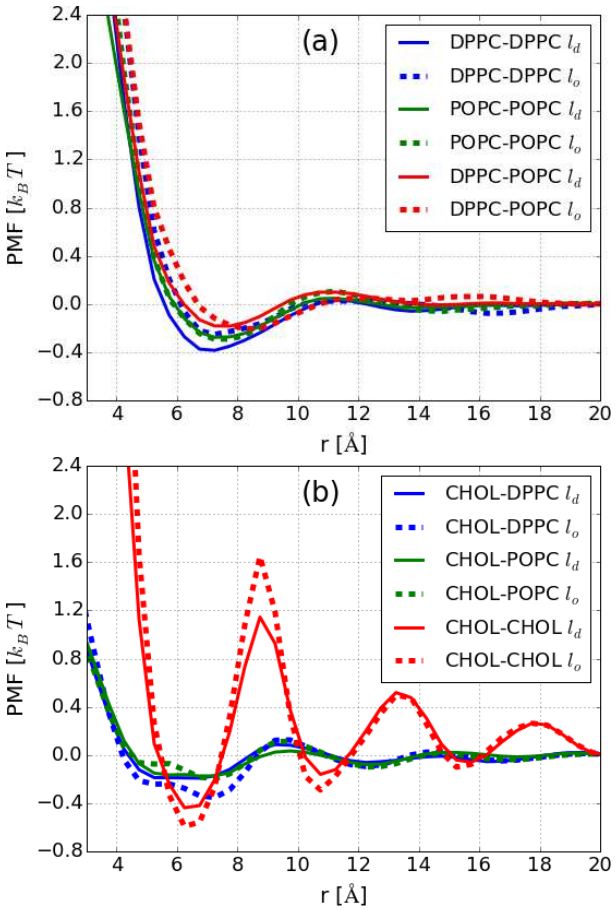

Figure 5.3: Potential of mean force (PMF) for lipid-lipid (a) and cholesterol-lipid (b) pairs in the l_d (solid line) and the l_o (dash line) phases.

al.[154] and indicate that the interactions of cholesterol-saturated phospholipids and those of cholesterol-unsaturated phospholipids are different. To have a more intuitive understanding of the effect of lipid saturation on cholesterol-lipid interactions, we obtain the lateral-vertical radial dis-

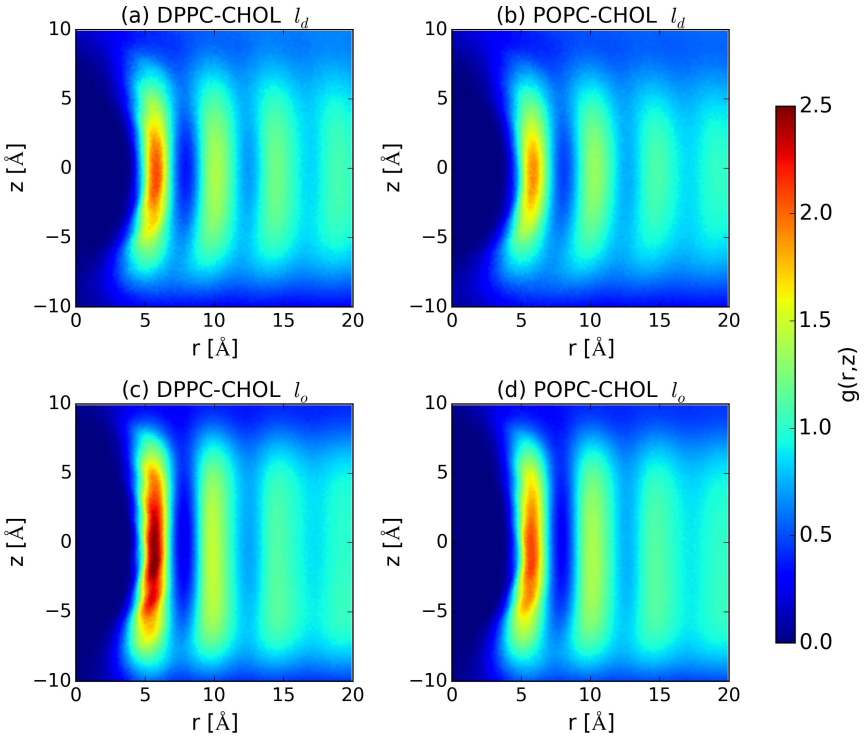

Figure 5.4: Lateral-vertical radial distribution function $g(r, z)$ between the center of mass of cholesterol and the carbon atoms of lipid tails.

tribution function $g(r, z)$ between cholesterol and carbon atoms in lipid tails, where r is the lateral distance between the cholesterol COM and a lipid tail carbon, and z is the vertical distance between the cholesterol COM and a lipid tail carbon. The positive direction of z is towards the membrane-water interface. As shown in Figure 5.4, DPPC has higher densities around CHOL in the z direction compared with POPC in a given phase. As the phase changes from l_d to l_o, the boundary curves between cholesterol and lipids are straightened for both DPPC and POPC, indicating that the change of lateral radial distribution function $g(r)$ in different

phases (Figure 5.2) may be attributed to the change of packing in the vertical direction. This straightening effect is consistent with the condensing effect of cholesterol on saturated and unsaturated lipid chains, which lengthens phospholipid molecules complexed with cholesterol and thickens lipid bilayers[145]. The vertical packing densities for DPPC-CHOL are enhanced significantly in the l_o phase, corresponding to a favorable pull [154]. Although the POPC-CHOL interaction is significant push in the l_d phase, they mix more ideally in the vertical direction as the lipid tails become more ordered in the l_o phase, resulting in neither attractive nor repulsive interactions in l_o phase [154, 150]. Consequently, the lateral-vertical packing property $g(r, z)$ provides a straightforward point of view to examine the interactions of cholesterol-lipid, and explain well the change of lateral packing property $g(r)$ in line with experiments.

5.4 Conclusions

We have systematically examined the mutual interactions among saturated phospholipids, unsaturated phospholipids, and cholesterol in the liquid-ordered and the liquid-disordered phases by performing microsecond MD simulations on the ternary mixtures of DPPC/ POPC/ cholesterol. The results show that there exits a competition between tighter packing of cholesterol-lipid and looser packing of lipid-lipid as the membrane changes from the liquid-disordered phase to liquid-ordered phase. Depending on the lipid saturation, the favor of lipid-lipid interactions is in the order of saturated-saturated > unsaturated-unsaturated > saturated-unsaturated. The cholesterol-saturated lipid interaction is more favorable than cholesterol-unsaturated lipid interaction, though the push force of the latter one reduces significantly as the mixtures condense. The results are consistent with the pull-push forces derived from experiments and give general insights on the interactions among membrane components.

6 Conclusions and Perspectives

6.1 Ion binding landscapes at phospholipid membrane surfaces

(1). The free-energy landscapes unveil specific binding behaviors of metal cations on phospholipid membranes. Na^+ and K^+ are more likely to stay in the aqueous solution, and can easily bind to a few lipid oxygens by overcoming low free-energy barriers. Ca^{2+} is most stable when bound to four lipid oxygens of the membranes, rather than being hydrated in the aqueous solution. Mg^{2+} is tightly hydrated, and can hardly lose a hydration water and bind directly to the membranes.

(2). When bound to the membranes, the cations' most favorable total coordination numbers with water and lipid oxygens are the same as their corresponding hydration numbers in aqueous solution, indicating a competition between ion binding to water and lipids. The binding specificity of metal cations on membranes is highly correlated with the hydration free energy and the size of the hydration shell.

(3). The binding landscapes of Na^+ at DMPC-cholesterol membranes show that the ionic affinity to membranes decreases as cholesterol concentration increases. When cholesterol concentration is greater than 30%, the ionic binding is significantly reduced, which coincides with the phase transition point of DMPC-cholesterol membranes from a liquid-disordered phase to

a liquid-ordered phase.

(4). We have also evaluated the contributions of different lipid head groups to the binding free energy separately. The DMPC's carbonyl group is the most favorable binding site for sodium, followed by DMPC's phosphate group and then the hydroxyl group of cholesterol.

6.2 Molecular dynamics of phospholipid membranes

(1). Molecular self-diffusion, reorientational motions and spectral densities of atomic species reveal a variety of time scales playing a role in membrane dynamics.

(2). The mechanisms of lipid motion strongly depend on the time scale considered, from fast ballistic translation at the scale of picoseconds to diffusive flow of a few lipids forming nanodomains at the scale of hundreds of nanoseconds. In the intermediate regime of sub-diffusion, collisions with nearest neighbors prevent the lipids to achieve full diffusion.

(3). Lipid reorientation along selected directions agree well with reported nuclear magnetic resonance data and indicate two different time scales.

(4). Calculated spectral densities corresponding to lipid and water reveal an overall good qualitative agreement with Fourier transform infrared spectroscopy experiments. Our simulations indicate a blue-shift of the low frequency spectral bands of hydration water as a result of its interaction with lipids.

(5). Our findings include a "wagging of the tails" frequency around 30 cm^{-1}, which essentially corresponds to motions of the tail-group along the

instantaneous plane formed by the two lipid tails, i.e., in-plane oscillations are clearly of bigger importance than those along the normal-to-the plane direction.

(6). Microsecond MD simulations on the ternary mixtures of DPPC/ POPC/ cholesterol show that there exits a competition between tighter packing of lipid-cholesterol and looser packing of lipid-lipid as the membrane changes from the liquid-disordered phase to liquid-ordered phase.

(7). Depending on the lipid saturation, the favor of lipid-lipid interactions is in the order of saturated-saturated > unsaturated-unsaturated > saturated-unsaturated. Cholesterol-saturated lipid interactions are more favorable than cholesterol-unsaturated lipid interactions.

(8). The results are consistent with the pull-push forces derived from experiments and give general insights on the interactions among membrane components.

6.3 Perspectives

Our work provides a general methodology to explore the free-energy landscapes for ions at complex biological interfaces. Furthermore, provided the importance in a variety of biological processes of the interaction of ions and charged interfaces in aqueous solution, our approach could be extended to explore other problems in colloidal chemistry and biology, and could be helpful to deepen our understanding of specific ion effects on soft matter and biological systems. It could be interesting to explore the binding landscapes of K^+, Ca^{2+}, Zn^{2+}, and Fe^{2+} at cholesterol-containing membranes, the free-energy landscapes of metal cations at a physiological concentration, and the binding of ions at protein surfaces.

Molecular dynamics of membranes reveal a variety of time scales playing a role in membrane dynamics. It could be interesting to explore the time scales of lipid-lipid and lipid-cholesterol interactions depending on the lipid saturation and membrane phases, which could be helpful to deepen our understanding of lipid rafts.

References

[1] D.P Tieleman, S.J Marrink, and H.J.C Berendsen. A Computer Perspective of Membranes: Molecular Dynamics Studies of Lipid Bilayer Systems. *Biochimica et Biophysica Acta (BBA) - Reviews on Biomembranes*, 1331(3):235–270, 1997.

[2] Alexander P. Lyubartsev and Alexander L. Rabinovich. Recent Development in Computer Simulations of Lipid Bilayers. *Soft Matter*, 7(1):25, 2011.

[3] J F Nagle and S Tristram-nagle. Structure of Lipid Bilayers. *Biochim. Biophys. Acta*, 1469:159–195, 2000.

[4] M.I. Gurr and J.L. Harwood. Lipid Biochemistry: An Introduction. *Springer Science and Business Media*, 1991.

[5] E J Veldhuizen, J J Batenburg, L M van Golde, and H P Haagsman. The role of surfactant proteins in DPPC enrichment of surface films. *Biophysical journal*, 79(6):3164–71, 2000.

[6] M R Vist and J H Davis. Phase Equilibria of Cholesterol/Dipalmitoylphosphatidylcholine Mixtures: 2H Nuclear Magnetic Resonance and Differential Scanning Calorimetry. *Biochemistry*, 29(2):451–464, 1990.

[7] Max L Berkowitz. Detailed Molecular Dynamics Simulations of

Model Biological Membranes Containing Cholesterol. *Biochim. Biophys. Acta*, 1788(1):86–96, 2009.

[8] Clare L Armstrong, Matthew a. Barrett, Arno Hiess, Tim Salditt, John Katsaras, An Chang Shi, and Maikel C Rheinstädter. Effect of Cholesterol on the Lateral Nanoscale Dynamics of Fluid Membranes. *Eur. Biophys. J.*, 41(10):901–913, 2012.

[9] Kai Simons and Mathias J Gerl. Revitalizing Membrane Rafts: New Tools and Insights. *Nature reviews. Molecular cell biology*, 11(10):688–99, October 2010.

[10] Deborah Brown. Structure and Function of Membrane Rafts. *International Journal of Medical Microbiology*, 291(6-7):433–437, January 2001.

[11] Peter J. Bond, John Holyoake, Anthony Ivetac, Syma Khalid, and Mark S P Sansom. Coarse-Grained Molecular Dynamics Simulations of Membrane Proteins and Peptides. *Journal of Structural Biology*, 157(3):593–605, 2007.

[12] Ilpo Vattulainen and Tomasz Rog. Lipid Simulations: a Perspective on Lipids in Action. *Cold Spring Harbor perspectives in biology*, 3(4):a004655, April 2011.

[13] Siewert J Marrink, H Jelger Risselada, Serge Yefimov, D Peter Tieleman, and Alex H de Vries. The MARTINI Force Field: Coarse Grained Model for Biomolecular Simulations. *The journal of physical chemistry. B*, 111(27):7812–24, July 2007.

[14] Indira Chandrasekhar, Mika Kastenholz, Roberto D Lins, Chris Oostenbrink, Lukas D Schuler, D Peter Tieleman, and Wilfred F van Gunsteren. A Consistent Potential Energy Parameter Set for Lipids:

Dipalmitoylphosphatidylcholine as a Benchmark of the GROMOS96 45A3 Force Field. *European biophysics journal : EBJ*, 32(1):67–77, 2003.

[15] Balázs Jójárt and Tamás A Martinek. Performance of the General Amber Force Field in Modeling Aqueous POPC Membrane Bilayers. *Journal of computational chemistry*, 28(12):2051–8, September 2007.

[16] R. W. Pastor and a. D. MacKerell. Development of the CHARMM Force Field for Lipids. *Journal of Physical Chemistry Letters*, 2(13):1526–1532, 2011.

[17] Jeffery B Klauda, Richard M Venable, J Alfredo Freites, Joseph W O'Connor, Douglas J Tobias, Carlos Mondragon-Ramirez, Igor Vorobyov, Alexander D MacKerell, and Richard W Pastor. Update of the CHARMM All-Atom Additive Force Field for Lipids: Validation on Six Lipid Types. *J. Phys. Chem. B*, 114(23):7830–7843, 2010.

[18] Scott E. Feller and Jr. Alexander D. MacKerell. An improved empirical potential energy function for molecular simulations of phospholipids. *The Journal of Physical Chemistry B*, 104(31):7510–7515, 2000.

[19] Jeffery B. Klauda, , Bernard R. Brooks, Jr. Alexander D. MacKerell, Richard M. Venable, , and Richard W. Pastor. An ab initio study on the torsional surface of alkanes and its effect on molecular simulations of alkanes and a dppc bilayer. *The Journal of Physical Chemistry B*, 109(11):5300–5311, 2005.

[20] M.P. Allen and D.J. Tildesley. Computer Simulation of Liquids. *Oxford Science Publications*, 1989.

[21] Daan Frenkel and Berend Smit. Understanding Molecular Simulation: From Algorithms to Applications, second edition. *Academic Press*, 2001.

[22] Jarosaw Meller. Molecular dynamics. *eLS*, 2001.

[23] Ludovico Sutto, Simone Marsili, and Francesco Luigi Gervasio. New Advances in Metadynamics. *Wiley Interdisciplinary Reviews: Computational Molecular Science*, 2(5):771–779, September 2012.

[24] Cameron Abrams and Giovanni Bussi. Enhanced Sampling in Molecular Dynamics Using Metadynamics, Replica-Exchange, and Temperature-Acceleration. *Entropy*, 16(1):163–199, 2014.

[25] Alessandro Barducci, Massimiliano Bonomi, and Michele Parrinello. Metadynamics. *Wiley Interdiscip. Rev. Comput. Mol. Sci.*, 1(5):826–843, 2011.

[26] G.M. Torrie and J.P. Valleau. Nonphysical Sampling Distributions in Monte Carlo Free-Energy Estimation: Umbrella Sampling. *Journal of Computational Physics*, 23(2):187–199, February 1977.

[27] Eric Darve, David Rodriguez-Gomez, and Andrew Pohorille. Adaptive Biasing Force Method for Scalar and Vector Free Energy Calculations. *The Journal of Chemical Physics*, 128(14):144120, 2008.

[28] Barry Isralewitz, Jerome Baudry, Justin Gullingsrud, Dorina Kosztin, and Klaus Schulten. Steered Molecular Dynamics Investigations of Protein Function. *Journal of Molecular Graphics and Modelling*, 19(1):13–25, February 2001.

[29] Alessandro Laio and Michele Parrinello. Escaping Free-Energy Minima. *Proc. Natl. Acad. Sci. U. S. A.*, 99(20):12562–12566, 2002.

[30] Vojtech Spiwok, Zoran Sucur, and Petr Hosek. Enhanced sampling techniques in biomolecular simulations. *Biotechnology Advances*, 33(6, Part 2):1130 – 1140, 2015.

[31] Alessandro Barducci, Giovanni Bussi, and Michele Parrinello. Well-Tempered Metadynamics: A Smoothly Converging and Tunable Free-Energy Method. *Phys. Rev. Lett.*, 100(2):20603, 2008.

[32] S. Schurch, Martin Lee, and Peter Gehr. Pulmonary Surfactant: Surface Properties and Function of Alveolar and Airway Surfactant. *Pure and Applied Chemistry*, 64(11):1745–1750, 1992.

[33] Siewert-Jan Marrink and Herman J C Berendsen. Simulation of Water Transport Through a Lipid Membrane. *Journal of Physical Chemistry*, 98(15):4155–4168, 1994.

[34] Shreyas Y Bhide and Max L Berkowitz. Structure and Dynamics of Water at the Interface with Phospholipid Bilayers. *The Journal of chemical physics*, 123(22):224702, 2005.

[35] Lula Rosso and Ian R Gould. Structure and Dynamics of Phospholipid Bilayers Using Recently Developed General All-Atom Force Fields. *Journal of computational chemistry*, 29(1):24–37, January 2008.

[36] Wei Zhao, David E. Moilanen, Emily E. Fenn, and Michael D. Fayer. Water at the Surfaces of Aligned Phospholipid Multibilayer Model Membranes Probed with Ultrafast Vibrational Spectroscopy. *Journal of the American Chemical Society*, 130(42):13927–13937, 2008.

[37] C. L. Armstrong, M. Trapp, J. Peters, T. Seydel, and M. C. Rheinstädter. Short Range Ballistic Motion in Fluid Lipid Bilayers Studied by Quasi-Elastic Neutron Scattering. *Soft Matter*, 7(18):8358,

2011.

[38] S. König, W. Pfeiffer, T. Bayerl, D. Richter, and E. Sackmann. Molecular Dynamics of Lipid Bilayers Studied by Incoherent Quasi-Elastic Neutron Scattering. *Journal de Physique II*, 2(8):1589–1615, August 1992.

[39] Emma Falck, Tomasz Róg, Mikko Karttunen, and Ilpo Vattulainen. Lateral Diffusion in Lipid Membranes through Collective Flows. *Journal of the American Chemical Society*, 130(1):44–45, 2008.

[40] Sebastian Busch, Luis Carlos Pardo, Christoph Smuda, and Tobias Unruh. The Picosecond Dynamics of the Phospholipid Dimyristoylphosphatidylcholine in Mono- and Bilayers. *Soft Matter*, 8(13):3576, 2012.

[41] Clare L. Armstrong, Martin D. Kaye, Michaela Zamponi, Eugene Mamontov, Madhusudan Tyagi, Timothy Jenkins, and Maikel C. Rheinstädter. Diffusion in Single Supported Lipid Bilayers Studied by Quasi-Elastic Neutron Scattering. *Soft Matter*, 6(23):5864, 2010.

[42] Andrey a. Gurtovenko and Ilpo Vattulainen. Molecular Mechanism for Lipid Flip-Flops. *Journal of Physical Chemistry B*, 111(48):13554–13559, 2007.

[43] Jordi Martí and Félix S. Csajka. Transition Path Sampling Study of Flip-Flop Transitions in Model Lipid Bilayer Membranes. *Physical Review E - Statistical, Nonlinear, and Soft Matter Physics*, 69:061918, 2004.

[44] Jakob Wohlert and Olle Edholm. Dynamics in Atomistic Simulations of Phospholipid Membranes: Nuclear Magnetic Resonance Relaxation Rates and Lateral Diffusion. *Journal of Chemical Physics*,

125(20):204703, 2006.

[45] Maciej Kozak, Aleksandra Wypych, Kamil Szpotkowski, Stefan Jurga, and Andrzej Skrzypczak. Structural and Spectroscopic Studies of DMPC/Cationic Surfactant System. *Journal of Non-Crystalline Solids*, 356(11-17):747–753, 2010.

[46] Elijah Flenner, Jhuma Das, Maikel C. Rheinstädter, and Ioan Kosztin. Subdiffusion and Lateral Diffusion Coefficient of Lipid Atoms and Molecules in Phospholipid Bilayers. *Physical Review E - Statistical, Nonlinear, and Soft Matter Physics*, 79(1):011907, 2009.

[47] F. Y. Hansen, G. H. Peters, H. Taub, and a. Miskowiec. Diffusion of Water and Selected Atoms in DMPC Lipid Bilayer Membranes. *Journal of Chemical Physics*, 137(20):204910, 2012.

[48] William L Jorgensen, Jayaraman Chandrasekhar, Jeffry D Madura, Roger W Impey, and Michael L Klein. Comparison of Simple Potential Functions for Simulating Liquid Water. *J. Chem. Phys.*, 79(2):926–935, 1983.

[49] J F Nagle, R Zhang, S Tristram-Nagle, W Sun, H I Petrache, and R M Suter. X-ray Structure Determination of Fully Hydrated L_α Phase Dipalmitoylphosphatidylcholine Bilayers. *Biophysical journal*, 70(3):1419–1431, 1996.

[50] James C Phillips, Rosemary Braun, Wei Wang, James Gumbart, Emad Tajkhorshid, Elizabeth Villa, Christophe Chipot, Robert D Skeel, Laxmikant Kalé, and Klaus Schulten. Scalable Molecular Dynamics with NAMD. *J. Comput. Chem.*, 26(16):1781–1802, 2005.

[51] Ulrich Essmann, Lalith Perera, Max L. Berkowitz, Tom Darden, Hsing Lee, and Lee G. Pedersen. A Smooth Particle Mesh Ewald

Method. *The Journal of Chemical Physics*, 103(19):8577, 1995.

[52] Prithvi Raj Pandey and Sudip Roy. Headgroup Mediated Water Insertion into the DPPC Bilayer: A Molecular Dynamics Study. *Journal of Physical Chemistry B*, 115(12):3155–3163, 2011.

[53] Jeffery B Klauda, Norbert Kucerka, Bernard R Brooks, Richard W Pastor, and John F Nagle. Simulation-Based Methods for Interpreting X-Ray Data from Lipid Bilayers. *Biophysical journal*, 90(8):2796–2807, 2006.

[54] H J C Berendsen, J P M Postma, W F van Gunsteren, a DiNola, and J R Haak. Molecular Dynamics with Coupling to an External Bath. *The Journal of Chemical Physics*, 81(8):3684–3690, 1984.

[55] Scott E. Feller, Yuhong Zhang, Richard W. Pastor, and Bernard R. Brooks. Constant Pressure Molecular Dynamics Simulation: The Langevin Piston Method. *The Journal of Chemical Physics*, 103(11):4613, 1995.

[56] E. Lindahl and O. Edholm. Molecular Dynamics Simulation of NMR Relaxation Rates and Slow Dynamics in Lipid Bilayers. *Journal of Chemical Physics*, 115(10):4938–4950, 2001.

[57] Gerald W. Stockton and Ian C.P. Smith. A Deuterium Nuclear Magnetic Resonance Study of the Condensing Effect of Cholesterol on Egg Phosphatidylcholine Bilayer Membranes. I. Perdeuterated Fatty Acid Probes. *Chemistry and Physics of Lipids*, 17(2-3):251–263, October 1976.

[58] Christofer Hofsäss, Erik Lindahl, and Olle Edholm. Molecular Dynamics Simulations of Phospholipid Bilayers with Cholesterol. *Biophysical journal*, 84(4):2192–2206, 2003.

[59] Theodore P Trouard, Alexander a Nevzorov, Todd M Alam, Constantin Job, Jaroslav Zajicek, and M F Brown. Influence of Cholesterol on Dynamics of Dimyristoylphosphatidylcholine Bilayers as Studied by Deuterium NMR Relaxation. *J. Chem. Phys.*, 110(17):8802–8818, 1999.

[60] H I Petrache, S W Dodd, and M F Brown. Area per Lipid and Acyl Length Distributions in Fluid Phosphatidylcholines Determined by ^{2}H NMR Spectroscopy. *Biophysical journal*, 79(6):3172–3192, 2000.

[61] P B Moore, C F Lopez, and M L Klein. Dynamical Properties of a Hydrated Lipid Bilayer from a Multinanosecond Molecular Dynamics Simulation. *Biophysical journal*, 81(5):2484–2494, 2001.

[62] Beate Griepernau and Rainer a Böckmann. The Influence of 1-Alkanols and External Pressure on the Lateral Pressure Profiles of Lipid Bilayers. *Biophysical journal*, 95(12):5766–5778, 2008.

[63] J. Gullingsrud, a. Babakhani, and J. a. McCammon. Computational Investigation of Pressure Profiles in Lipid Bilayers with Embedded Proteins. *Molecular Simulation*, 32(10-11):831–838, 2006.

[64] Justin Gullingsrud and Klaus Schulten. Lipid Bilayer Pressure Profiles and Mechanosensitive Channel Gating. *Biophysical journal*, 86(6):3496–3509, 2004.

[65] K Tu, D J Tobias, J K Blasie, and M L Klein. Molecular Dynamics Investigation of the Structure of a Fully Hydrated Gel-Phase Dipalmitoylphosphatidylcholine Bilayer. *Biophysical journal*, 70(2):595–608, 1996.

[66] F. Brochard, P.G. De Gennes, and P. Pfeuty. Surface Tension and Deformations of Membrane Structures : Relation to Two-

Dimensional Phase Transitions. *Journal de Physique*, 37(10):1099–1104, October 1976.

[67] H Schindler. Formation of Planar Bilayers from Artificial or Native Membrane Vesicles. *FEBS letters*, 122(1):77–79, 1980.

[68] D Peter Tieleman and Herman Jc Berendsen. Molecular Dynamics Simulations of a Fully Hydrated Dipalmitoylphosphatidylcholine Bilayer with Different Macroscopic Boundary Conditions and Parameters. *J Chem Phys*, 105(11):4871, 1996.

[69] F Jähnig. What is the Surface Tension of a Lipid Bilayer Membrane? *Biophysical journal*, 71(3):1348–1349, 1996.

[70] E. a. Disalvo, F. Lairion, F. Martini, E. Tymczyszyn, M. Frías, H. Almaleck, and G. J. Gordillo. Structural and Functional Properties of Hydration and Confined Water in Membrane Interfaces. *Biochimica et Biophysica Acta - Biomembranes*, 1778(12):2655–2670, 2008.

[71] Ravinath Kausik and Songi Han. Dynamics and State of Lipid Bilayer-Internal Water Unraveled with Solution State ^{1}H Dynamic Nuclear Polarization. *Physical chemistry chemical physics : PCCP*, 13(17):7732–7746, 2011.

[72] Nikolay a. Krylov, Vladimir M. Pentkovsky, and Roman G. Efremov. Nontrivial Behavior of Water in the Vicinity and Inside Lipid Bilayers as Probed by Molecular Dynamics Simulations. *ACS Nano*, 7(10):9428–9442, 2013.

[73] Kazimierz Krynicki, Christopher D. Green, and David W. Sawyer. Pressure and Temperature Dependence of Self-Diffusion in Water. *Faraday Discuss. Chem. Soc.*, 66:199–208, 1978.

[74] A L Kuo and C G Wade. Lipid Lateral Diffusion by Pulsed Nuclear

Magnetic Resonance. *Biochemistry*, 18(11):2300–2308, 1979.

[75] Takahiro Fujiwara, Ken Ritchie, Hideji Murakoshi, Ken Jacobson, and Akihiro Kusumi. Phospholipids undergo Hop Diffusion in Compartmentalized Cell Membrane. *Journal of Cell Biology*, 157(6):1071–1081, 2002.

[76] P Schwille, J Korlach, and W W Webb. Fluorescence Correlation Spectroscopy with Single-Molecule Sensitivity on Cell and Model Membranes. *Cytometry*, 36(3):176–182, 1999.

[77] J. Tabony and B. Perly. Quasielastic Neutron Scattering Measurements of Fast Local Translational Diffusion of Lipid Molecules in Phospholipid Bilayers. *Biochimica et Biophysica Acta (BBA) - Biomembranes*, 1063(1):67–72, 1991.

[78] Giulia Palermo, Pablo Campomanes, Marilisa Neri, Daniele Piomelli, Andrea Cavalli, Ursula Rothlisberger, and Marco De Vivo. Wagging the tail: Essential role of substrate flexibility in faah catalysis. *Journal of Chemical Theory and Computation*, 9(2):1202–1213, 2013.

[79] Jae Hyung Jeon, Hector Martinez Seara Monne, Matti Javanainen, and Ralf Metzler. Anomalous Diffusion of Phospholipids and Cholesterols in a Lipid Bilayer and Its Origins. *Physical Review Letters*, 109(18):1–5, 2012.

[80] Eli Barkai, Yuval Garini, and Ralf Metzler. Strange Kinetics of Single Molecules in Living Cells. *Physics Today*, 65(8):29–35, 2012.

[81] Igor M. Sokolov. Models of Anomalous Diffusion in Crowded Environments. *Soft Matter*, 8(35):9043, 2012.

[82] W L Vaz, R M Clegg, and D Hallmann. Translational Diffusion of Lipids in Liquid Crystalline Phase Phosphatidylcholine Multibi-

layers. A Comparison of Experiment with Theory. *Biochemistry*, 24(3):781–786, 1985.

[83] Matej Praprotnik and Dušanka Janežič. Molecular Dynamics Integration and Molecular Vibrational Theory. III. The Infrared Spectrum of Water. *Journal of Chemical Physics*, 122(17), 2005.

[84] J. Marti, E. Guardia, and J. a. Padro. Dielectric Properties and Infrared Spectra of Liquid Water: Influence of the Dynamic Cross Correlations. *The Journal of Chemical Physics*, 101(12):10883, 1994.

[85] G. E. Walrafen, M. R. Fisher, M. S. Hokmabadi, and W.-H. Yang. Temperature Dependence of the Low- and High-Frequency Raman Scattering from Liquid Water. *The Journal of Chemical Physics*, 85(12):6970, December 1986.

[86] Iwao Ohmine and Hideki Tanaka. Fluctuation, Relaxations, and Hydration in Liquid Water. Hydrogen-Bond Rearrangement Dynamics. *Chem. Rev. (Washington, D. C.)*, 93(7):2545–2566, 1993.

[87] Ananya Debnath, Biswaroop Mukherjee, K. G. Ayappa, Prabal K. Maiti, and Shiang T. Lin. Entropy and Dynamics of Water in Hydration Layers of a Bilayer. *Journal of Chemical Physics*, 133(17), 2010.

[88] J.B. Hasted, S.K. Husain, F.A.M. Frescura, and J.R. Birch. Far-Infrared Absorption in Liquid Water. *Chemical Physics Letters*, 118(6):622–625, August 1985.

[89] Joan Angel Padro and Jordi Mart. Response to Comment on An Interpretation of the Low-Frequency Spectrum of Liquid Water [J. Chem. Phys. 118, 452 (2003)]. *The Journal of Chemical Physics*, 120(3):1659, 2004.

[90] E. a. Disalvo and M. a. Frias. Water State and Carbonyl Distribution Populations in Confined Regions of Lipid Bilayers Observed by FTIR Spectroscopy. *Langmuir*, 29(23):6969–6974, 2013.

[91] M. Moskovits and K. H. Michaelian. A Reinvestigation of the Raman Spectrum of Water. *The Journal of Chemical Physics*, 69(6):2306, August 1978.

[92] W. Pohle, D. R. Gauger, H. Fritzsche, B. Rattay, C. Selle, H. Binder, and H. Böhlig. FTIR-Spectroscopic Characterization of Phosphocholine-Headgroup Model Compounds. *Journal of Molecular Structure*, 563-564:463–467, 2001.

[93] H Binder. The Molecular Architecture of Lipid Membranes - New Insights from Hydration-Tuning Infrared Linear Dichroism Spectroscopy. *Appl. Spectrosc. Rev.*, 38(August 2002):15–69, 2003.

[94] W Hübner and H H Mantsch. Orientation of Specifically ^{1}3C=O Labeled Phosphatidylcholine Multilayers from Polarized Attenuated Total Reflection FT-IR Spectroscopy. *Biophysical journal*, 59(6):1261–1272, 1991.

[95] H Binder, T Gutberlet, a Anikin, and G Klose. Hydration of the Dienic Lipid Dioctadecadienoylphosphatidylcholine in the Lamellar Phase–An Infrared Linear Dichroism and X-Ray Study on Headgroup Orientation, Water Ordering, and Bilayer Dimensions. *Biophysical journal*, 74(4):1908–1923, 1998.

[96] S. Krishnamurty, M. Stefanov, T. Mineva, S. Bégu, J. M. Devoisselle, a. Goursot, R. Zhu, and D. R. Salahub. Density Functional Theory-Based Conformational Analysis of a Phospholipid Molecule (Dimyristoyl phosphatidylcholine). *Journal of Physical Chemistry B*, 112(42):13433–13442, 2008.

[97] Dorit R. Gauger and Walter Pohle. FT-IR Spectroscopy for Exposing the CH Vibrational Bands from the Polar Parts of Phospholipids. *Journal of Molecular Structure*, 744-747(SPEC. ISS.):211–215, 2005.

[98] Richard W. Pastor, Richard M. Venable, Martin Karplus, and Attila Szabo. A Simulation Based Model of NMR T1 Relaxation in Lipid Bilayer Vesicles. *The Journal of Chemical Physics*, 89(2):1128, 1988.

[99] Richard W. Pastor, Richard M. Venable, and Scott E. Feller. Lipid Bilayers, NMR Relaxation, and Computer Simulations. *Accounts of Chemical Research*, 35(6):438–446, 2002.

[100] Michael Patra, Mikko Karttunen, Marja T. Hyvonen, Emma Falck, and Ilpo Vattulainen. Lipid Bilayers Driven to a Wrong Lane in Molecular Dynamics Simulations by Truncation of Long-Range Electrostatic Interactions. pages 4485–4494, 2004.

[101] Jeffery B. Klauda, Nadukkudy V. Eldho, Klaus Gawrisch, Bernard R. Brooks, and Richard W. Pastor. Collective and Noncollective Models of NMR Relaxation in Lipid Vesicles and Multilayers. *Journal of Physical Chemistry B*, 112(19):5924–5929, 2008.

[102] Jeffery B Klauda, Mary F Roberts, Alfred G Redfield, Bernard R Brooks, and Richard W Pastor. Rotation of Lipids in Membranes: Molecular Dynamics Simulation, ^{31}P Spin-Lattice Relaxation, and Rigid-Body Ddynamics. *Biophysical journal*, 94(8):3074–3083, 2008.

[103] Pierandrea Lo Nostro and Barry W Ninham. Hofmeister Phenomena: An Update on Ion Specificity in Biology. *Chem. Rev.*, 112(4):2286–2322, 2012.

[104] Werner Kunz. Specific Ion Effects in Colloidal and Biological Systems. *Curr. Opin. Colloid Interface Sci.*, 15(1-2):34–39, 2010.

[105] Max L Berkowitz, David L Bostick, and Sagar Pandit. Aqueous Solutions Next to Phospholipid Membrane Surfaces: Insights from Simulations. *Chem. Rev.*, 106(4):1527–1539, 2006.

[106] Max L Berkowitz and Robert Vácha. Aqueous Solutions at the Interface with Phospholipid Bilayers. *Acc. Chem. Res.*, 45(1):74–82, 2012.

[107] Hans Binder and Olaf Zschörnig. The Effect of Metal Cations on the Phase Behavior and Hydration Characteristics of Phospholipid Membranes. *Chem. Phys. Lipids*, 115(1-2):39–61, 2002.

[108] L Herbette, C A Napolitano, and R V McDaniel. Direct Determination of the Calcium Profile Structure for Dipalmitoyllecithin Multilayers Using Neutron Diffraction. *Biophys. J.*, 46(6):677–685, 1984.

[109] Nadia N Casillas-Ituarte, Xiangke Chen, Hardy Castada, and Heather C Allen. Na+ and Ca2+ Effect on the Hydration and Orientation of the Phosphate Group of DPPC at Air-Water and Air-Hydrated Silica Interfaces. *J. Phys. Chem. B*, 114(29):9485–9495, 2010.

[110] Piotr Jurkiewicz, Lukasz Cwiklik, Alžběta Vojtíšková, Pavel Jungwirth, and Martin Hof. Structure, Dynamics, and Hydration of POPC/POPS Bilayers Suspended in NaCl, KCl, and CsCl Solutions. *Biochim. Biophys. Acta - Biomembr.*, 1818(3):609–616, 2012.

[111] Benjamin Klasczyk, Volker Knecht, Reinhard Lipowsky, and Rumiana Dimova. Interactions of Alkali Metal Chlorides with Phosphatidylcholine Vesicles. *Langmuir*, 26(24):18951–18958, 2010.

[112] Sagar A Pandit, David Bostick, and Max L Berkowitz. Molecular

Dynamics Simulation of a Dipalmitoylphosphatidylcholine Bilayer with NaCl. *Biophys. J.*, 84(6):3743–3750, 2003.

[113] Rainer A Böckmann, Agnieszka Hac, Thomas Heimburg, and Helmut Grubmüller. Effect of Sodium Chloride on a Lipid Bilayer. *Biophys. J.*, 85(3):1647–1655, 2003.

[114] Rainer A. Böckmann and Helmut Grubmüller. Multistep Binding of Divalent Cations to Phospholipid Bilayers: A Molecular Dynamics Study. *Angew. Chemie - Int. Ed.*, 43(8):1021–1024, 2004.

[115] Arnau Cordomí, Olle Edholm, and Juan J Perez. Effect of Ions on a Dipalmitoyl Phosphatidylcholine Bilayer. A Molecular Dynamics Simulation Study. *J. Phys. Chem. B*, 112(5):1397–1408, 2008.

[116] Andrey A. Gurtovenko. Asymmetry of Lipid Bilayers Induced by Monovalent Salt: Atomistic Molecular-Dynamics Study. *J. Chem. Phys.*, 122(24):244902, 2005.

[117] Andrey A. Gurtovenko and Ilpo Vattulainen. Effect of NaCl and KCl on Phosphatidylcholine and Phosphatidylethanolamine Lipid Membranes: Insight from Atomic-Scale Simulations for Understanding Salt-Induced Effects in the Plasma Membrane. *J. Phys. Chem. B*, 112(7):1953–1962, 2008.

[118] Robert Vácha, Shirley W I Siu, Michal Petrov, Rainer A. Böckmann, Justýna Barucha-Kraszewska, Piotr Jurkiewicz, Martin Hof, Max L Berkowitz, and Pavel Jungwirth. Effects of Alkali Cations and Halide Anions on the DOPC Lipid Membrane. *J. Phys. Chem. A*, 113(26):7235–7243, 2009.

[119] Christophe Chipot. Frontiers in Free-Energy Calculations of Biological Systems. *Wiley Interdiscip. Rev. Comput. Mol. Sci.*, 4(1):71–89,

2014.

[120] Niels Hansen and Wilfred F Van Gunsteren. Practical Aspects of Free-energy Calculations: A Review. *J. Chem. Theory Comput.*, 10(7):2632–2647, 2014.

[121] Nina Vlachy, Barbara Jagoda-Cwiklik, Robert Vácha, Didier Touraud, Pavel Jungwirth, and Werner Kunz. Hofmeister Series and Specific Interactions of Charged Headgroups with Aqueous Ions. *Adv. Colloid Interface Sci.*, 146(1-2):42–47, 2009.

[122] Sunhwan Jo, Taehoon Kim, Vidyashankara G Iyer, and Wonpil Im. CHARMM-GUI: A Web-Based Graphical User Interface for CHARMM. *J. Comput. Chem.*, 29(11):1859–1865, 2008.

[123] Sunhwan Jo, Joseph B Lim, Jeffery B Klauda, and Wonpil Im. CHARMM-GUI Membrane Builder for Mixed Bilayers and Its Application to Yeast Membranes. *Biophys. J.*, 97(1):50–58, 2009.

[124] Marta Pasenkiewicz-Gierula, Yuji Takaoka, Hiroo Miyagawa, Kunihiro Kitamura, and Akihiro Kusumi. Hydrogen Bonding of Water to Phosphatidylcholine in the Membrane as Studied by a Molecular Dynamics Simulation: Location, Geometry, and Lipid-Lipid Bridging via Hydrogen-Bonded Water. *J. Phys. Chem. A*, 101(20):3677–3691, 1997.

[125] J Yang, C Calero, and J Martí. Diffusion and Spectroscopy of Water and Lipids in Fully Hydrated Dimyristoylphosphatidylcholine Bilayer Membranes. *J. Chem. Phys.*, 140(10):104901, 2014.

[126] Jean-Paul Ryckaert, Giovanni Ciccotti, and Herman J.C Berendsen. Numerical Integration of the Cartesian Equations of Motion of a System with Constraints: Molecular Dynamics of N-Alkanes. *Journal*

of Computational Physics, 23(3):327–341, 1977.

[127] Shuichi Miyamoto and Peter A. Kollman. Settle: An Analytical Version of the SHAKE and RATTLE Algorithm for Rigid Water Models. *Journal of Computational Chemistry*, 13(8):952–962, 1992.

[128] William Hoover. Canonical Dynamics: Equilibrium Phase-Space Distributions. *Physical Review A*, 31(3):1695–1697, 1985.

[129] Joakim P M Jämbeck and Alexander P Lyubartsev. Exploring the Free Energy Landscape of Solutes Embedded in Lipid Bilayers. *J. Phys. Chem. Lett.*, 4(11):1781–1787, 2013.

[130] Christian L Wennberg, David Van Der Spoel, and Jochen S Hub. Large Influence of Cholesterol on Solute Partitioning into Lipid Membranes. *J. Am. Chem. Soc.*, 134(11):5351–5361, 2012.

[131] Ilja V Khavrutskii, Alemayehu A. Gorfe, Benzhuo Lu, and J Andrew McCammon. Free Energy for the Permeation of Na+ and Cl- Ions and Their Ion-Pair Through a Zwitterionic Dimyristoyl Phosphatidylcholine Lipid Bilayer by Umbrella Integration with Harmonic Fourier Beads. *J. Am. Chem. Soc.*, 131(5):1706–1716, 2009.

[132] Igor Vorobyov, Timothy E Olson, Jung H Kim, Roger E Koeppe, Olaf S Andersen, and Toby W Allen. Ion-Induced Defect Permeation of Lipid Membranes. *Biophys. J.*, 106(3):586–597, 2014.

[133] Massimiliano Bonomi, Davide Branduardi, Giovanni Bussi, Carlo Camilloni, Davide Provasi, Paolo Raiteri, Davide Donadio, Fabrizio Marinelli, Fabio Pietrucci, Ricardo a. Broglia, and Michele Parrinello. PLUMED: A Portable Plugin for Free-energy Calculations with Molecular Dynamics. *Comput. Phys. Commun.*, 180(10):1961–1972, 2009.

[134] Gareth A. Tribello, Massimiliano Bonomi, Davide Branduardi, Carlo Camilloni, and Giovanni Bussi. PLUMED 2: New Feathers for an Old Bird. *Comput. Phys. Commun.*, 185(2):604–613, 2014.

[135] Olof Allnér, Lennart Nilsson, and Alessandra Villa. Magnesium Ion-Water Coordination and Exchange in Biomolecular Simulations. *Journal of Chemical Theory and Computation*, 8(4):1493–1502, 2012.

[136] R Mancinelli, A Botti, F Bruni, M A Ricci, and A K Soper. Hydration of Sodium, Potassium, and Chloride Ions in Solution and the Concept of Structure Maker/Breaker. *J. Phys. Chem. B*, 111(48):13570–13577, 2007.

[137] Sameer Varma and Susan B Rempe. Coordination Numbers of Alkali Metal Ions in Aqueous Solutions. *Biophys. Chem.*, 124(3):192–199, 2006.

[138] Michael Peschke, Arthur T Blades, and Paul Kebarle. Hydration Energies and Entropies for Mg2+, Ca2+, Sr2+, and Ba2+ from Gas-Phase Ion-Water Molecule Equilibria Determinations. *J. Phys. Chem.*, 102:9978–9985, 1998.

[139] Matthew F Bush, Jeremy T O'Brien, James S Prell, Chih Che Wu, Richard J Saykally, and Evan R Williams. Hydration of Alkaline Earth Metal Dications: Effects of Metal Ion Size Determined Using Infrared Action Spectroscopy. *J. Am. Chem. Soc.*, 131(37):13270–13277, 2009.

[140] Lorena Redondo-Morata, Marina I Giannotti, and Fausto Sanz. Structural Impact of Cations on Lipid Bilayer Models: Nanomechanical Properties by AFM-Force Spectroscopy. *Molecular membrane biology*, 31(1):17–28, 2014.

[141] Frédérick J M De Meyer, Ayelet Benjamini, Jocelyn M Rodgers, Yannick Misteli, and Berend Smit. Molecular Simulation of the DMPC-Cholesterol Phase Diagram. *J. Phys. Chem. B*, 114(32):10451–10461, 2010.

[142] Ximena L Raffo Iraolagoitia and M Florencia Martini. Ca2+ Adsorption to Lipid Membranes and the Effect of Cholesterol in Their Composition. *Colloids Surfaces B Biointerfaces*, 76(1):215–220, 2010.

[143] Aniket Magarkar, Vivek Dhawan, Paraskevi Kallinteri, Tapani Viitala, Mohammed Elmowafy, Tomasz Róg, and Alex Bunker. Cholesterol Level Affects Surface Charge of Lipid Membranes in Saline Solution. *Sci. Rep.*, 4:5005, 2014.

[144] Joseph B Lim, Brent Rogaski, and Jeffery B Klauda. Update of the Cholesterol Force Field Parameters in CHARMM. *J. Phys. Chem. B*, 116(1):203–210, 2012.

[145] Wei-Chin Hung, Ming-Tao Lee, Fang-Yu Chen, and Huey W Huang. The Condensing Effect of Cholesterol in Lipid Bilayers. *Biophysical journal*, 92(11):3960–3967, 2007.

[146] Jianjun Pan, Thalia T. Mills, Stephanie Tristram-Nagle, and John F. Nagle. Cholesterol Perturbs Lipid Bilayers Nonuniversally. *Physical Review Letters*, 100(19):198103, 2008.

[147] M Bonomi, A Barducci, and M Parrinello. Reconstructing the Equilibrium Boltzmann Distribution from Well-Tempered Metadynamics. *J. Comput. Chem.*, 30(11):1615–1621, 2009.

[148] Henna Ohvo-Rekilä, Bodil Ramstedt, Petra Leppimäki, and J. Peter Slotte. Cholesterol Interactions with Phospholipids in Membranes. *Progress in Lipid Research*, 41(1):66–97, 2002.

[149] T. P W McMullen, R. N a H Lewis, and Ronald N. McElhaney. Cholesterol-Phospholipid Interactions, the Liquid-Ordered phase and Lipid Rafts in Model and Biological Membranes. *Current Opinion in Colloid and Interface Science*, 8(6):459–468, 2004.

[150] Martin R. Krause, Trevor a. Daly, Paulo F. Almeida, and Steven L. Regen. Push-Pull Mechanism for Lipid Raft Formation. *Langmuir*, 30(12):3285–3289, 2014.

[151] Hermann-Josef Kaiser, Daniel Lingwood, Ilya Levental, Julio L Sampaio, Lucie Kalvodova, Lawrence Rajendran, and Kai Simons. Order of Lipid Phases in Model and Plasma Membranes. *Proceedings of the National Academy of Sciences of the United States of America*, 106(39):16645–16650, 2009.

[152] Paulo F F Almeida. Thermodynamics of Lipid Interactions in Complex Bilayers. *Biochimica et Biophysica Acta - Biomembranes*, 1788(1):72–85, 2009.

[153] Serhan Turkyilmaz, Paulo F. Almeida, and Steven L. Regen. Effects of Isoflurane, Halothane, and Chloroform on the Interactions and Lateral Organization of Lipids in the Liquid-Ordered Phase. *Langmuir*, 27(23):14380–14385, 2011.

[154] Chang Wang, Martin R. Krause, and Steven L. Regen. Push and Pull Forces in Lipid Raft Formation: The Push Can Be as Important as the Pull. *Journal of the American Chemical Society*, 137(2):664–666, 2015.

[155] Linda J. Pike. The challenge of lipid rafts. *Journal of Lipid Research*, 50(Supplement):S323–S328, 2009.

[156] Sunhwan Jo, Taehoon Kim, Vidyashankara G Iyer, and Wonpil

Im. CHARMM-GUI: A Web-Based Graphical User Interface for CHARMM. *J. Comput. Chem.*, 29(11):1859–1865, August 2008.

[157] Sunhwan Jo, Joseph B Lim, Jeffery B Klauda, and Wonpil Im. CHARMM-GUI Membrane Builder for Mixed Bilayers and Its Application to Yeast Membranes. *Biophys. J.*, 97(1):50–58, July 2009.

[158] William L. Jorgensen, Jayaraman Chandrasekhar, Jeffry D. Madura, Roger W. Impey, and Michael L. Klein. Comparison of Simple Potential Functions for Simulating Liquid Water. *J. Chem. Phys.*, 79(2):926–935, 1983.

[159] Jeffery B Klauda, Richard M Venable, J Alfredo Freites, Joseph W O'Connor, Douglas J Tobias, Carlos Mondragon-Ramirez, Igor Vorobyov, Alexander D MacKerell, and Richard W Pastor. Update of the CHARMM All-Atom Additive Force Field for Lipids: Validation on Six Lipid Types. *J. Phys. Chem. B*, 114(23):7830–7843, June 2010.

[160] Joseph B Lim, Brent Rogaski, and Jeffery B Klauda. Update of the Cholesterol Force Field Parameters in CHARMM. *J. Phys. Chem. B*, 116(1):203–210, January 2012.

[161] Louic S. Vermeer, Bert L. De Groot, Valérie Réat, Alain Milon, and Jerzy Czaplicki. Acyl Chain Order Parameter Profiles in Phospholipid Pilayers: Computation from Molecular Dynamics Simulations and Comparison with 2H NMR Experiments. *European Biophysics Journal*, 36(8):919–931, 2007.

[162] a M Smondyrev and M L Berkowitz. Structure of Dipalmitoylphosphatidylcholine/Cholesterol Bilayer at Low and High Cholesterol Concentrations: molecular dynamics simulation. *Biophysical journal*, 77(4):2075–2089, 1999.

[163] T. Róg and M. Pasenkiewicz-Gierula. Cholesterol Effects on a Mixed-Chain Phosphatidylcholine Bilayer: a Molecular Dynamics Simulation Study. *Biochimie*, 88(5):449–460, 2006.

[164] Sagar a. Pandit, See Wing Chiu, Eric Jakobsson, Ananth Grama, and H. L. Scott. Cholesterol Packing around Lipids with Saturated and Unsaturated Chains: A Simulation Study. *Langmuir*, 24(13):6858–6865, 2008.

[165] Chunkit Hong, D Peter Tieleman, and Yi Wang. Microsecond Molecular Dynamics Simulations of Lipid Mixing. *Langmuir : the ACS journal of surfaces and colloids*, 30(40):11993–2001, 2014.

[166] Kun Huang and Angel E García. Acceleration of Lateral Equilibration in Mixed Lipid Bilayers Using Replica Exchange with Solute Tempering. *Journal of chemical theory and computation*, 10(10):4264–4272, October 2014.

[167] Jeff Timko, Alexandra De Castro, and Serdar Kuyucak. Ab initio calculation of the potential of mean force for dissociation of aqueous ca-cl. *The Journal of Chemical Physics*, 134:204510, 2011.

Publications and Conferences

Publications

1. Jing Yang, Carles Calero, and Jordi Martí.

Diffusion and Spectroscopy of Water and Lipids in Fully Hydrated Dimyristoylphosphatidylcholine Bilayer Membranes.
Journal of Chemical Physics, 140, 104901 (2014).
JCR-Year: 2013 Impact factor: 3.122

2. Jing Yang, Carles Calero, Massimiliano Bonomi, and Jordi Martí.

Specific Ion Binding at Phospholipid Membrane Surfaces.
Journal of Chemical Theory and Computation, 11, 4495 (2015).
JCR-Year: 2014 Impact factor: 5.498

3. Jing Yang, Massimiliano Bonomi, Carles Calero, and Jordi Martí.

Free Energy Landscapes of Sodium Ions at DMPC-Cholesterol Membrane Surfaces.
(Submitted to Physical Chemistry Chemical Physics)

4. Jing Yang, Jordi Martí, and Carles Calero.

Pair Interactions among Ternary DPPC/POPC/Cholesterol Mixtures in Liquid-Ordered and Liquid-Disordered Phases.
(Submitted to Soft Matter)

Conferences

1. Jing Yang, Carles Calero, Massimiliano Bonomi, and Jordi Martí.

Oral communication: Free Energy Landscapes of Metal Ions at Phospholipid Membrane Surfaces.

Workshop on biomaterials and their interactions with biological and model membranes. Salou, Spain, October 19-21, 2015.

2. Jing Yang, Carles Calero, and Jordi Martí.

Poster: Molecular Dynamics Simulation Study of the Influence of Cholesterol on Ionic Adsorption in Biological Membranes.

CECAM Tutorial: Enhancing molecular simulations with PLUMED. Belfast, United Kingdom, May 28-June 2, 2014.

3. Jing Yang, and Jordi Martí.

Poster: Structure and Dynamics of Aqueous Dimyristoylphosphatidylcholine Bilayer Membranes.

Conference: Faraday Discussion 161: Lipids and Membrane Biophysics. London, United Kingdom, September 11-13, 2012.